Russian Original Vol. 40, No. 1, January, 1976

July, 1976

SATEAZ 40(1) 1-118 (1976)

SOVIET ATOMIC ENERGY

АТОМНАЯ ЭНЕРГИЯ
(ATOMNAYA ÉNERGIYA)

TRANSLATED FROM RUSSIAN

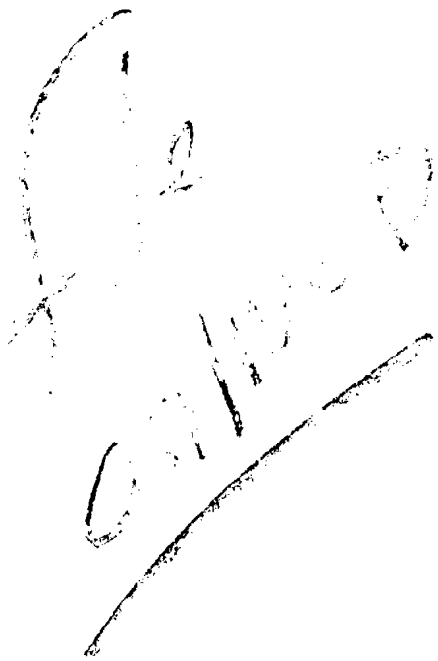

CONSULTANTS BUREAU, NEW YORK

SOVIET ATOMIC ENERGY

Soviet Atomic Energy is a cover-to-cover translation of *Atomnaya Énergiya*, a publication of the Academy of Sciences of the USSR.

An agreement with the Copyright Agency of the USSR (VAAP) makes available both advance copies of the Russian journal and original glossy photographs and artwork. This serves to decrease the necessary time lag between publication of the original and publication of the translation and helps to improve the quality of the latter. The translation began with the first issue of the Russian journal.

Consultants Bureau journals appear about six months after the publication of the original Russian issue. For bibliographic accuracy, the English issue published by Consultants Bureau carries the same number and date as the original Russian from which it was translated. For example, a Russian issue published in December will appear in a Consultants Bureau English translation about the following June, but the translation issue will carry the December date. When ordering any volume or particular issue of a Consultants Bureau journal, please specify the date and, where applicable, the volume and issue numbers of the original Russian. The material you will receive will be a translation of that Russian volume or issue.

Subscription
$107.50 per volume (6 Issues)
2 volumes per year

Single Issue: $50
Single Article: $15

Prices somewhat higher outside the United States.

CONSULTANTS BUREAU, NEW YORK AND LONDON

227 West 17th Street
New York, New York 10011

Published monthly. Second-class postage paid at Jamaica, New York 11431.

Soviet Atomic Energy is abstracted or indexed in *Applied Mechanics Reviews, Chemical Abstracts, Engineering Index, INSPEC—Physics Abstracts and Electrical and Electronics Abstracts, Current Contents,* and *Nuclear Science Abstracts.*

SOVIET ATOMIC ENERGY

A translation of *Atomnaya Énergiya*

July, 1976

Volume 40, Number 1 January, 1976

CONTENTS

CONTENTS

(continued)

The Russian press date (podpisano k pechati) of this issue was 12/23/1975. Publication therefore did not occur prior to this date, but must be assumed to have taken place reasonably soon thereafter.

ARTICLES

ROLE OF GAS AS A COOLANT IN THE DEVELOPMENT OF NUCLEAR POWER STATIONS

E. P. Anan'ev and G. N. Kruzhilin

UDC 621.039.524.46.034.3

Gas-cooled reactors, of both the thermal and fast varieties, are again exciting considerable interest. Gas cooling in general, and helium cooling in particular, is in fact now being considered and developed as a technical alternative to cooling with molten sodium in fast reactors, since as regards the breeding of plutonium and the generation of water vapor for the power cycle the parameters of the two coolants are sufficiently close to make no practical difference. Such difference as exists is mainly of a technological character. There is of course a considerable difference in the arrangements for the cooling of the active zone in any hypothetical emergency, since the heat capacity of the gas in this zone is quite negligible compared with that of sodium.

As regards thermal reactors, helium cooling appears to be quite a promising solution; in this case the temperature of the gas at the outlet from the reactor may extend to 750-850°C or even higher. There is thus a real possibility of generating steam at high temperatures and pressures, such as those characteristic of modern thermal power installations, giving a power cycle efficiency of 41-42% as compared with 30-34% in the case of the saturated-vapor cycle obtained in installations with water-cooled reactors. Clearly, if we take no account of the possible nuclear superheating of the steam in certain types of reactors, this effect will be of no great importance in view of the low fuel component of the cost of electrical power in nuclear power stations with saturated-vapor cycles. Nevertheless, the degree of use of the nuclear fuel improves in the presence of a high efficiency factor and the ejection of heat through the condenser into the cooling water diminishes, i.e., the "thermal contamination" of the water and the corresponding harmful effect on Nature is reduced.

Considerable interest also arises in relation to high-temperature helium coolants at the present time in view of the special requirements of a number of branches of industry (metallurgical, chemical, etc.) for high-temperature heat; these are branches which at present consume some 25% of recoverable organic fuel. One of the most important problems facing the power industry will be that of directing nuclear power into the multipurpose complex production of electrical power and other types of product [1]. Here we have a real prospect of using high-temperature gas heated in a nuclear reactor for industrial purposes.

It is interesting to consider gas-cooled reactors of the kind which have been developed most extensively in Britain and France. The development of a gas reactor was started in the USSR even at the end of the 40's. However, only a nuclear power station with an electrical power of 150 MW (incorporating a gas-cooled reactor using natural uranium with a heavy-water moderator), built in Czechslovakia, was in fact fully developed.

The first British nuclear power station with a gas reactor (essentially a demonstration model) was started in Calder Hall in 1956 (power 42.0 MW) [2]. The reactor in this power station uses natural uranium and has a graphite moderator situated in a steel housing 11.2 m in diameter with a wall thickness of 50 mm. The cooling gas is CO_2, the fuel elements are metallic uranium (cylindrical elements with a core diameter of 29.6 mm) covered with a magnesium alloy (Magnox) can. Since the melting point of Magnox is 640°C, the maximum temperature of the fuel-element can is only ~450°C, and correspondingly the temperature of the cooling gas at the reactor outlet is 345°C. The reactor has four loops with a pipe diameter

Translated from Atomnaya Énergiya, Vol. 40, No. 1, pp. 3-11, January, 1976. Original article submitted April 9, 1975.

of 1370 mm; the gas coolant circulates through these at a pressure of 7.8 atm. Each loop has a gas blower with a power of 1500 kW and a steam generator (boiler) which produces superheated water vapor at a pressure of 14 atm and a temperature of 320°C. The steam generator is placed alongside the reactor in a vertical steel housing of diameter 5.5 m and is furnished with a drum separator. Repeated circulation of the water in the boiler is effected on the La Monte forced-flow principle. The efficiency of the unit is 19.2%.

In order to intensify heat transfer, the fuel-element can is ribbed transversely with a rib height of 12 and a step of 7 mm. This ribbing is certainly very original, since the gas flows longitudinally around the fuel elements in the graphite stack. The mean thermal loading is 1.65 MW/ton of U, or $0.19 \cdot 10^6$ kcal/m$^2 \cdot$h referred to the surface area of the uranium cores.

The groups of boiler tubes are flushed transversely by the gas. In order to intensify heat transfer, these tubes (carbon steel, 51 mm in diameter) also have transverse ribbing. This configuration is produced by the automatic welding of sector ribs on to the tube, the weld contour amounting to 1/3 of the length of the outer circumference of the tube cross section. The total surface of the rib is thus roughly four times greater than that of the outer surface of the tube.

Clearly the ribbing of the fuel elements and boiler pipes is in this case perfectly acceptable, since the circulating gas does not contain any particles such as might become deposited on the pipes and ribs in the manner of, for example, coal installations.

After the British nuclear power station in Calder Hall had been tested, a number of industrial nuclear power stations were built with analogously constructed uranium-graphite gas reactors using fuel elements of natural uranium and Magnox cans; reactors of this kind have become known as the "Magnox" type [2]. Eighteen industrial power units with a total power of 5000 MW have been constructed in Britain. The unit electrical power of these installations has gradually increased from 138 to 590 MW, with a parallel rise in efficiency from 24.6 to 33.6%. These indices were largely achieved by correspondingly enlarging the active zone, raising the pressure of the cooling gas in the circuit to 27 atm, and increasing the gas temperature at the reactor outlet to 410°C, and also by providing for a corresponding rise in boiler steam temperature and pressure, namely, superheating to 393°C and 100 atm. Another important feature was a further improvement to the fuel-element ribbing, in that the transverse ribs were replaced by an optimum configuration of inclined ribs (chevrons). The diameter of the fuel-element core was also reduced to 28 mm. Altogether the mean thermal loading of the fuel elements was increased to 3.15 MW/ton of U or $0.35 \cdot 10^6$ kcal/m$^2 \cdot$h.

The increase in the dimensions of the active zone resulted in a corresponding increase in the size of the reactor vessel. This latter increment, together with the rise in circuit gas pressure, necessitated an increase in reactor wall thickness. The nuclear power station in Sizewell, in which the unit power is 290 MW and the gas pressure 18.56 atm, has the largest steel spherical vessel, 19.4 m in diameter, with a wall thickness of 105 mm. Vessels of this kind are made directly on the site in the form of individual sheets welded together manually. This extremely laborious work is executed by hundreds of welders over several months.

Under the conditions existing on the building site severe difficulties were encountered in ensuring a metal temperature sufficient for welding and subsequent heat treatment. Such difficulties increased with vessel wall thickness. The next British gas reactors with higher cooling gas pressures were therefore made not of steel but of prestressed reinforced concrete.

The first reinforced-concrete vessel was made for the nuclear power station in Oldbury. This cylindrical vessel (internal diameter and height 23.5 and 18.3 m, wall thickness 4.5 m) was designed for a pressure of 24.6 atm. The second was a spherical vessel for the Magnox reactor of the nuclear power station in Wylfa, designed for a unit having an electrical power of 590 MW with an internal diameter and wall thickness of 29 and 3.36 m and a gas pressure of 27 atm. In both reactors the boilers and gas blowers are sited in chambers inside the walls of the concrete reactor vessel, and in this sense the composition of the equipment may be regarded as integrated.

Such a compact arrangement is undoubtedly economical and also entirely reasonable from the point of view of ensuring more reliable hermetization of the circuit.

An important technological characteristic of the British Industrial Magnox reactors is the method of fuel recharging, which ensures a high use coefficient and improves the physical characteristics of the fuel cycle.

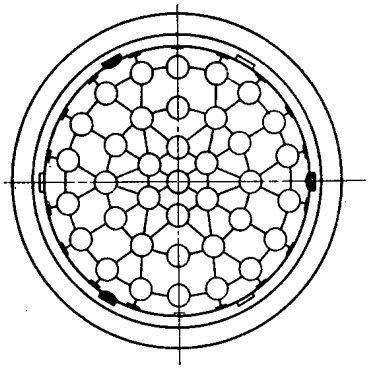

Fig. 1. Cross section of a fuel cassette in the Hinckley Point nuclear power station.

The Magnox reactors were constructed and are being used on a two-purpose principle: for breeding plutonium and for producing electrical power. The fuel consumption is accordingly relatively small and amounts to 3000-3600 MW·day/ton of U. The campaign of the fuel elements in the reactor lasts up to six years [3]. Reliable hermetization of the fuel elements is required for such a long campaign. In the few cases in which the hermetization of the fuel elements is breached, the release of the carbon dioxide is quite a slow process. There is accordingly no need for any urgent discharging, and the recharging is planned as an ordinary operation.

Up to 1971 there had been only one emergency in Magnox reactors involving the melting of the fuel elements in one channel of the Chapel Cross reactor, probably due to the breakdown of a graphite bushing, with the partial closing of the channel cross section. An important point noted in 1968 was the considerable corrosion of the carbon steel in the CO_2 atmosphere [3]. It was found that this gas had no effect on the open surfaces, including the vessel and the boiler pipes, but that serious corrosion took place at the contacts between nuts and bolts. Magnetite (Fe_3O_4) was formed in volumes two or three times greater than the volume of the actual metal, and in some cases this led to the fracture of the bolts. Carbon steel bolts are used for fixing purposes in the reactors and boilers of all Magnox nuclear power stations. It was therefore decided in 1969 to reduce the pressure at the reactor output to 360°C, and this reduced the power of these nuclear power stations by 20-25%, i.e., to a total value of about 1000 MW.

The considerable experience gained in the building and practical exploitation of the British Magnox reactors formed a basis for the manufacture of improved powerful gas reactors of the AGR series, using enriched uranium. The planned cost of electrical power in nuclear power stations using these reactors was estimated as being 40% below the best nuclear power stations with Magnox reactors and 10% below power stations using organic fuel. Typical of this series is the AGR reactor in the Hinckley Point B nuclear power station with a unit power of 660 MW, and cylindrical fuel elements 1016 mm long made of enriched (2.06-2.57% [4]) uranium dioxide (core diameter 14.5 mm). The mean depth of burn-up is 18,000 MW·days/ton of U. The cooling gas (CO_2) circulates at a pressure of 43 atm. The gas temperature at the inlet into the active zone is 282°C and at the outlet 665°C. As a result of this the boilers produce superheated steam at 170 atm and 540°C; secondary superheating of the steam is also effected at 41 atm and up to 540°C. The turbine operates with a condenser pressure of 0.041 atm with a cooling water temperature of 12°C. The efficiency is 41.7%.

It follows from Fig. 1 that the rod-type fuel elements are assembled in a cassette with a cylindrical graphite housing having internal and external diameters of 190 and 238 mm. The cassette contains 36 fuel elements. Eight cassettes are connected together vertically, using a special suspension, and the group is let down into the channel of the graphite stack through a special adjusting tube. The diameter of the channel is 263 mm, the gap between the channel and the graphite casing of the cassette 12.5 mm, so that the cassette passes freely into the channel. Mounted on the suspension are biological shielding units, sensors measuring the temperature at the outlet from the channel, and a mechanism for changing the flow of gas through the latter. Altogether there are 308 channels; the average electrical power of one channel is 2.13 MW. The step between the channels is 460 mm.

The average thermal loading of the fuel elements is 12.2 MW/ton of U ($0.67 \cdot 10^6$ kcal/m^2·h). The maximum temperatures in the center of the fuel element and on the can are 1500 and 800°C. These temperatures are reached in approximately the middle cross section of the channel, at which the gas temperature is ~480°C, so that the can/gas temperature drop is ~320°C. Taking account of this, we may consider that the heat-transfer coefficient from the can to the gas averages ~2100 kcal/m^2·h·°C. This large value for the gas coolant is achieved by circulating the gas under high pressure (43 atm at a mean velocity of 12 m/sec) and by creating artificial roughness on the fuel-element can, in the form of a fine rectangular thread with a pitch of 2 mm.

The reactor vessel is cylindrical, made of prestressed reinforced concrete with an internal diameter of 18.9 m. The boiler and gas blower are integrated, as in the Oldbury power station. The four direct-flow boilers associated with each reactor are sited in individual chambers, the gas circulation through each being effected by means of two gas blowers. The eight gas blowers ensure a gas circulation with a

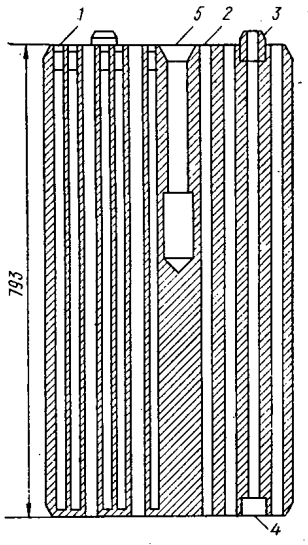

Fig. 2. Block-type fuel element of the reactor in the Fulton nuclear power station.

total flow rate of 3512 kg/sec for a pressure drop of 2.5 atm. The gas-blower power is 3.5 MW (28 MW for all eight) amounting to 4.1% of the power of the whole unit.

The heating surface of the direct-flow boiler is made of three kinds of steel. The economizer part is made of mild carbon steel tubes, in view of the fact that their surface temperature will never exceed 350°C (this is based on corrosion considerations). The evaporating part of the boiler is made of chromium steel tubes with a chromium content of 9%. In the steam-generating part, austenitic chromium-nickel steel tubes are employed. From considerations of the strength and welding requirements, transitional sections of Niconel-600 are placed between the chromium and austenitic steel tubes; if the tubes were welded directly there would be harmful effects associated with their different thermal expansions and also with carbon diffusion. In order to avoid stress corrosion moisture must be prevented from falling into the austenitic steel tubes. In order to intensify heat transfer the first two kinds of tube are provided with different transverse ribbing. No ribbing is provided on the austenitic steels. It is interesting to note that the temperature difference between the gas leaving the reactor and the superheated steam in nuclear power stations of this type is ~130°C, while in Magnox power stations, in which the boilers are made of ribbed carbon tubes, this difference is only 17°C. The temperature of the graphite stack in reactors of this type is under 500°C. This limit is chosen because at higher temperatures the graphite starts oxidizing seriously as a result of interaction with the oxygen released by the decomposition of the CO_2 (partly due to radiation). In addition to this, methane is added as an inhibitor to retard the oxidation of the graphite. In order to ensure the required temperature the graphite is gas-cooled. Hence after leaving the gas blower at a temperature of 200°C the gas first passes through the graphite stack, including the annulae gaps between the channels in the stack and the graphite housings of the fuel cassettes. Then the gas passes through the fuel-element cassettes, in which it is heated to 670°C.

The reinforced-concrete reactor vessel is cooled with water passing through a special tube system, the temperature of the concrete being held below 70°C. The construction of the vessel is quite specific owing to the large number of metal tubes with wire cables ~100 mm in diameter passing through them, the tension in these creating the stressed state of the vessel. The calculated tensile-strength reserve factor is taken as three. When testing model vessels on 1/8 and 1/5 scales, the maximum loads were applied to the models. When the pressure rises in the vessel, cracks start propagating, and the rupture process is of a completely different character from that in which walls made of brittle materials fracture. It is therefore quite reasonable to assume that a hypothetical accident (with the swift collapse of the vessel and a total loss of coolant) is much less likely in this case than in that of a system with a steel vessel.

As far as radiation safety is concerned, it is especially important to consider the problem of preventing the active zone from melting. In reactors of this series, this requirement is chiefly guaranteed by the low temperature of the active-zone graphite. Thus if the gas circulation ceases as a result of (for example) accidental disconnection of the gas blower (when emergency shielding also comes into action) the remaining heat evolution of the fuel elements will be largely carried out into the "cold" graphite stack as a result of radiant heat transfer. According to calculations, in this emergency situation the fuel element can will only rise to 1000°C after 4 h (at which point it may well break down, although its melting point is actually 1400°C). In this time it should be possible to correct the fault in the electrical supply system which caused gas circulation to cease.

It is interesting to note that during the development of nuclear power stations containing AGR reactors the boiler tubes vibrated; this was prevented, after certain experiments, by appropriate clamping of the tubes. The vibrations arose both from the mechanical pressure of the dense gas on the tubes and from acoustic resonance in the gas itself. In view of the latter the number of gas blowers had to be increased to eight (3.5 MW each as in the Hinckley Point station). Even so during tests on the first unit of this nuclear power station the severe noise from the gas blowers gave serious problems: The regulating valves at the outlet from the gas blowers were damaged and severe vibrations of the adjusting tubes took place. It was indicated in August 1974 [5] that because of this the initiation of the unit would be delayed for 20 weeks. So far nothing further has been said about this.

TABLE 1. Basic Characteristics of Certain Reactors with Gas Cooling

Indices	Peach Bottom, USA	Fort St. Wrayne, USA	Fulton, USA	Hinckley Point, Britain
Coolant	Helium	Helium	Helium	CO_2
Power, MW:				
thermal	115	842	3000	1500
electrical	40	330	1160	625
Efficiency, %	35	39	38,6	41,7
Temperature, °C:				
at the inlet	340	405	318	282
at the outlet	715	780	740	665
Height of active zone, m	2,28	4,75	6,34	—
Diameter of active zone, m	2,79	5,94	8,47	—
Internal diameter of vessel, m	—	—	—	18,9
Gas pressure, atm	24	49	51	43

Earlier it was indicated that the AGR reactor (unit) Dungeness B would be first to start (in 1970). Then in 1972 it was proposed to start the reactor of the Hinckley Point nuclear power station and later to initiate other AGR reactors. According to the data of the International Agency on Atomic Energy [6], however, all the AGR reactors will only just now have started operation; this implies a delay of 5-6 years, involving direct economic losses and certain difficulties in estimating the prospects of such reactors. This is why the discussions regarding future nuclear-power developments held in Britain in 1973-1974 were so acrimonious and prolonged. It was pointed out [7] that the main reason for the delay in starting the AGR was the necessity of replacing certain carbon steel parts in these reactors. A number of the first reactors of this series were already largely completed as regards the construction of the reinforced concrete vessels when it became known that dangerous corrosion of carbon steel took place in Magnox reactors working in an atmosphere of CO_2 at 360°C. The carbon steel therefore had to be replaced by more heat-resistant varieties in the already completed structures, a task by no means simple.

In addition to this [8] difficulties arose with the fuel-element cassettes, since earlier tests on these in the experimental Windscale AGR reactor did not entirely correspond to the operating conditions of industrial reactors in the power system. Subsequently further tests were made, the thermal loads being varied cyclically from 40 to 100%. The tests showed that, under these conditions, and subject to high fuel burn-up values, the uranium dioxide fuel-element cores swelled. However, fuel-element cores with a central aperture swelled in the direction of the aperture and may therefore be regarded as more promising than solid versions. The aperture in the core promotes a more vigorous diffusive evolution of gaseous fission products from the fuel; this might be compensated by changing to coarser UO_2 granules in preparing the cores by the sintering method. These tests also showed that carbon was deposited on the fuel-element cans. This is an undesirable feature, since under nominal loads the can temperature may rise to 800°C.

In the opinion of the former Director of the British Atomic Energy Authority Sir Christopher Hinton it will be necessary to reduce the gas temperature and pressure very considerably in the AGR reactors, reducing the power to some 60% of the original plan [9]. Naturally this raises the question as to whether it might not be better to use helium as a reactor coolant [10], a possibility not seriously considered before on account of the difficulty of making a circuit with a reinforced-concrete vessel sufficiently gastight.

Thermal reactors with helium cooling are intended to heat the gas to higher temperatures than AGR reactors. This leads to a considerable contraction in the heating surface of the boilers, which is quite substantial and expensive when using gas coolants. An increase in the gas temperature also means an increase in the temperature of the fuel elements. Thus in high-temperature reactors fuel elements with stainless steel coatings (as employed in the AGR) cannot be used; for these reactors fuel elements of a special construction with graphite coatings have been developed, and the temperature of such coatings may exceed 1000°C. This means that CO_2 cannot be used as a coolant, since it reacts vigorously with graphite even at under 500°C. Hydrogen cooling is also impossible, since at temperatures above 700°C it starts reacting with carbon to form hydrocarbons. Thus helium cooling of the high-temperature reactor is the most favorable method. However, even helium has to be purified from H_2, CO, and CO_2, since these gases appear in the coolant, for example, when water leaks out of the boiler.

Helium is a comparatively rare gas and quite expensive. It is therefore very important to prevent losses such as might occur if the circuit is not hermetized and leaks occur. We may note that the reinforced-concrete vessel of the Magnox reactor in Oldbury, for example, gave a CO_2 leakage of about 1000

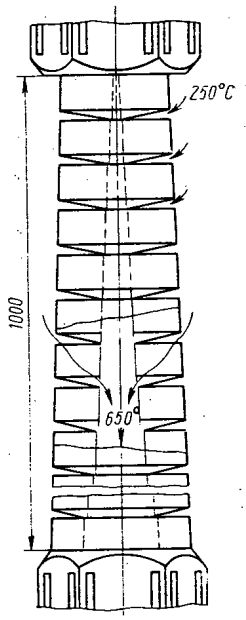

Fig. 3. Construction of a fuel element for a high-temperature helium-cooled reactor.

kg per day at the very beginning, [11], which later of course increased. For helium cooling this is quite unacceptable.

Some interesting developments were started by S. M. Feinberg in cooperation with other scientists on a helium breeder reactor of module construction [12].

Helium-cooled reactors have perhaps been most persistently developed in the United States (Table 1). An experimental helium reactor with a power of 40 MW (electrical) was constructed and started in 1966 in Peach Bottom. Then a demonstration helium reactor with an electrical power of 330 MW was constructed in Fort St. Wrayne, being in a state of imminent operation in 1974 [10]. Recently the design of a large power reactor with helium cooling and an electrical power of 1160 MW was completed for the Fulton nuclear power station; construction is expected to be complete in 1982 [13].

According to design the Fulton nuclear power unit will have six direct-flow boilers (steam pressure 177 atm, temperature 513°C) and two turbogenerators of 600 MW each. It is well known that US industry already produces turbogenerators of 1300 MW with high steam parameters. In the Fulton nuclear power station design we thus see a clear departure from the principle of the monolithic unit hitherto ruling in United States nuclear power.

In the Fulton nuclear power station (as in Fort St. Wrayne) the fuel elements are made of a graphite block of hexagonal cross section with gage dimensions of 359 mm and a height of 793 mm (Fig. 2). A block-type fuel element of this kind contains 128 channels 16 mm in diameter accommodating the fuel 1, and 72 open channels 21 mm in diameter through which the helium passes 2. In addition to this there are six channels 12.7 mm in diameter, containing burning-out absorbent. Eight such fuel elements are arranged over the height of the active zone in the Fulton nuclear power station. These are joined by means of projections 3 and corresponding depressions 4. The central upper depression 5 serves for taking hold of the block when recharging.

The fuel employed comprises UC and ThC granules ~0.8 mm in size coated successively with layers of pyrolytic graphite and silicon carbide to a total thickness of ~0.2 mm. The granules are mixed with graphite and resin and pressed into rods 16 mm in diameter and 6 cm long, which are then loaded into the channels of the graphite block.

The coating of the granules with layers of graphite and silicon carbide fails to make them completely hermetic; some of the fission fragments diffuse into the coolant, which becomes radioactive. In order to reduce the radioactivity, devices are incorporated to trap the radioactive contaminants with activated charcoal, in conjunction with cryogenic traps. According to experience gained in the use of this experimental type of reactor, the total radioactivity of the gas in the circuit stabilizes at a level of 20-30 Ci. This indicates that no developing discontinuities occur in the layered can for burn-ups of up to $100 \cdot 10^3$ MW·day/ton of U, and in this case the cans operate reliably for the temperatures indicated in Table 1. This is an extremely important and favorable result.

At higher temperatures, however, when the diffusion of the fission fragments through the solid wall becomes substantial, the radioactivity of the helium in the circuit will be higher. A rise in temperature may also lead to damage in the fuel-element cans. These circumstances (especially the second) prevent increasing the gas temperature when using such fuel elements. The new type of fuel-element construction illustrated in Fig. 3 is perhaps a more promising version; in this the fuel granules are placed in protective graphite cans over the height of the fuel elements in the form of free layers, having the high porosity characteristic of a layer filling. The fuel element is cooled by gas passing through the layers of granules, there being a relatively low temperature difference between the gas and the can. Hence the gas temperature may lie close to the permissible can temperature, exceeding 1000°C. Unfortunately fuel elements of this kind have not yet been developed. However, it is easily seen that the construction will not be a simple matter, since in view of the high gas temperature the housing of such a fuel element will have to be made of heat-resistant ceramic. The development of such fuel elements will take time and effort. No experimental data have yet been obtained as to the permissible upper temperature of the can.

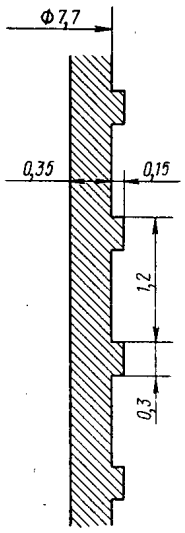

Fig. 4. Longitudinal section of the fuel-element can of a fast helium-cooled reactor.

Attention should also be paid to certain other characteristics of high-temperature gas reactors. In particular, the motion of the gas from bottom to top used for the active zones of the Magnox and AGR reactors must now be replaced by motion from top to bottom, since if the gas in the active zone moved from bottom to top and had an outlet temperature of 750°C the current servicing of the upper part of the reactor, the recharging of the fuel elements, the functioning of the control and safety-rod system, and the regulation of the gas flow along the channels would be very difficult.

One interesting feature is the transition to a new, compact construction of the direct-flow boiler in the Fulton station. The power-station unit provides for six boilers, each producing ~600 tons/h of steam. The total boiler heating surface is therefore very large. The over-all dimensions nevertheless have to be limited, since the whole equipment of the circulating circuit is made in integrated form in a common prestressed-concrete housing. According to design the boiler will therefore be made from coils wound around a cylindrical surface. In the concrete reactor vessel, this fairly powerful boiler is to be sited in a cylindrical cavity only 3.2 m in diameter. It would thus be very difficult to repair the boiler if any leaks developed. In the majority of cases it would be necessary to extract the whole boiler and spend a great deal of time on servicing. It is therefore vital that the boiler should be made as reliable as possible.

The question of radiation hazard is especially important, since the cooling gas of these reactors contains fission fragments diffusing through the cans of the fuel granules. This complicates operations in the recharging of the fuel, and also repair operations within the circuit. Problems of general safety are here approximately the same as in the AGR reactors. There is also a great deal of graphite in the active zone of these reactors. Hence if the gas circulation is accidently cut off the residual heat will pass into the graphite stack without damaging the granule cans for some considerable time. The systems are also provided with special emergency cooling systems.

Fast helium-cooled reactors with a prestressed reinforced concrete vessel are also planned. These also envisage integrated construction, i.e., all the equipment resides inside the reinforced concrete vessel. Owing to the absence of a moderator the active-zone dimensions of a fast reactor are much smaller. In the design for the fast helium reactor GBR-4 with an electrical power of 1200 MW [14] the diameter and height of the active zone are 4 and 1.4 m. The fuel elements are cylindrical, the can is of stainless steel 7.7 mm in external diameter. As indicated in Fig. 4, the outer surface of the fuel-element can has a fine rectangular thread to intensify heat transfer. Such fuel elements are assembled in a hexagonal cassette with a gage dimension of 213 mm and are arranged in a triangular lattice with a step of 11.65 mm, i.e., with a gap of about 4 mm. Altogether the cassette contains 321 fuel elements.

It is well known that the main characteristic of a fast reactor is its extremely high thermal loadings. In the GBR-4 reactor the maximum loads are about 400 MW/ton of U or $1.5 \cdot 10^6$ kcal/m$^2 \cdot$h of the surface of the fuel element. In view of this the problem of cooling the active zone in the case of an accidental disconnection of the gas blowers is extremely vital. In the reactor design this problem is intended to be solved by means of three loops capable of operating with natural circulation of cooling water and cooled gas. When an emergency stoppage occurs in the gas blower, the reactor is protected by continued circulation of the gas through the active zones, promoted by the difference between the densities of the gas in the active zone and the sets of tubes forming the emergency loop. For the normal gas pressure in the circuit (90 atm) this gas circulation is sufficient to prevent melting of the active zone, at least for a while, so giving time to restore the gas circulation by means of the gas blowers [14]. In addition to this, these emergency loops have their own gas blowers, driven by emergency Diesel generators, which may be automatically brought into action at short notice. With this arrangement the chief danger clearly arises in the very first moments, in which the residual heat has to be carried away by natural gas circulation.

Another original feature of the design is the fact that the lower part of the fuel-element assembly is filled with activated charcoal, designed to absorb gaseous fission fragments. In addition to this, in a fast gas-cooled reactor it is desirable to use fuel elements made from granules with a graphite can (Fig. 3).

The search for other coolants (apart from those already known) to be used in fast reactors has so far met with little success. As an alternative it has been proposed to use dissociating nitrogen tetroxide

N_2O_4 [15]. According to A. K. Krasin et al., a reactor with a coolant of this kind may provide a doubling time equivalent to that of sodium reactors.

Thus it may now confidently be stated that gas-cooled reactors will shortly be capable of effective use not only in nuclear power stations but also as sources of high-temperature heating for technological processes in industry. The development of the latter aspect has only just started, and cannot of course be very rapid, since it depends on both reactor development and special technologies. Nevertheless, it is becoming more and more evident that nuclear reactors are excellently suited to high-temperature gas heating. It should furthermore be noted that extremely heat-resistant materials (molybdenum, niobium, tantalum, and their alloys) may also find employment in future high-temperature reactors. It may well be that these new materials will be required for the heat exchangers, in which high-temperature helium from the reactor will heat the gas directly used in the technological process.

Finally it is appropriate to note that, in the possible development of the technological aspect, there is yet another specific limitation which has to be taken into account; namely, that arising from radioactivity; it is accordingly essential to ensure that the practical exploitation of the nuclear reactor should be characterized by great efficiency and reliability. It is reasonable to assert that there should not be too many technological undertakings with nuclear reactors, and the latter should therefore have a very high unit power, or a correspondingly high thermal power, at least of the order of 1000 MW. The technological undertakings should be correspondingly powerful.

LITERATURE CITED

1. A. P. Aleksandrov, At. Énerg., 25, No. 5, 356 (1968).
2. Brit. Nucl. Export Executive Rev., No. 1 (1966); No. 2 (1967); No. 3 (1968).
3. R. Kutter, Fourth Intern. Conf., Geneva (1971), Rep. 49/p./468.
4. Nucl. Engng. Intern., 20, No. 229, 412 (1975).
5. Nucl. Engng. Intern., 19, No. 219, 623 (1974).
6. Power and Research Reactors in Member States, IAEA, Vienna (1974).
7. Appl. Atomics, No. 857 (1972); No. 936 (1973).
8. Nucl. Engng. Intern., 19, No. 220, 689 (1974).
9. Electr. Rev., Feb. 8 (1974); Electr. Rev., Oct. 25 (1974).
10. J. Nucl. Energy, 26, No. 1, 49 (1972).
11. Brit. Nucl. Export Executive Rev., No. 3, 75 (1968).
12. S. M. Feinberg, At. Énerg., 37, No. 1, p. 3.
13. V. Boyer and J. Gibbons, Nucl. Engng. Intern., 19, No. 219, 635 (1974).
14. Nucl. Engng. Intern., 19, No. 218, 566 (1974).
15. A. K. Krasin et al., 4th Geneva Conf., Soviet Paper No. 431 (1971).

EXPERIENCE IN THE USE OF A NUCLEAR REACTOR IN THE NORIL'SK MINING-METALLURGICAL COMPLEX

V. N. Nikitin, V. N. Pavlova,
A. I. Petrov, and A. M. Shchetinin

UDC 621.039

The diverse analytical problem in the practical training of the Noril'sk mining-metallurgical complex requires constant development, modernization, and unrestricted industrial application of the most modern chemical, physicochemical and physical methods for investigating the elementary composition of the natural raw material and the products of its technological processing. The correct technology for processing the raw material and for the extraction of metals depends on the speed and quality of the analysis, and the detection and elimination of channels of loss of industrially valuable elements depends on the sensitivity of the methods [1].

Among the physicochemical and physical methods which have become classical, activation analysis possesses a number of additional potentialities with respect to sensitivity, rapidity and efficiency. Therefore, an activation analysis laboratory was built in the complex with an RG-1M research nuclear reactor [2, 3], which in the first place should solve the problems of the high-sensitivity determination of the content of metals of the platinum group and the rare elements, should ensure a higher efficiency for the analysis of geological and technological materials in nonferrous and rock-forming elements and should carry out radioisotopic investigations of technological processes.

The thermal-power design of the reactor (5 kW) was increased during the start-up adjustment period to 30 kW [4, 5] and in April 1970 the RG-1M reactor was brought on stream. As a result of redesign after two years of operation and after the investigations carried out, simultaneously with the installation of a five-channel pneumatic rabbit system a further increase of its power was achieved [6]. The thermal neutron flux at the center of the reactor core is now $2.7 \cdot 10^{12}$ n/(cm^2 · sec) and, by using a neutron trap, it is doubled.

The heterogeneous RG-1M reactor, of the swimming-pool type, has 11 vertical experimental channels in ten of which the thermal neutron flux amounts to 0.4 to $2.7 \cdot 10^{12}$ n/(cm^2 · sec) and in one channel the fast neutron flux (energies greater than 5 MeV) has a value of 10^8 n/(cm^2 · sec). Five channels are equipped with a pneumatic rabbit system for transporting samples into the reactor and out of the reactor to the store position after irradiation or measurement. The times of irradiation, holding and address for conveyance of the samples in ampoules are provided automatically. The pneumatic rabbit equipment, developed and manufactured in the All-Union Scientific-Research Institute of Reactor Technology, has shown high operating qualities during two years. The magnitude of the neutron flux in the reactor channels and the pneumatic rabbit equipment permit neutron activation analysis to be carried out with a sensitivity and accuracy, satisfactory for industrial requirements, in two alternatives: radiochemically with the use of long- and average-life isotope-tracers and nondestructively with the use predominantly of short-lived activities. Single-shift operation of the reactor was found to be sufficient for the irradiation of samples being analyzed according to a manufacturing scheme.

The activation analysis laboratory has six work points for radiochemical treatment of irradiated samples, in combination with two scintillation spectrometers based on multichannel pulse analyzers AI-128 and USD-1 universal scintillation data units, and two industrial facilities for instrumental activation analysis, including NTA-512 and LP-4840 multichannel pulse analyzers with a bank of scintillation and

Translated from Atomnaya Énergiya, Vol. 40, No. 1, pp. 11-16, January, 1976. Original article submitted March 3, 1975.

TABLE 1. Characteristics of Radioactivation Analysis Procedures

Element determined	Thresh. of sensitiv. for 5-h irrad., %	Wt. of sample to be analyzed, g	No. of samples in single batch	Time of analysis of single batch, h	Sample output per week
Radiochemical version					
Au	10^{-7}	0,5—1,0	18	18	36
Pt	$5 \cdot 10^{-5}$	0,2—0,5	6	18	12
Pd	$2 \cdot 10^{-6}$	0,2—0,5	6	18	12
Ir	$2 \cdot 10^{-7}$	0,5—1,0	20	36	20
Ru	$2 \cdot 10^{-6}$	0,5—1,0	20	36	20
Os	$5 \cdot 10^{-7}$	0,5—1,0	20	36	20
Re	10^{-6}	0,1—1,0	24	36	24
Ag	10^{-4}	0,1—1,0	30	36	30
Instrumental version					
Cu (in core samples)	10^{-2}	up to 200	1—2	0,15	up to 200
Co(^{60}Co)	$2 \cdot 10^{-5}$	1—2	40—50	168—336	200—250
Co(^{60m}Co)	10^{-3}	0,2—1	2	0,18	200
Si	10^{-1}	0,5—1	2	0,18	200
Al	10^{-2}	1—2	1—2	0,15	240
Au	10^{-4}	1—5	40—50	72—120	200—250
Ir	10^{-5}	1—5	40—50	168—240	200—250

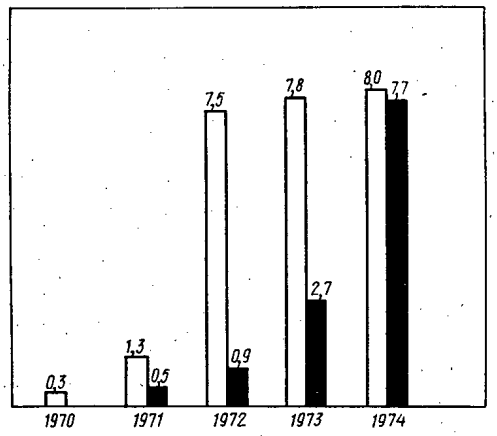

Fig. 1. Radioactivation analyses by means of the RG-1M reactor (thousands of element-determinations). □) Radioisotope analysis; ■) instrumental activation analysis.

semiconductor Ge(Li) detectors. In addition to this, the laboratory is equipped with an AI-4096-3M amplitude—time analyzer, an "Angara" coincidence spectrometer, an MIR-1 electronic computer, and a satisfactory amount of electronic—physical, radiometric, and dosimetric equipment.

Considerable assistance in equipping the laboratory with modern equipment and plant was afforded by the combine of the organization GKAÉ (State Committee for the Utilization of Atomic Energy) of the USSR, treating the activation analysis laboratory of the Noril'sk Mining-Metallurgical Complex as an experimental-industrial proving ground for the application of achievements in the field of applied nuclear physics to the national economy. Many instruments and methods, developed in the All-Union Scientific-Research Institute for Reactor Technology (VNIIRT), are introduced and used in the Noril'sk Mining-Metallurgical Complex, and joint scientific-research and systematic work are undertaken.

About 20 procedures have been developed and introduced into analytical practice in the laboratory during a year of experimental-industrial operation (industrial since 1972). The characteristics of the continuously used procedures are given in Table 1. When solving analytical problems by radioactivation analysis methods, the requirement for high sensitivity was taken into account (especially when determining the content of metals of the platinum group and of the rare elements), which was lacking in the methods previously used. Radioactivation analysis provides better characteristics of productivity and rapidity and replaces the more laborious classical methods of analysis. As a result of this, the accuracy of the analysis is increased, especially for industrial products, by which a technological balance is set up. Only the use of this method makes it possible to determine the content of elements in samples of very small weight, in unique samples or in undisintegrated samples, when the use of other methods is impossible; moreover, the list of elements being determined is supplemented.

The advantages of activation analysis in sensitivity and productivity in comparison with chemical methods have permitted two fields of its industrial application to be defined: for determining the content of microquantities of elements of the platinum group and the rare elements in so-called low-grade products [7, 8] and for the bulk analysis of geological specimens and products of the average monthly technological assay on the content of ferrous metals and certain elements of the silicate group. Thus, the

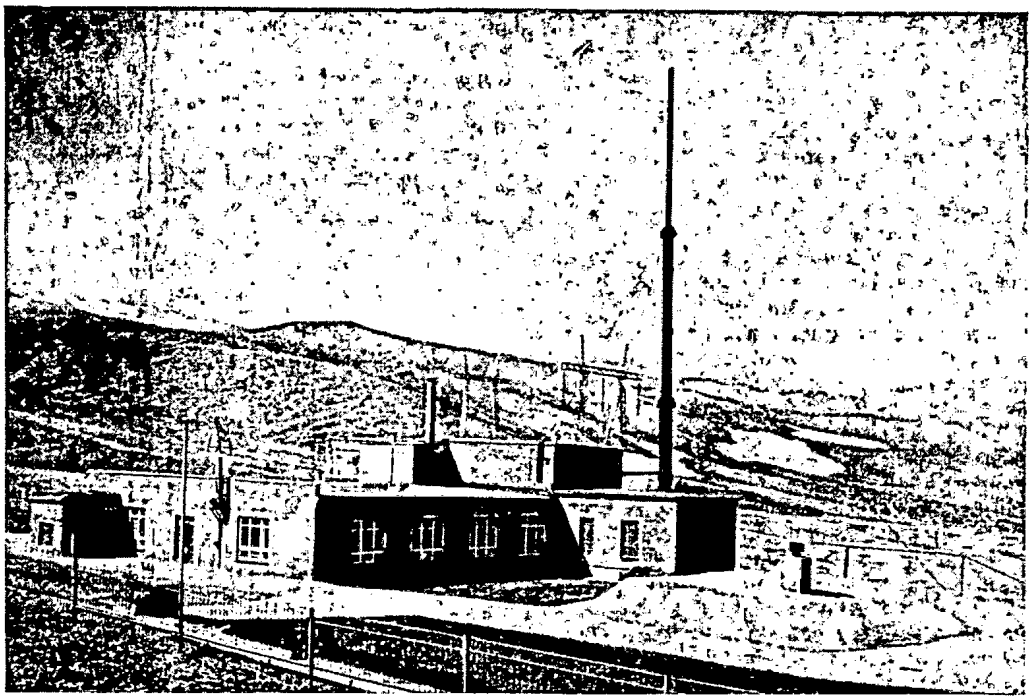

Fig. 2. The RG-1M reactor building of the Noril'sk complex.

TABLE 2. Economical Efficiency of Experiments Carried Out on the RG-1M Nuclear Reactor, Thousands of Rubles

Type of expts.	1970	1971	1972	1973	1974
Radiochemical analyses	2,0	4,8	31,9	33,0	39,0
Instrumental activation analyses	—	2,8	4,5	6,5	18,0
Reduction of sample irradiation cost	—	—	36,0	48,0	67,0
Total	2,0	7,6	72,4	87,5	124,0

introduction of procedures for the radiochemical determination of the Ir, Os, Ru, and Re content has significantly supplemented the capabilities for the analytical service of the complex, and the use of instrumental activation analysis of ores and industrial products for the content of cobalt and aluminum has increased significantly the productivity of the analytical operations, has increased their quality, and has shortened the times.

The determination of the microelemental composition of the environmental contamination, the analysis of dust samples and of certain industrial solutions, the nondestructive analysis of large bulk-samples, etc., illustrate the merits of this method. Problems of determining the degree of contamination of the environment, the effects of copper — nickel production waste on the plant and animal world of Zapolyar'ya at the present time are acquiring particular importance in connection with the increase of the volumes of industrial output. The capabilities of activation analysis are of great importance in these investigations. A series of analyses of the snow cover, selected in the Noril'sk region, carried out by the method of nondestructive multielemental analysis using Ge(Li) detectors with a volume of 60 cm^3 and a resolution of 3 to 4 keV, permitted the content of more than 20 elements to be estimated quantitatively, including Hg, As, Se, Te, Go, Ni, Cu, Fe, Cr, etc.

The instrumental determination of the content of native copper in core samples with a weight of up to 200 g permitted the error, due to the nonrepresentativeness of the balance used in chemical and x-ray spectral methods, and losses of metal on grinding the samples to be reduced.

The use of both versions of the neutron-activation method in analytical practice of the Noril'sk complex is shown by the histogram (see Fig. 1) and at the present time an increase is being restrained only by the shortage of laboratory accommodation. By means of radioactive isotopes, it has become possible to use successfully the two versions of radioisotopic investigations: the introduction of labelled materials into a production process with the subsequent removal of technological samples for measurements under laboratory conditions and radiometric measurements directly on industrial plants.

The first method was used to investigate the depletion process of converter slags and the behavior of the noble metals during the conversion of nickel-containing white matte, when the compounds being studied,

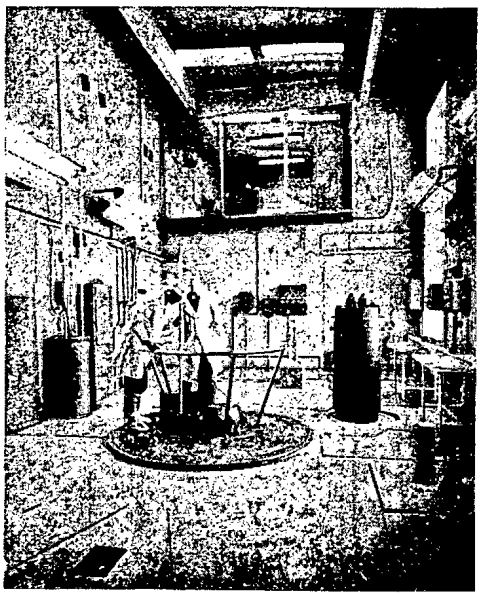

Fig. 3. The reactor hall.

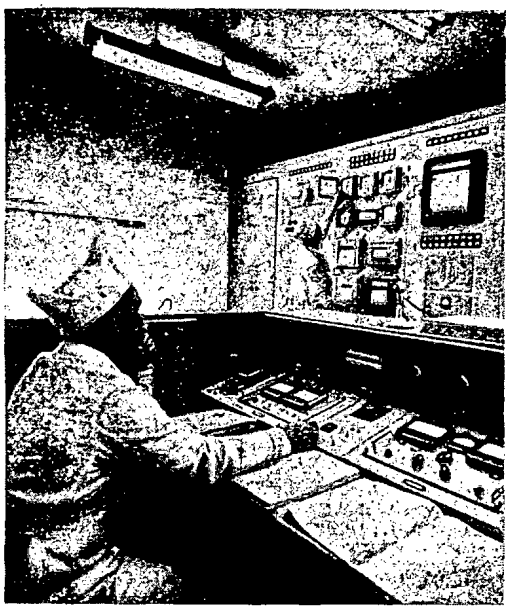

Fig. 4. Reactor control desk.

labelled with short-lived radioactive isotopes of Cu, Co, Ni, Au, Pt, Pd, Os, Se, and other elements, were introduced into materials being processed in the industrial plants. Analysis of selected samples assisted in drawing the appropriate conclusions concerning the distribution of these metals in the metallurgical products [9].

In the second case, direct examination was accomplished without sampling of the calcination of nickelous oxide in rotating tubular furances and recommendations have been made for the optimization of this technological process. Similar investigations are being planned for the future.

The first stage for the introduction into industry of applied methods of nuclear physics and equipment, combined with overcoming difficulties of an organizational-technical and psychological nature, can be assumed to have been completed successfully. In making an attempt to assess the economical efficiency of the all-round utilization of a nuclear reactor (Table 2), it is still not possible to talk about the considerable achievements which, to a known degree, are explained by the insufficiently complete utilization of all its capabilities and the mass use of activation analysis first of all because of the absence of an industrial-experimental basis. The fraction of activation analyses (about 20 thousand elemental-determinations per year) in comparison with the total volume of the annual analytical operations of the complex (more than 2 million element-determinations) amounts to about 1%; even among similar operations carried out by other methods, this contribution still amounts to 5-6%. Clearly, tendencies are seen to increase the quantity and efficiency of the operations carried out by means of a reactor, to approach self-repayment of the annual costs on the content of the laboratory which, according to our forecasts, will be reached in 1976. Over 5 years, more than 36 thousand element-determinations have been carried out. A further increase of the volume of activation analyses by a factor of ten may even give an annual economy of about 0.5 million rubles.

A new stage of development of activation analysis and radioisotpe investigations at the Noril'sk Mining-Metallurgical Complex using the RG-1M nuclear reactor provides for a widening of the circle of industrial materials to be analyzed (including solutions) and an increase of the number of elements to be determined; the mass use of the procedures introduced; the development partially or completely of automated analytical cycles with data processing on a computer and, in the first place, of the multielement instrumental version of analysis; the application of activation analysis for investigating plant samples, animal tissues and other biological items; the carrying out of analyses for ecological investigations; the expansion of radioisotope investigations of technological processes for their optimization and the reduction of the loss of valuable metals, etc. [10].

Five years of industrial operation of the research nuclear reactor at one of the largest-scale mining-metallurgical plants of the country and the experience built up permit a positive conclusion to be drawn concerning the prospects for further extension of operations by means of nuclear-physical methods of investigation in the application to problems of nonferrous metallurgy and of the mining industry, and give a

basis for optimistic conclusions concerning their increasing industrial-practical importance.

LITERATURE CITED

1. B. I. Kolesnikov, in: The State of Technology for the Extraction and Analysis of the Content of Metals of the Platinum Group in the Process for the Concentration of Copper — Nickel Ores [in Russian], Izd. TsNIIinformtsvetmet, Moscow (1967), p. 3.
2. Yu. M. Bulkin et al., At. Énerg., 21, No. 4, 319 (1966).
3. A. S. Shtan', At. Énerg., 33, No. 4, 858 (1972).
4. V. I. Alekseev et al., At. Énerg., 32, No. 4, 315 (1972).
5. A. M. Benevolenskii, V. T. Shentsev, and A. M. Shchetinin, in: Collection of Scientific Proceedings of NVII No. 15. Physicotechnical Issue [in Russian], Izd. Krasnoyarsk Polytechnical Institute, Krasnoyarsk (1973), p. 5.
6. A. M. Shchetinin et al., At. Énerg., 38, No. 2, 97 (1975).
7. V. N. Pavlova et al., Zh. Analit. Khim., 29, No. 11, 2088 (1974).
8. V. P. Razhdaev and V. N. Nikitin, Zh. Analit. Khim., 29, No. 11, 2172 (1974).
9. The Use of Isotopes and Ionizing Radiations in the National Economy of the Urals. Data for Reports at the 3rd Zonal Conference on the Use of Isotopes in the National Economy of the Urals (Thesis of Reports) [in Russian], Sverdlovsk (1973).
10. V. N. Nikitin, in: The 9th All-Union Conference on the Chemistry, Analysis, and Technology of the Noble Metals (Thesis of Reports) [in Russian], Krasnoyarsk (1973), p. 183.

TESTING OF EXPERIMENTAL BN-600-TYPE FUEL ELEMENTS IN THE BOR-60 REACTOR UP TO DIFFERENT BURNUPS

M. M. Antipina, Yu. K. Bibilashvili,
I. S. Golovnin, V. M. Gryazev,
E. F. Dyvydov, G. V. Kalashnik,
A. V. Medvedev, T. S. Men'shikova,
V. S. Mukhin, A. A. Petukhov,
A. V. Sukhikh, V. N. Syuzev,
L. I. Sytov, and V. L. Timchenko

UDC 621.039.542.342:621.039.548

Tests in the BOR-60 of experimental fuel elements — prototype fuel elements for high-capacity power reactors — complete the work on the creation of a fuel-element design. These tests and post-irradiation investigations permit the operating qualities of the design to be analyzed, the assumed design and technological solutions to be refined or confirmed, and also the route for further optimization of the fuel element to be designated.

In this present paper, the generalized results are given of an investigation of three experimental bundles, with fuel elements based on oxide fuel, which were irradiated in the BOR-60 reactor to burnups of 4.3, 8, and 10.3% of heavy atoms.

The principal structural and thermal parameters of the fuel elements did not differ from the working parameters of the BN-600 fuel elements. However, the neutron fluence for the claddings of the experimental fuel elements are lower than is required for the BN-600 fuel elements ($\sim 7.5 \cdot 10^{22}$ instead of $\sim 3.5 \cdot 10^{23}$ n/cm^2). This difference is quite significant and must be taken into account in the analysis of the results of the tests. All the experimental fuel elements achieved the stated burnup without damage to the completeness of the cladding and loss of hermiticity.

The results of the post-radiation investigations permitted the degree and nature of the chemical interaction of the cladding and the fuel with the fission fragments to be estimated, the magnitude of the deformation stored up after the run as a result of the mechanical action of the fuel core and swelling of the steel, and it permitted the gas release from the fuel to be measured and the structural changes in the core to be determined.

Structure and Manufacturing Technology of the Fuel Elements. In the principal structural characteristics (diameter and thickness of the cladding, pitch of positioning in the bundle, effective fuel density and density of the sintered pellets, the cladding-fuel gap), the experimental fuel elements irradiated in the BOR-60 reactor are similar to the regular fuel elements of the BN-600 reactor [1].

The structure of the experimental fuel element is shown in Fig. 1. The outside diameter of the cladding, of OKH16N15M3B steel from electroslag remelting, is 6.9 mm and the wall thickness is 0.4 mm. In the single cladding are located the active section and the upper and lower reflectors. The length of the core of the active section, in the form of sintered sleeved pellets of 90% enriched uranium dioxide, is 500 mm. The density of the pellets is 10-10.6 g/cm^3. The nominal value of the effective fuel density in the fuel element is 8.25 g/cm^3. The upper and lower reflectors, with a length of 50 m, are made from depleted uranium dioxide with a density of not less than 10 g/cm^3 and directly touch the core of the active section.

Translated from Atomnaya Énergiya, Vol. 40, No. 1, pp. 16-27, January, 1976. Original article submitted April 28, 1975.

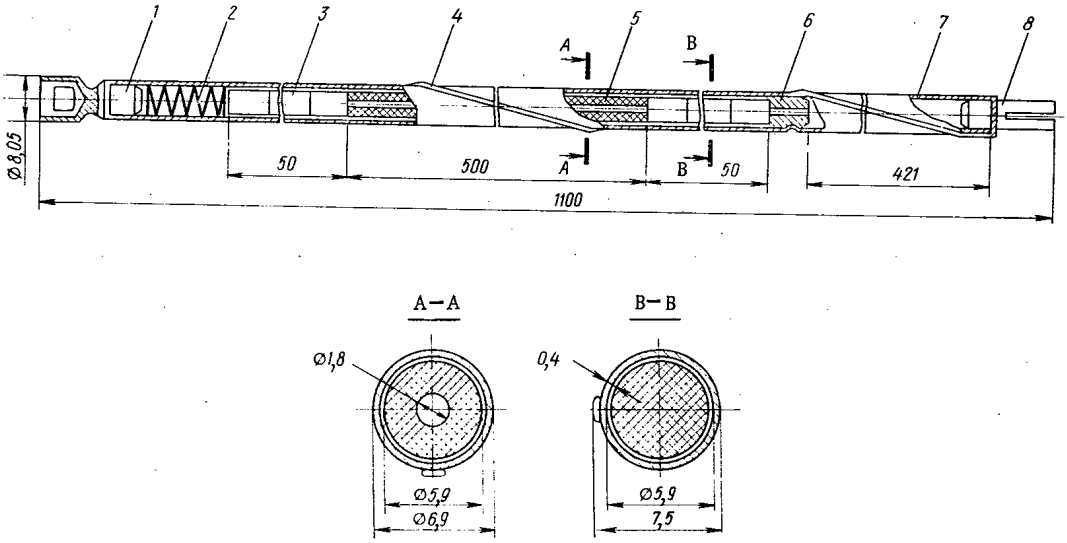

Fig. 1. Structure of an experimental fuel element of the BN-600 reactor: 1) upper cap; 2) spring; 3) reflector; 4) spacer band; 5) active section of fuel element; 6) sleeve; 7) fuel element cladding; 8) lower cap.

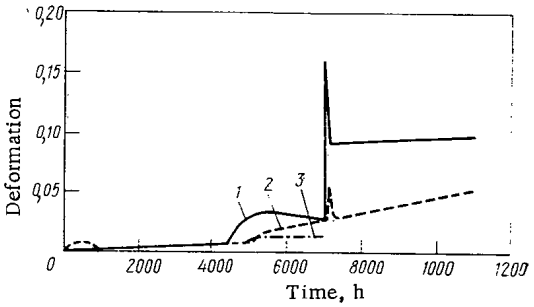

Fig. 2. Nature of change of mechanical deformation over the run in the average cross section of the fuel element (375 mm from the lower end of the cap) on the time of operation at nominal power when γ_0 = 10.3 g/cm^3: 1, 2, 3) fuel elements of Type I and II (see [2]) zones of high enrichment and zone of low enrichment, respectively.

The pellets are prepared by a cold pressing method, using a rotary automatic press, and with subsequent sintering at a temperature of 1650°C during 3 h in metal heater furnaces. Before loading the pellets in the fuel element cladding, chemical, x-ray and metallographic analysis was carried out in order to determine the content of uranium, oxygen and other admixtures. The characteristics of the pellets are as follows: the content of fluorine, carbon and other admixtures to a total of < 0.02; ≤ 0.02 and ≤ 0.7 mass %, respectively; the oxygen coefficient is 2.00 to 2.02; outside and inside diameter are 5.9 and 1.8 mm.

In the lower section of the fuel element there is a compensation space, intended for reducing the pressure of the fission gases beneath the fuel element cladding. The compensation space and the core of the fuel element are separated by a steel sleeve, which is secured at the required height by necking at three points. The ratio between the size of the compensation space and the amount of fuel is chosen so that at the end of the test run, the pressure of the fission gases in the experimental fuel elements was approximately 20% higher than in the regular fuel elements of the BN-600 reactor. The fuel elements are hermetically sealed by means of plugs. The lower plug was welded to the cladding by an argon-arc weld, and the upper by an helium-arc weld in a chamber filled with helium. This hermetic sealing technology ensured that the fuel element was filled with helium of purity not less than 95%.

Spacing of the fuel elements in a bundle was achieved by means of a wire with a diameter of 1.05 mm, wound on the cladding of the inner fuel elements of the bundle and a tape of elliptical cross section 1.3 × 0.6 mm for the near-wall fuel elements. The use of the tape allowed the surrounding temperature nonuniformity at the cladding of the near-wall fuel elements to be reduced from 70-80 to 40-45°C. The wire and the tape were secured by a contact weld to the ends of the cladding and by an argon-arc to the cap of the fuel element.

An assembly of 19 fuel elements was loaded into a hexahedral tube of Kh18N10T steel with a gauge "below key" of 38 mm and with a wall thickness of 0.8 mm. The fuel elements in the bundle were secured by welding the lower caps to the grid, but the upper caps remained unsecured.

Radiation Tests of the Experimental Bundles. Comparison of the Test Conditions of the Experimental Fuel Elements with the Operating Conditions of the Regular BN-600 Fuel Elements. The principal

TABLE 1. Comparative Parameters of the Experimental and Regular BN-600 Fuel Elements

Parameters	Regular fuel elements	Expt. fuel elements
Diam. and wall thickness of cladding, mm	6.9; 0.4	6.9; 0.4
Type of fuel	UO_2; content of carbon ≤ 0.02 mass %. Oxygen coefficient 2.01 ± 0.01	
Isotopic enrichment for ^{235}U:	21 and 33%	90%
Density of pellets of active part of fuel element, g/cm^3	10.0-10.6	10.0-10.6
Effective density of fuel along active part of fuel element, g/cm^3	8.25	8.25
Max. thermal loading per unit length of fuel element, W/cm	490-530	404, 490, and 490 for bundles B-159, B-164 and B-165
Ma. temp. at inside surface of cladding, °C	680-710*	650, 720, and 720 for bundles B-159, B-164, and B-165
Max. fuel burnup, % heavy atoms	7 and 10 for the zones of low and high enrichment	4.3, 8.03, and 10.3 for bundles B-159, B-164, and B-165
Max. neutron flux density, n/(cm^2 · sec)	$1 \cdot 10^{16}$	$3 \cdot 10^{15}$
Neutron fluence of all energies at end of run, n/cm^2	$(3-4) \cdot 10^{23}$	$2.75 \cdot 10^{22}$, $5.5 \cdot 10^{22}$, and $7.3 \cdot 10^{22}$ for bundles B-159, B-164, and B-165
Pressure of fission gases at end of run, kg/cm^2	40†	55
Max. sodium flow rate in bundle, m/sec	up to 8	8

*The temperature is shown, taking into account superheating factor.
†For 100% escape of fission gases from the fuel.

TABLE 2. Variation of Relative Coolant Flow Rate through Bundle B-165

Control meas.	Burnup, % heavy atoms	Hel. coolant flow rate
12.X.71	4,3	1,00
9.X.72	8,0	0,965
24.XI.72	8,2	0,935
27.III.73	10,3	0,91

irradiation parameters of the fuel elements in the reactor are shown in Table 1. In the controlled measurements during irradiation, no deviations from the nominal values of the coolant flow through the B-159 and B-164 bundle were observed; the bundles were discharged from the reactor after attaining burnups in the fuel elements of 4.3 and 8% of heavy atoms, respectively. For the B-165 bundle, whose fuel elements achieved burnups of 10.3% of heavy atoms, some reduction of flow rate was observed (Table 2).

During reactor shutdown, the bundles were regularly checked for leak-tightness. No breakdown of hermiticity of the fuel elements was detected. After reactor shutdown, the bundles remained in the active zone in the sodium medium during 25-30 days, after which the residual heat release amounted to 0.3 to 0.4 kW. The bundles then were stored in a water pond. Estimates showed that in this case the temperature of the central fuel element and the sheath of the bundle did not exceed 550 and 300°C, respectively.

The main difference between the conditions of testing of the experimental and regular fuel elements of the BN-600 reactor is because of the use in the experimental fuel elements of highly enriched nuclear fuel. On reaching a burnup of 10% the neutron fluence for the cladding of the experimental elements was $7.3 \cdot 10^{22}$ n/cm^2; for the regular fuel elements with this same burnup, at the end of the run it should amount to $3-4 \cdot 10^{23}$ n/cm^2. In this case, the fraction of fast neutrons with energies greater than 0.1 MeV, which cause the principal defects in the fuel elements, should be taken into account. For the BN-600

TABLE 3. Yield of Fission Gases from Fuel

Bundle	Calc. quantity of fission gases, formed as a result of the fission of nucl., $N \cdot cm^3$	Vol. of gases escaping below fuel-element cladding, $N \cdot cm^3$	Av. % yield of fission gases from fuel	Fission-gas pressure in element at end of irradiation, kg/cm^2
B-159	110	50—73	65	17
B-164	208	158—174	80	39
B-165	268	232—251	90	55

reactor, this fraction amounts to ~0.6; and for the fifth row of the BOR-60, where the experimental bundles were irradiated, it is 0.8.

There is still one important special feature in the functioning of the BN-600 regular fuel elements. During the run, in the zone of high enrichment interchange of the bundles was provided from a region with low heat release [2], for the purpose of improving the physical and economic characteristics of the reactor.

With nominal power output of the reactor, in the claddings of fuel elements transposed into a region with higher heat release, additional stresses are created, due to the different thermal expansion of the fuel and the cladding. These stresses might be the cause of the additional plastic deformation, the magnitude of which depends on the rate of rise of power of the fuel element. With increase of the rate the deformation increases. Limit calculations (for instantaneous power output) show that the plastic deformation may reach 0.1% (Fig. 2).

It should be noted that interchange of the bundles into a zone of high enrichment of the BN-600 reactor was simulated partially by overloading the power of the BOR-60 reactor.

Examination and Treatment of the Irradiated Bundles. After testing the bundles were found to be in a satisfactory state without visible defects. The sheath of bundle B-165 had a small buckling along the active zone. The maximum sag amounted to ~8 mm. The sheaths of all bundles were removed from the fuel element pencil without difficulty.

No defects were observed in the fuel elements of all assemblies. The peripheral fuel elements had buckling along the active section, oriented from the center of the bundle. Buckling of the fuel elements of all bundles is approximately identical and amounts to ~20 mm for a freely laid fuel element. The fuel elements of the inner rows maintained their rectilinearity.

Yield of Fission Gases from the Fuel. The quantity of fission gases escaping below the fuel element cladding was measured with an accuracy of ± 0.5 $N \cdot cm^3$ (Table 3). The fuel elements of all bundles were leak-tight.

Deformation of Fuel Element Claddings. Estimate of the Contribution of Radiation Swelling of Steel. The dimensions of the hexahedral sheaths of all fuel assemblies were measured with a micrometer at six points along the active section. The measurements showed that the gauge "below key" remained within tolerance limits and amounted to 37.77-37.93 mm.

The diameter of the fuel element claddings (after cleaning the surface with a 10% solution of nitric acid) was measured with an accuracy of ± 0.01 mm. The diameter of the fuel elements of assembly B-159

TABLE 4. Diameter of Fuel Element Claddings of Assembly B-164

No. of fuel element	Fuel-element diam. over height of active section, at a distance from the lower end of the core, mm								Magnitude of maximum residual deformation $(d-d_0)/d_0$, %
	compensation space, d_0	100	200	250	300	350	400	500	
31	6,92	6,92	6,92	6,92	6,93	—	6,92	6,92	0,1
40	6,86	6,93	6,92	—	6,94	6,91	6,91	6,90	1,1
36	6,92	6,93	6,96	6,96	6,97	6,99	6,93	6,88	0,9
62	6,92	6,91	6,97	6,97	6,93	6,93	6,90	6,92	0,7
65	6,91	6,92	6,96	6,94	6,92	6,91	6,90	6,90	0,7
32	6,88	6,92	6,92	6,92	6,90	6,89	—	—	0.6
33	6,90	6,87	6,89	—	6,96	6,89	6,96	—	0,9
35	6,89	6,89	6,89	—	6,92	—	6,88	6,91	0.4
37	6,89	6,91	6,95	6,97	6,97	6,99	6,95	—	1.4
43	6,88	6,88	6,90	—	6,92	—	6,91	—	0,5
42	6,89	6,89	6,90	—	6,94	7,00	6,92	—	1.6
41	6,87	6,88	6,92	—	6,93	—	6,89	—	0,9
39	6,86	6,89	6,94	6,92	—	—	—	—	0.9
34	6,89	6,88	6,89	6,89	6,91	—	—	—	0,4
63	6,86	6,88	6,95	6,88	6,89	—	6,89	6,90	1,4
66	6,86	6,90	6,91	—	6,94	6,88	6,89	—	1,2
68	6,87	6,89	6,91	—	6,98	6,88	6,89	—	1,6
67	6,87	6,87	6,92	—	6,90	—	6,87	6,86	0,4

TABLE 5. Diameter of the Fuel Element Claddings of Assembly B-165

No. of fuel element	Fuel-element diam. over height of active section, at a distance from the lower end of the core, mm								Magnitude of maximum residual deformation $(d-d_0)/d_0$, %
	compensation space, d_0	80	130	180	230	280	330	380	
1	6,90	6,92	6,93	6,98	6,93	6,93	6,90	—	1,1
4	6,92	6,93	6,96	6,98	7,00	6,97	7,00	6,95	1,1
7	6,91	6,92	6,97	6,94	6,98	6,99	6,96	—	1,1
13	6,90	6,93	6,99	7,02	6,99	6,91	6,92	6,92	1,7
17	6,91	6,92	6,97	7,03	6,96	6,95	6,94	6,92	1,7
19	6,90	6,92	6,97	7,02	6,97	6,88	6,91	6,91	1,7
No number	6,91	6,92	6,91	6,91	6,95	6,97	6,90	6,90	0,9
Ditto	6,93	6,92	6,94	7,02	6,99	6,93	6,91	6,92	1,3
»	6,92	6,92	6,95	7,00	6,99	6,96	6,92	—	1.1

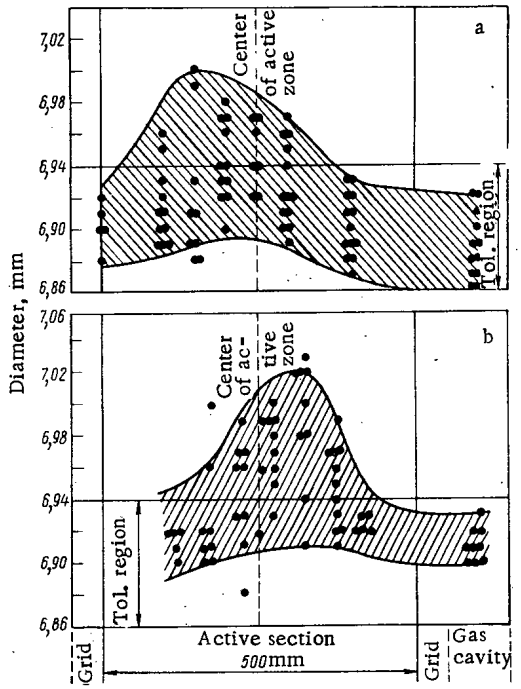

Fig. 3. Deformation of cladding over height of fuel elements for a burnup of (a) 8 and (b) 10.3% of heavy atoms.

did not fall outside the tolerance limits at the shell tubes and amounted to 6.89-6.93 mm. The results of the measurements of the fuel element diameters of assemblies B-164 and B-165 are shown in Tables 4 and 5 and in Fig. 3.

A significant scatter is observed from fuel element to fuel element in the magnitude of the deformation built up, especially in assembly B-164. The maximum residual deformation is 1.6 and 1.7% for the fuel elements of assemblies B-164 and B-165. For the fuel elements with 8% burnup of heavy atoms, the deformation of the cladding lay within the limits of 0.1 to 0.5% (elements No. 31, 35, 42, 34, 67) up to 0.9 to 1.6% (element Nos. 40, 36, 33, 37, 42, 41, 39, 63, 66, 68), and for fuel elements with 10% burnup, within the limits of 0.9 to 1.7%.

For assembly B-165, electron-microscopic investigations were carried out on the section of the fuel-element cladding with maximum increase of diameter (Fig. 4). It was established that the maximum swelling of the cladding material was found to be at a distance of 200-250 mm from the bottom of the active zone of the element and amounted to 4%.

The scatter in the porosity values for different sections of the sample being examined did not exceed 35%. The data obtained on swelling show that a "power" deformation, built up by the cladding as a result of mechanical action of the core, amounts to 0.3 to 0.4%. It should be noted that the calculations give approximately the same ratio between the deformations built up as a result of swelling, and radiation creep of steel (Fig. 5).

Over the entire height of the active section of the fuel element, a three-zoned structure was observed in the core cross section: a zone of columnar crystals, a zone of equiaxial grains, and a zone with the original structure. The dependence of the deformation built up in the cladding during the run on the thickness of the zone with the original structure (Fig. 6) shows that deformation of the cladding increases sharply after reducing the thickness of the zone by 0.2 mm or less. This, obviously, can be explained by an increase of the fraction of "power" deformation built up in the cladding due to radiation creep as a result of the effect of the swollen core. In this case, the hydrostatic component of radiation creep should affect the deformation to a greater degree. The dimensions of the zone with the original structure depend significantly on the initial assembly gap between the fuel pellets and the cladding. It is extremely desirable, therefore, to reduce also the deviations of this parameter.

The characteristic structure of the cladding at sections with no interaction with fission fragments is shown in Fig. 7. In the lower sections, where the temperature did not exceed 400°C, the original structure of the steel was preserved (see Fig. 7c). In individual cases, with increase of the total neutron dose,

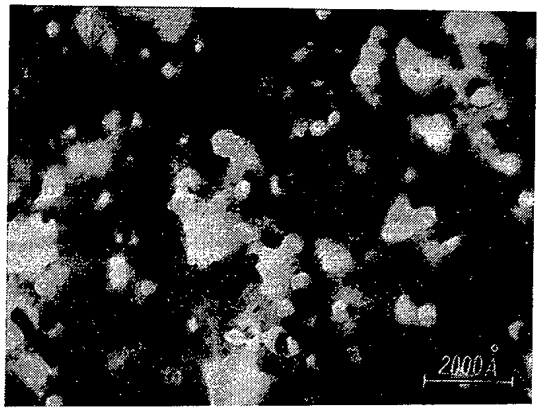

Fig. 4. Porosity in the cladding material at the section with maximum increase of diameter.

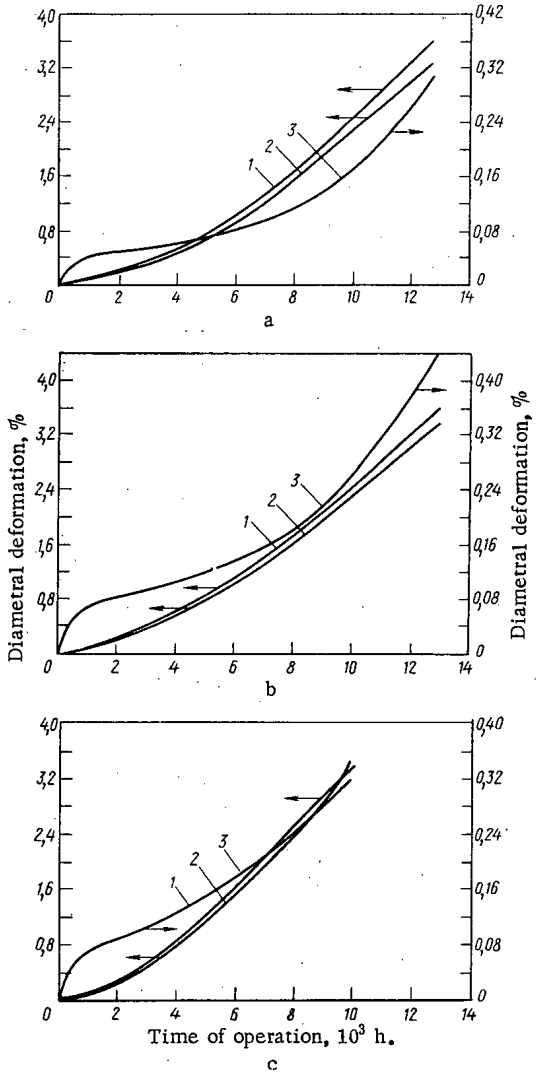

Fig. 5. Calculated deformation of BN-600 reactor fuel elements (center of active zone): a, b) fuel elements of Type I and II of zone of high enrichment for γ_{eff} = 78% of theoretical, and 11.5% burnup of heavy atoms; c) low-enrichment fuel elements for γ_{eff} = 78% of theoretical and 8.5% burnup of heavy atoms, 1) total deformation, 2, 3) deformation from swelling of steel and as a result of radiation and thermal creep, respectively.

some increase of corrosion of the inside surface of the cladding is noted. No changes of microhardness were observed over the thickness of the cladding, but with burnup its value increases from 270 to 370 kg/mm^2 (for β = 4 and 10% heavy atoms respectively). In the central sections, with temperatures of 550°C and somewhat higher, increased corrosion is observed of the grain boundaries on the inside surface of the cladding (see Fig. 7b). The microhardness, just as in the lower sections, increases with increase of burnup from 300 to 340 kg/mm^2. In individual cases, with small burnups, an increase of microhardness is noted up to 460 kg/mm^2 on the inside layer of the cladding. In the upper sections of the fuel elements, where the temperature is a maximum, the structure is characterized by sharp boundaries of the grains. The microhardness of the fuel element cladding of assembly B-159 was equal to 200 kg/mm^2 and was

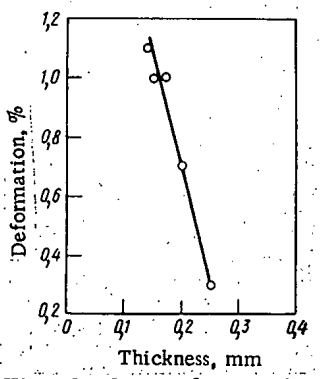

Fig. 6. Dependence of change of deformation of fuel element cladding on the thickness of the zone with original structure: q_l = 470–485; T_{cl} = 550°C; burnup 10.3% of heavy atoms.

unchanged over the thickness of the wall. In the fuel elements of assemblies B-164 and B-165 the microhardness of the cladding increased up to 270 kg/mm^2. On sections of interaction, a reduction of the microhardness to 200 kg/mm^2 and an increase up to 290 kg/mm^2 was observed.

Interaction of Fission Fragments with the Fuel and the Cladding. During the investigation of the regular and experimental fuel elements, in individual cases (Table 6), interaction of fission products with the cladding and the fuel was observed, mostly localized in the hottest sections of the cladding. The thickness of the interaction layer depends on many factors, in particular on the temperature and the burnup (Table 7, Figs. 8 and 9). The initial stage of interaction is characterized by increased etchability of the grain boundaries on the inside surface of the cladding (Fig. 10) at a temperature of 500°C.

With increase of temperature, two types of interaction are noted; intercrystallite corrosion with chipping of the individual grains of steel (Fig. 11) and the formation of layers of chemical interaction products (Fig. 12). The maximum depth of interaction reaches 110 μ (burnup 10.3% of heavy atoms, temperature 700°C). In individual fuel elements, scaling of the cladding material was observed on sections extending to approximately two thirds of the perimeter of the circumference and to 12-15 mm along the height of the fuel element (Figs. 13 and 14).

The effect of UO_2 stochiometry on the degree of interaction was investigated on regular BOR-60 fuel elements (Fig. 15). It can be seen that the oxygen coefficient has significantly affected the depth of interaction, which in the second case reached 40–50 μ. The presence of carbon in the fuel (in fuel elements of the BN-600 type, not more than 0.02 mass %, and in regular BOR-60 fuel elements approximately 0.02 to 0.05 mass %) favors the interaction process. Carbon, being an oxygen carrier, leads to a change of stochiometry along the radius of the fuel pellet. As a result, at the fuel-cladding interface it increases

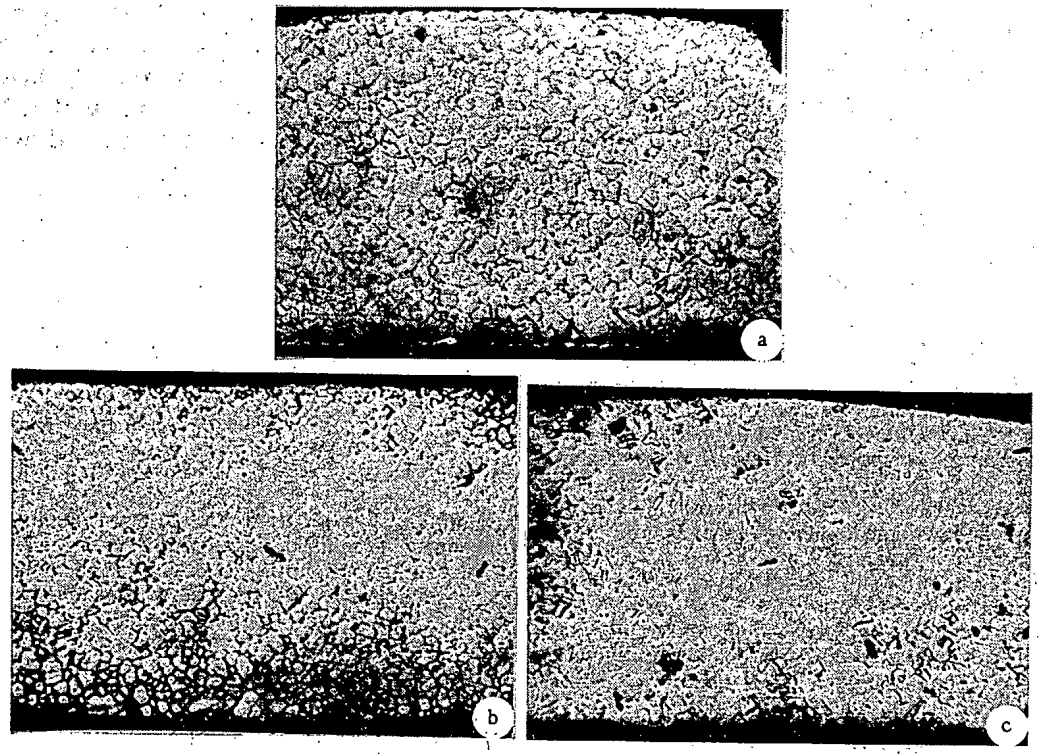

Fig. 7. Microstructure of cladding over height of fuel element. Burnup 10.3% of heavy atoms (×200): a, b, c) upper, central, and lower parts of active section.

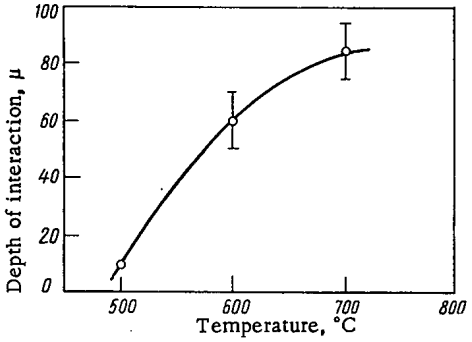

Fig. 8

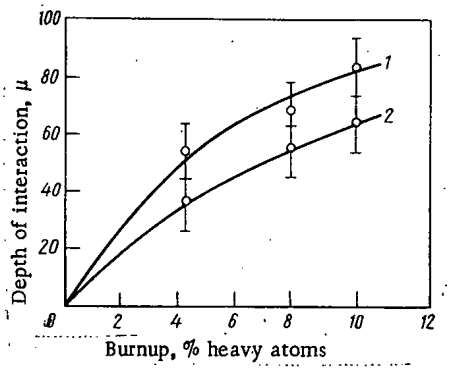

Fig. 9

Fig. 8. Dependence of thickness of interaction layer on temperature, for 10.3% burnup of heavy atoms.

Fig. 9. Change of depth of interaction layer in the fuel element cladding, with increase of burnup at (1) 700 and (2) 600°C.

TABLE 6. Interaction of Fission Fragments with Fuel and Cladding

Fuel elements	No. of fuel elements investigated	No. of fuel elements in which interaction is observed	Achieved burnup, % heavy atoms
Regular BOR-60 fuel elements	8	1	2,3
Prototype BN-600 fuel elements	4,3	4	4,3
Regular	12	3	5,6
Regular Prototype	10	4	8
Regular Prototype	12	7	10

and without such a high oxygen potential that it promotes interaction of the fission fragments with the fuel and the cladding. In our opinion, the content of carbon in the UO_2 pellets should be less than 0.01 mass %.

Fuel elements, in which corrosion interaction was detected, were investigated also by the γ-spectrometry method in order to determine the nature of the principal fission product distribution over the height and radius of the fuel element. As a result of the investigations, it was ascertained that the fission products dissolved in the UO_2 (zirconium, cerium) are uniformly distributed over the diametral cross

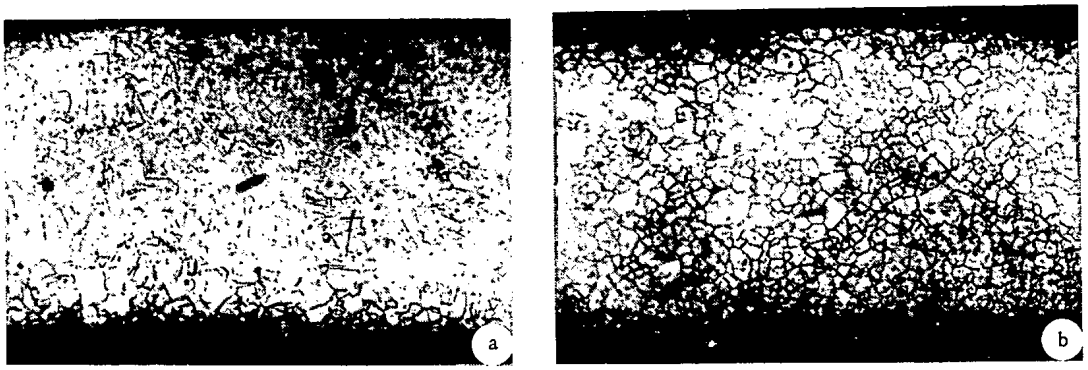

Fig. 10. Microstructure of cladding, characteristic for the initial stage of interaction: increased etchability of grain boundaries on the inside surface of the cladding for T = 500 (a) and 600 (b) °C (×200).

TABLE 7. Nature of Interaction in Investigations of the Type BN-600 Fuel Elements

Temp., °C	Burnup, %heavy atoms		
	4,3	8	10,3
500	No interaction	No interaction	Increased etchability of grain boundaries, without change of microhardness
600	Increased etchability of grain boundaries, without change of microhardness	Local intercryst. corrosion at a depth to 50 μ, no change of microhardness	Intercryst. corrosion over entire perim. of cladding, depth to 60 μ, decrease of microhardness
700	Local intercryst. corrosion at depth to 50 μ with increase of microhardness in the zone of interaction	Intercryst. corrosion over entire perim. of cladding, at depth to 70 μ, no change of microhardness	Formation of interaction layers and intercryst. corrosion over entire perim. of cladding at depth to 100 μ, decrease of microhardness

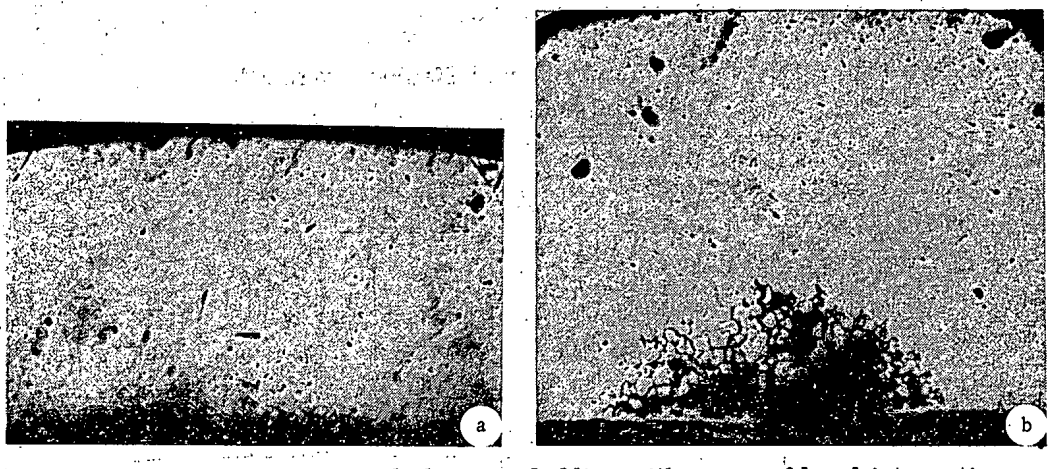

Fig. 11. Microstructure of fuel element cladding with zones of local interaction, for a burnup of 2.3 (a) and 8 (b) % of heavy atoms.

section of the fuel elements. The volatile elements (cesium and antimony) are concentrated predominantly at the fuel — cladding interface (Figs. 16 and 17). Migration of these elements is significant also along the length of the fuel elements (Fig. 18).

Figure 19 shows the results of measurements of the distribution of the two radioactive elements ^{54}Mn and ^{58}Co over the radius of the fuel element. These isotopes are the products of the nuclear reactions $^{54}Fe(np)^{54}Mn$ and $^{58}Ni(np)^{58}Co$. The $^{54}Mn/^{58}Co$ ratio in different sections, measured through a cylindrical collimator with an aperture diameter of 0.25 mm, varies from 2.5 (for the cladding) to 9 (for the start of the zone of columnar grains), which shows the selective migration of the components of the cladding into the core of the fuel element.

Corrosion interaction between the oxide fuel and the cladding is one of the factors limiting the

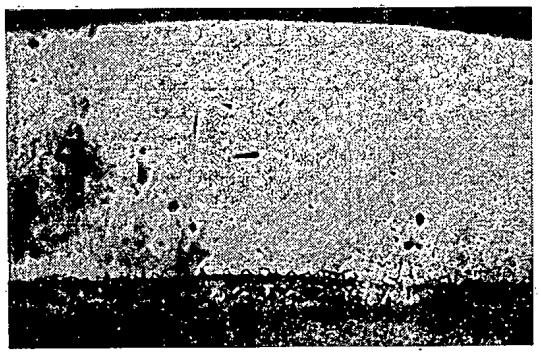

Fig. 12. Microstructure of cladding of a regular BOR-60 fuel element with a section of the interaction layer.

Fig. 13. Section of interaction in the upper part of a fuel element of the BN-600 type (×100).

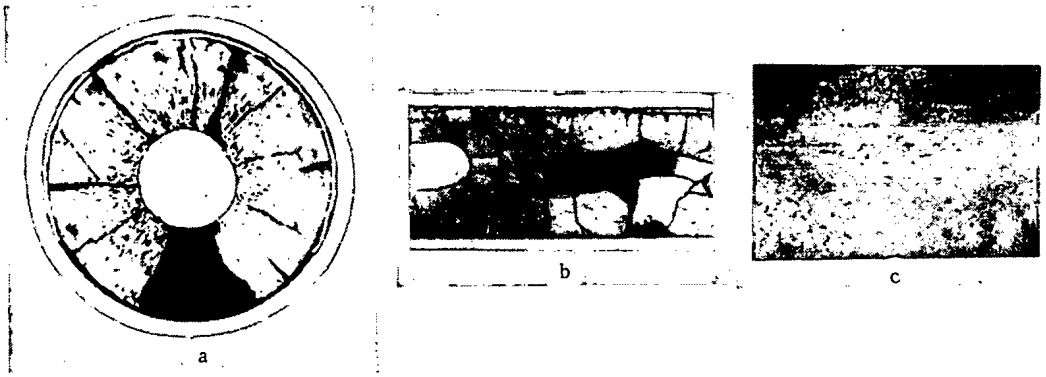

Fig. 14. Nature of interaction of cladding with fission fragments (upper part of fuel element): a) chipping of part of cladding to approximately two-thirds of the perimeter (×13); b) chipping of cladding, longitudinal microsection ~12 mm (×6); c) section of interaction (×200).

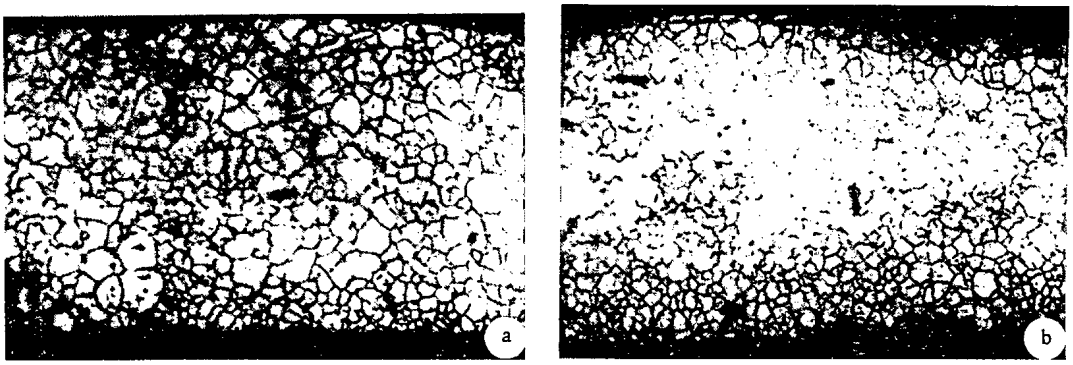

Fig. 15. Microstructure of fuel element cladding with UO_2 of different composition, irradiated up to a burnup of 10% of heavy atoms. Oxygen coefficient: a) 2.01 ± 0.01 (no interactions); b) 2.02 ± 0.01 (interaction with chipping of grains).

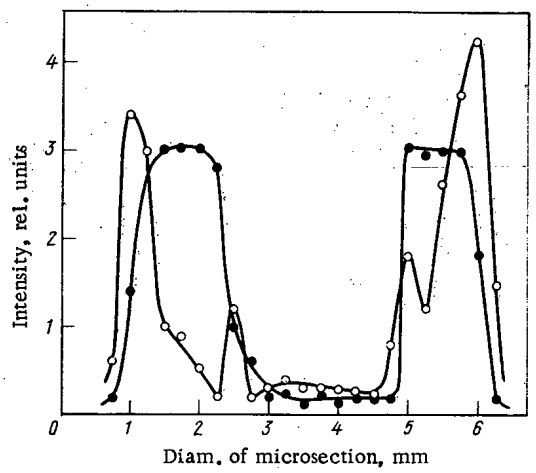

Fig. 16

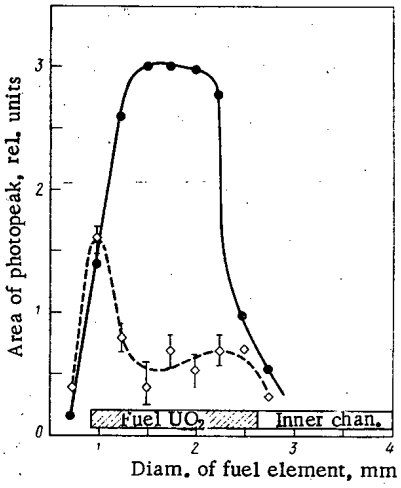

Fig. 17

Fig. 16. Distribution of ^{137}Cs (○) and ^{95}Zr (●) over the diameter of the fuel element with UO_2 (sleeve core with diameter of original channel 1.8 mm): T_{sur} = ~900°C; T_{cen} = ~1900°C; upper section.

Fig. 17. Distribution of ^{125}Sb (◇) and ^{95}Zr (●) along the radius of the fuel element: T_s = ~ 900°C; T_c = ~1900°C; upper section.

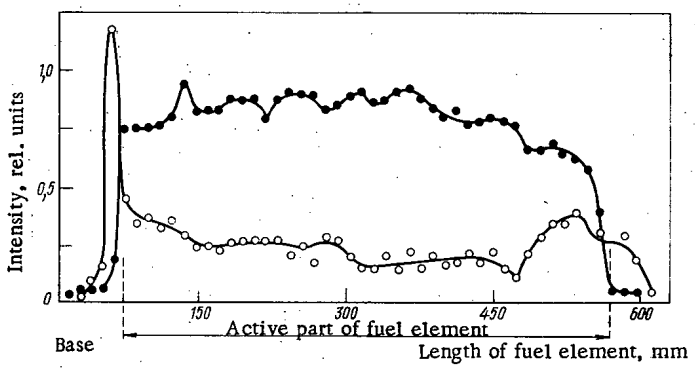

Fig. 18. Distribution of ^{95}Zr (●) and ^{137}Cs (○) along the height of the fuel element, for a burnup of 10.3% of heavy elements.

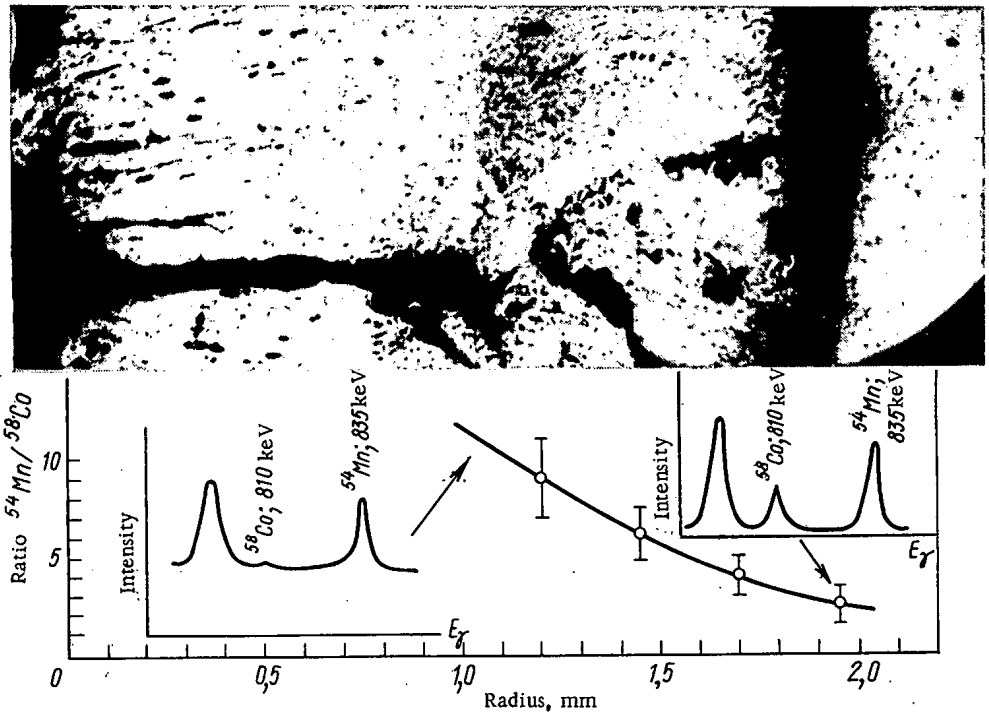

Fig. 19. Change of concentration of components of steel along the radius of the fuel element.

efficiency of fuel elements for fast reactors. The mechanism of the corrosion interaction of fission products with the fuel and the cladding has not yet been studied. The factors which determine the type of interaction have not been established. However, the experience built up during the testing of fuel elements with UO_2 in the BOR-60 reactor shows that corrosion prevents the achievement of burnups of 10-11% of heavy atoms with a cladding thickness of 0.3 to 0.4 mm and a temperature of 700°C.

In order to achieve deeper burnups or an increase of pressure of the fission gases (in excess of 50-60 kg/cm^2), it will be necessary to search for a means of limiting or totally eliminating this corrosion interaction which, other conditions being equal, is manifested particularly in the case of the use of uranium — plutonium oxide fuel [2].

LITERATURE CITED

1. I. S. Golovnin, Yu. K. Bibilashvili, and T. S. Men'shikova, At. Énerg. 34, No. 3, 147 (1973).
2. I. S. Golovnin et al., IAEA Symposium on Fuel and Fuel Elements for Fast Reactors, July 2-6, 1973 [in Russian], Report No. SM-173/69.

PREDICTING THE EFFICIENCY (SERVICEABILITY) OF OXIDE FUEL ELEMENTS FOR FAST SODIUM REACTORS

I. S. Golovnin and Yu. I. Likhachev

UDC 54:621.039.52.034.6

Fundamental Parameters Determining the Efficiency of Oxide Fuel Elements for Fast Sodium Reactors

The economic indices and exploitational (service) reliability of the oxide fuel elements used for fast sodium reactors determine the following main constructional parameters [1, 2]: 1) the diameter and thickness of the can wall; 2) the effective density of the fuel; 3) the working temperatures of the can; 4) the specific energy evolution; 5) the depth of fuel burn-up.

The optimum fuel-element can diameter is determined by two conditions: a) that the specific energy evolution should be no less than the economically viable value for the particular installation, allowing for the cost of the whole fuel cycle (such estimates may be based on published data [3-5]; in the case of a reactor with oxide fuel the minimum energy evolution is 250 W/g [6]); b) that the maximum linear power of the fuel element should be limited (in order to avoid the melting of the fuel) over the whole campaign, with due allowance for the initial compaction of the central regions of the core and the reduction in the melting point of the fuel which occurs as fission fragments accumulate.

The thickness of the fuel-element can wall is chosen in such a way as to ensure that the thermal stresses shall not exceed the elastic limit of the steel. In this case the influence of low-cycle fatigue (associated with the transient operating conditions of the installation) and stress relaxation on the strength characteristics of the steel [2] is eliminated. Allowance is made for the fact that an increase in the diameter of the fuel elements increases the internal conversion ratio and lowers the cost of production. The choice of fuel-element can dimensions [2] is illustrated in Fig. 1.

The effective density of the fuel situated in the active volume of the fuel element determines the working temperature of the core and also the useful extent to which the fuel element may be charged with fuel and breeding material [3, 7]. As a result of this, the effective density is related to the specific energy evolution in the fuel element, the temperature conditions of the can, and the depth of fuel burn-up. In

TABLE 1. Comparative Characteristics of the Fuel Elements of Certain Reactors

Parameters	Reactors						
				Rhapsodie			
	BOR -60	BN -350	BN -600	first charging	improved charging	Phenix	PFR
Diam. and thick. of can wall, mm	6,0×0,3	6,1×0,35	6,9×0,4	6,7×0,45	5,1×0,4	6,55×0,45	5,84×0,38
Effective density of fuel, % of theor. density	73,5±9	73,5±9	77,0±8	88—94	85—94	80—85	80
Max. linear power, W/cm	550	430	490—520	390	430	430	480

Translated from Atomnaya Énergiya, Vol. 40, No. 1, pp. 27-37, January, 1976. Original article submitted May 4, 1975.

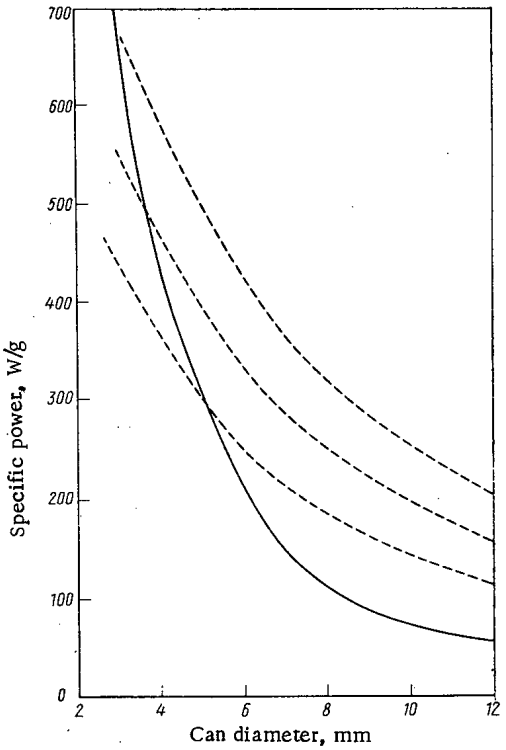

Fig. 1. Choice of optimum values of the fuel-element can diameter and thickness in fast oxide-fuel reactors having an effective density equal to 80% of theoretical: – – – –) loads for which the thermal stresses in the cans are equal to the elastic limit of the OKh16N15M3B steel composing them for wall thicknesses of 0.3, 0.4, and 0.5 mm respectively; ——) loads leading to the melting of the core center (for a constant heat evolution over the whole campaign).

constructing fuel elements we should choose a comparatively low effective density of the fuel in combination with as high a specific energy evolution as possible, this latter being limited by the temperature at the center of the core (Table 1 gives the comparative characteristics of the fuel elements of several reactors [1, 3], [7-13]); this enables us to use fuel elements with relatively high core surface temperatures and reduces the mechanical load on the cans [1, 3, 7]. We may make use of existing experimental data regarding the swelling of an oxide core surrounded by a retaining can (the mean volume increment is approximately 1% for 1% burn-up of the heavy atoms, Fig. 2) [14] and the dependence of the volumetric swelling on the actual initial density of the core material (Fig. 3) [15]; we must also allow for the 150-200°C fall in the melting point of the fuel after fragments have accumulated to the extent of ~100 kg/ton of fuel [16].

In practice the swelling of the core is reduced and the diametral deformation of the fuel element restrained in the following ways: 1) by using tablets with an optimum initial density; 2) by choosing the optimum assembly gap between the can and the core; 3) by maintaining sufficient purity of the helium filling the working space of the fuel element during the initial period of irradiation.

Under these conditions there is a high contact thermal conductivity at the core/can interface at the onset of fuel-element operation, which ensures the maintenance of the original structure in the outer layer of the fuel and reduces the diametral deformation [8], as indicated in Fig. 4. Figures 5 and 6 present some experimental data regarding the influence of the initial relative gap, the medium in the fuel element, and the linear power on the contact thermal conductivity. The influence of the initial density of the tablets on the calculated reserve of strength in the BN-600 fuel-element cans [2] is illustrated in Fig. 7.

Thus, a reduction in the tolerances imposed upon the main design characteristics is a very real way of increasing

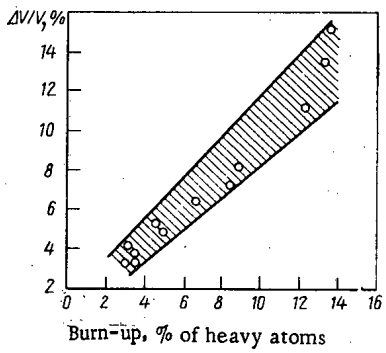

Fig. 2

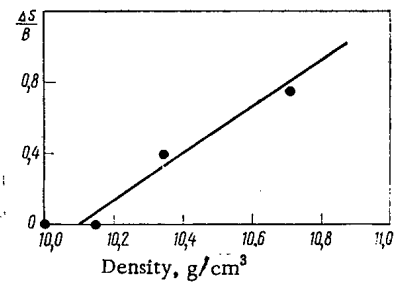

Fig. 3

Fig. 2. Swelling of the oxide fuel in cylindrical fuel elements in relation to burn-up.

Fig. 3. Specific swelling of UO_2 tablets ($\Delta S/B$) as a function of the original density for a linear loading of 250-410 W/cm in the fuel element and a burn-up of 4.2-6.1% of the heavy atoms. $\Delta S/B$ is the ratio of the increment in the cross-sectional area of the core (%) to the burn-up (%).

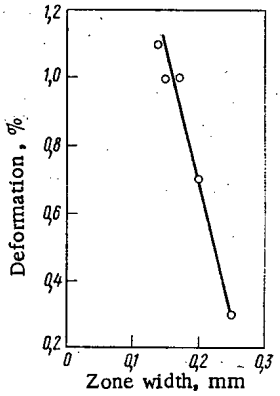

Fig. 4

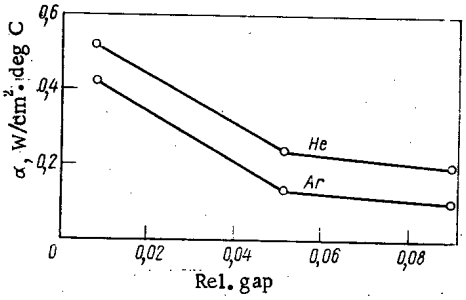

Fig. 5

Fig. 4. Deformation of the fuel-element cans as a function of the width of the zone maintaining the original structure of the UO_2 core for ql = 470-485; B = 10.3% of the heavy atoms; T_{irr} = 550°C.

Fig. 5. Influence of the initial relative diametral gap and the medium inside the fuel element on the contact thermal conductivity α.

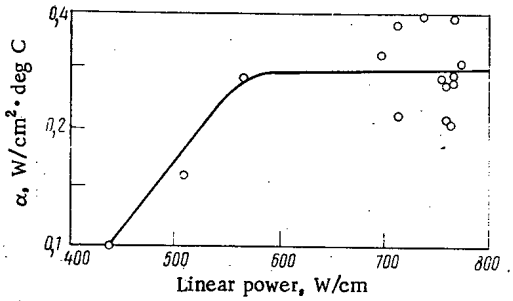

Fig. 6. Influence of the linear power on the contact thermal conductivity for a relative gap of 0.0523.

the service reliability and economic efficiency of the fuel elements.

A considerable influence on the serviceability of the fuel-element cans is exerted by fragment-induced damage of the inner surface which occurs in the presence of oxide fuel at a high oxidizing potential. Investigations revealed that the interaction was of an intercrystallite character, involving the formation of a layer of corrosion products as the process developed. The fragment interaction appears at a temperature of 500°C and experiences a tendency toward saturation as the corrosion layer advances (Figs. 8 and 9) [8]. In these experiments the depth of interaction was no greater than 110 μ (burn-up 10.3% of the heavy atoms,

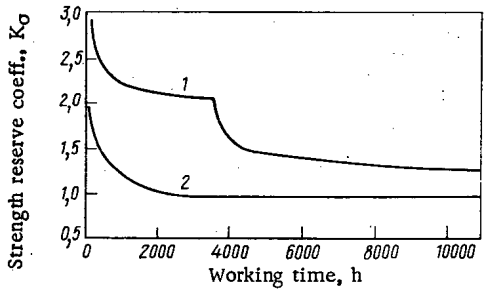

Fig. 7

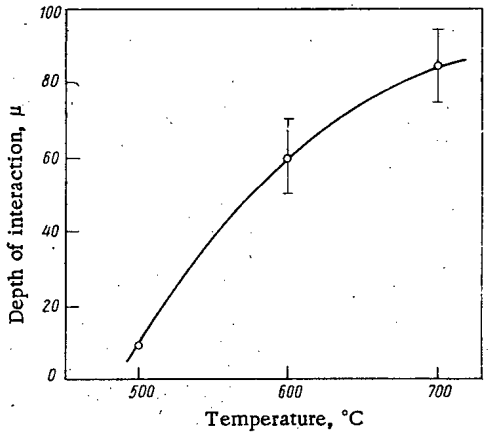

Fig. 8

Fig. 7. Influence of the original density of the tablets on the reserve of strength in the BN-600 fuel-element cans: 1, 2) tablet density 95 and 98-100% of theoretical respectively (the time to rupture of the steel is reduced by 100 times).

Fig. 8. Influence of temperature on the depth of fragment interaction at the point of contact of the ÖKh16N15M3B steel can with the UO_2 core for a burn-up of 10.3% of the heavy atoms.

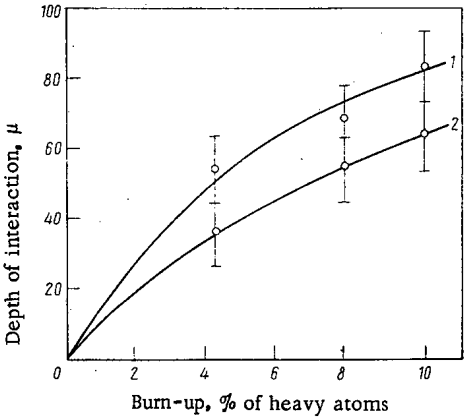

Fig. 9

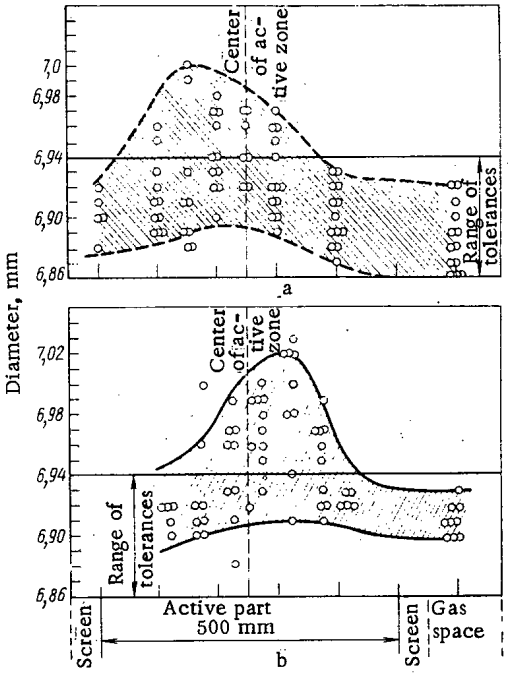

Fig. 10

Fig. 9. Influence of burn-up on the depth of fragment interaction at the point of contact between the OKh16N15M3B steel can and the UO_2 fuel: 1) 700; 2) 600°C.

Fig. 10. Change in the diametral deformation along a BN-600 fuel element on irradiation in a BOR-60 reactor to a burn-up of: a) 8%; b) 10.3% of the heavy atoms. The statistical spread of the deformations is obtained by measuring the fuel elements of one pack.

temperature 700°C). Local fission-fragment interaction appears in roughly 40% of the fuel elements tested. Thus an increase in the purity of the core material (carbon and moisture content, etc.), exact maintenance of the specified stoichiometric composition, and measures to ensure reproducibility of the fuel properties may substantially reduce or even eliminate corrosion.

On the whole the picture of the processes developing in the oxide fuel element during its service life are fairly complicated. In view of the considerable fall in temperature along the fuel-element can, and also the thermal and radiation-induced softening of the fuel and construction materials, this picture differs at different points along the fuel elements and also varies in time. As an illustration we may consider the distribution of the diametral deformation of the fuel elements along the length of the latter (Figs. 10 [8] and 11 [2]). The contribution to the total deformation arising from radiation-induced swelling in the range 400-500°C may be very considerable, as indicated in Fig. 12 [8]. An experimental investigation into the basic processes taking place in oxide fuel elements during service led to the following [1]:

1. The oxide fuel in sodium-cooled fast reactors with a burn-up of over 3% of the heavy atoms and a linear fuel-element power of over 400 W/cm is almost entirely (more than 80%) free from gaseous fragments.

2. Under transient conditions the oxide core of the fuel element is subject to crack formation, with subsequent healing in the steady state (on the evaporation-condensation principle), if the linear power of the fuel elements of real dimensions exceeds 350 W/cm. This same mechanism leads to a fall in the original gap under transient conditions.

3. The recrystallization of the core is accompanied by the formation of a central aperture (or the enlargement of an existing one). As burn-up advances in any particular cross section of the fuel element there is either a reduction in the central aperture or else deformation of the can, as determined by the holding capacity of the latter.

4. The swelling of the fuel together with gas pressure imposes mechanical loading upon the can. This loading is created by the outer layers of the core if their temperature is lower than 930-950°C. At

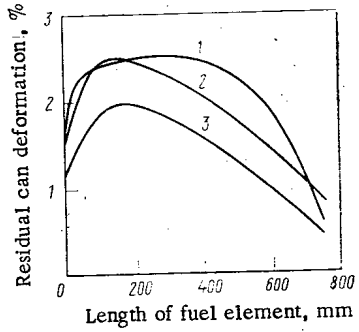

Fig. 11

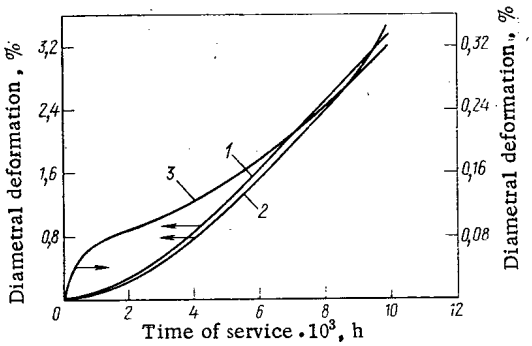

Fig. 12

Fig. 11. Calculated change in the diametral deformation of the fuel elements of the BN-600 reactor at the end of the campaign: 1, 2) Outer and intermediate rows of packs in the active zone respectively; 3) packs in the inner part of the active zone.

Fig. 12. Calculated dependence of the diametral deformation of a fuel element of the BN-600 reactor on the period of irradiation required to burn up 8.5% of the heavy atoms (original effective density of the fuel 78% of the theoretical density): 1) total deformation; 2, 3) deformation due to the radiation-induced swelling of the steel and thermal creep accelerated by irradiation, respectively.

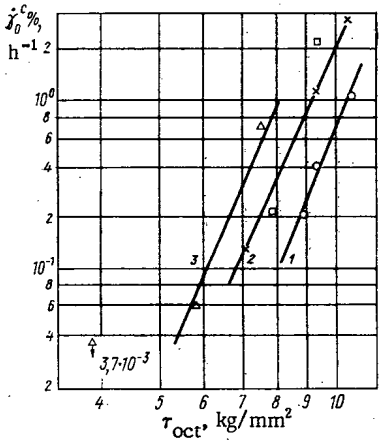

Fig. 13. Octahedral rate of creep-induced shear deformation as a function of the octahedral tangential stress for various plane-stressed states $K = \sigma_1/\sigma_3$; $\psi = \sigma/\sigma_i$: □) $K = \infty$, $\psi = 0.333$; ○) $K = -1$; $\psi = 0$; △) $K = -1.5$; $\psi = 0.076$; ×) $K = -3.3$; $\psi = 0.295$.

higher temperatures of the outer layer the ceramic fuel is softened and deforms in the direction of the axis of the fuel element. The volumetric swelling of the oxide core is ~1% for 1% burn-up of the heavy atoms, the contribution of "solid" swelling not exceeding 0.4 vol. %. The existence of initial porosity in the strong outer layer of the core partly counteracts the mechanical loading.

5. The radiation-induced swelling and creep of the can material have a great influence on the mechanical loading.

6. The corrosion damage to the can arising from fission fragments may be taken into account by introducing a correction when calculating the can thickness. Dynamic models of the phenomena have been constructed to act as a basis for the analytical prediction of the service reliability of fuel elements subject to burn-ups of no less than 10% of the heavy atoms and a neutron flux of ~10^{23} neutrons/cm^2.

Basic Calculations of the Efficiency (Serviceability) of the Fuel Elements

In order to determine the efficiency of hermetic cylindrical fuel elements of various constructions under specified conditions we use two models for the combined operation of the fuel and the can [17].

Gas Model. Between the fuel and the can we envisage a gap filled with gas or liquid metal (such as sodium) in the working temperature range. In this case the following effects may occur in the fuel-element can: 1) stresses due to the pressure of the coolant and gaseous fission fragments proceeding from the fuel into the compensation space; 2) stresses due to inhomogeneous, time-varying thermal fields (steady and transient operation of the reactor); 3) stresses due to the radiation-induced swelling of the steel, nonuniformly distributed over the circumference and thickness of the can.

In fast power reactors the pressure of the liquid metal coolant is low (up to 10 atm) and has little effect on the efficiency of the fuel element. For a high pressure of the coolant (for example, in gas-cooled or water-cooled reactors), there is a danger of the loss of stability by the fuel-element can, and the

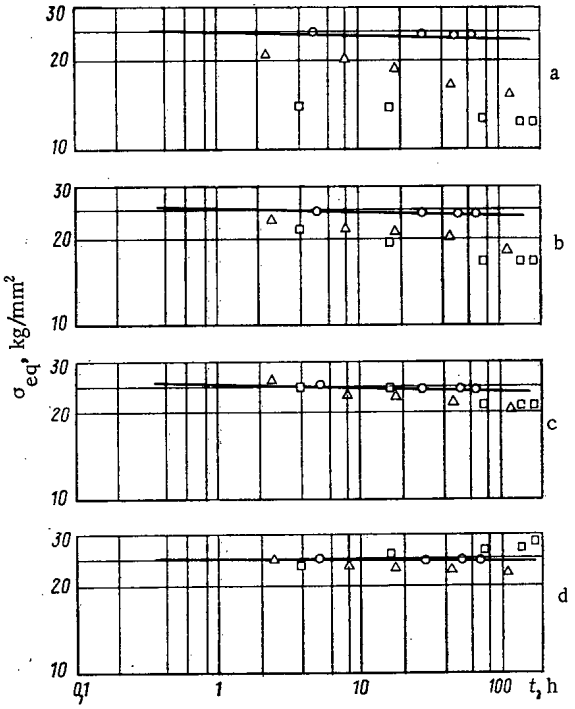

Fig. 14

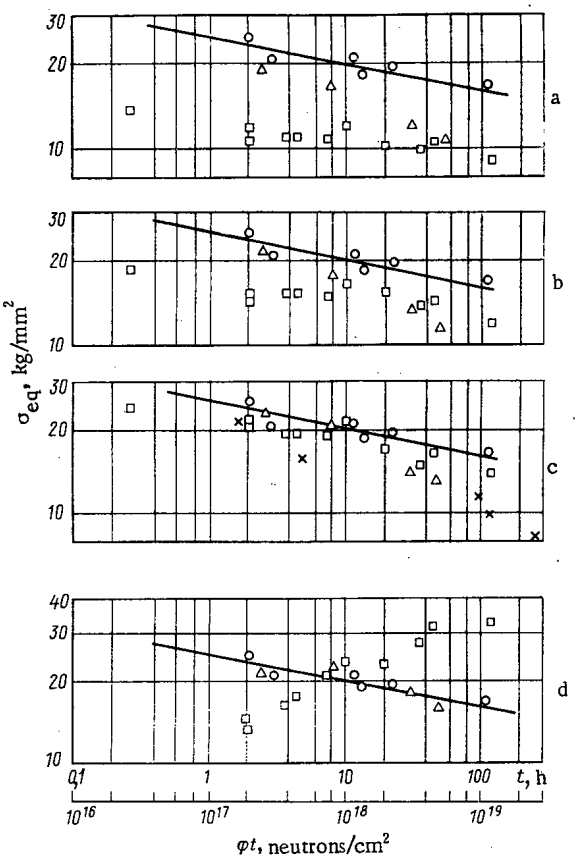

Fig. 15

Fig. 14. Results of long-term (creep) strength tests on nonirradiated Kh16N15M3B steel tubes in plane-stressed states, expressed in terms of various equivalent stresses: a) $\sigma_{eq} = \sigma$; b) $\sigma_{eq} = (\sigma_1+\sigma_i)/2$; c) $\sigma_{eq} = \sigma_i$, $\sigma_i = \sqrt{\sigma_1^2 - \sigma_1 \cdot \sigma_3 + \sigma_3^2}$; d) $\sigma_{eq} = \chi\sigma_i + (1 - \chi)\sigma_1 \cdot A^{1-I}$: ○, □, △) $\sigma_1/\sigma_3 = \infty$; −1; −3.3 respectively.

Fig. 15. Results of reactor tests on the long-term (creep) strength of Kh16N15M3B steel tubes (notation as in Fig. 14; × — — 1.5).

following must be taken into account: 1) the initial ellipticity of the can; 2) the effect of nonuniform swelling of the can material; 3) the possibility of a collapse of the compensation volume, with the formation of a longitudinal corrugation in those parts in which the can rests on the fuel core; 4) the possibility of an irreversible elongation of the can during the reactor cooling periods (axial "ratchet" effect) [17, 20].

Contact Model. Here we assume that from a certain instant of time the can and the fuel core are in contact with one another, and thus in addition to the loads already mentioned the can has to withstand the pressure of the swelling fuel. The time required for the gap to vanish between the core and the can is determined by the mass-transfer process, with the formation of three structural zones and a cavity in the center of the fuel tablet.

During the reactor cooling periods the UO_2 or $(UPu)O_2$ oxide fuel, which is characterized by high radial temperature gradients, cracks, and for this reason fails to draw the can behind it, even if the fuel and can have become diffusion-welded during the steady operation of the reactor. It may be considered that when the power of the reactor is subsequently restored the same compressive stresses as before develop in the fuel.

On using carbide or metallic fuel (which do not crack during the reactor cooling periods), either unilateral or reversing plastic deformations may take place in the can if this is firmly connected to the core. In this case we may find that the efficiency of the fuel element is determined by the low-cycle fatigue of the can material. This should be taken into account when designing the system by matching the thermal expansions of the fuel and can.

In order to determine the kinetic characteristics of the changes taking place in the stressed and strained state of a fuel-element can subject to nonisothermal loading (both in the steady state, and especially

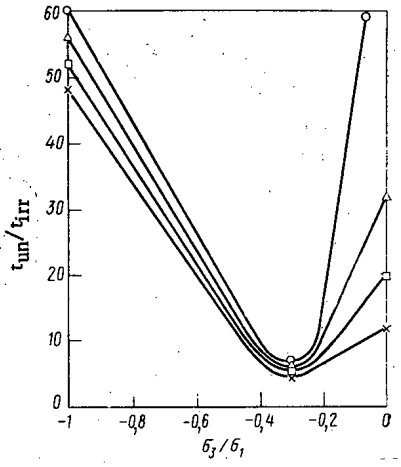

Fig. 16.

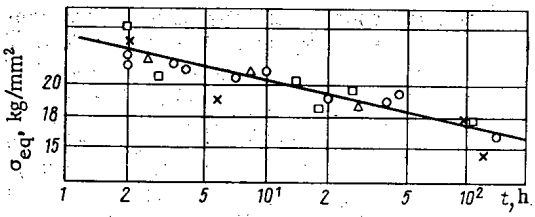

Fig. 17.

Fig. 16. Effect of the form of the stressed state on the relative time to failure for prolonged reactor tests on Kh16N15M3B steel tubes with various values of σ_i, kg/mm^2: ○) 22.7; △) 23; □) 23.3; ×) 23.5.

Fig. 17. Results of reactor tests on the long-term strength of Kh16N15M3B steel tubes for various forms of stress, expressed in terms of the V. N. Kiselevskii criterion (notation as in Fig. 14; ×) −1.5).

under transient reactor operating conditions) with due allowance for the "instantaneous" plastic and viscous deformations, the method of variable elasticity parameters is commonly employed [17-19].

In theories relating to the creep and plastic yield of an irradiated solid, the following assumptions are usually made: 1) volume changes are elastic; 2) the stress deviator is proportional to the deviator of the increments in plastic and viscous (including creep) deformations; 3) the relationship between the stress intensity and the plastic and creep-deformation velocity intensities is invariant relative to the form of the stressed state. We assume the existence of a surface of plastic yield in the irradiated solid:

$$f(\sigma_i,\ T,\ \varepsilon_i^p,\ H^p) = 0, \tag{1}$$

where $\sigma_i = \sqrt{3/2 S_{ij}S_{ij}}$ is the stress intensity ($S_{ij} = \sigma_{ij} - \delta_{ij}\sigma$); T is the temperature; $\varepsilon_i^p = \int d\varepsilon_i^p$ is the accumulated plastic deformation (Odqvist parameter) in which $d\varepsilon_i^p = \sqrt{2/3 d\varepsilon_{ij}^p d\varepsilon_{ij}^p}$; H^p is a parameter defining the influence of irradiation on the plastic-deformation process. In the simplest case H^p is equal to the integrated neutron flux for an energy exceeding a certain threshold value E_0. Equation (1) may be derived from a set of tensile curves plotted at various temperatures after carrying out short-term tests on samples irradiated up to specific levels of radiation damage at working temperatures.

The influence of irradiation on the creep-deformation process is taken into account by adding a radiation-creep component to the thermal creep

$$\underset{Q}{\xi_i^c} = \xi_{iT}^c + \xi_{iH}^c, \tag{2}$$

where $\xi_{iT}^c = A(t)e^{-(Q/RT)}\sigma_i^n$ is the intensity of the thermal creep velocity; $\xi_{iH}^c = B(t)\bar{E}\varphi\sigma_i$ is the intensity of the radiation creep velocity; R is the gas constant; A(t) is a function of time; B(T) is a weak function of temperature; $\bar{E}$ is the mean neutron energy; φ is the total flux density of neutrons with an energy $E > 0$; Q is the activation energy.

We note that the foregoing hypotheses, which have been reliably confirmed for nonirradiated materials (tests on thin-walled tubes), have never been verified experimentally under irradiation conditions.

By applying torsion and tensile tests to tubular samples made from Kh16N15M3B austenitic steel in the SM-2 reactor at 650°C, with fast and thermal neutron fluxes of $3.7 \cdot 10^{14}$ and $3.3 \cdot 10^4$ neutrons/(cm^2 · sec), respectively, it was shown in [21] that the function $\dot{\gamma}_0^c = f(\tau_0)$ depended on the form of stressed state (Fig. 13). Here $\dot{\gamma}_0^c = 2\xi_i^c$ and $\tau_0 = \sqrt{2/3} \cdot \sigma_i$ are the octahedral rate of shear strain (deformation) due to creep and the octahedral tangential stress, respectively. Due allowance for the observed nonconservative change in volume associated with creep [22] may bring curve 2 closer to curve 1, but curve 3 will hardly change its position at all. This very fact emphasizes the importance of further development in the study

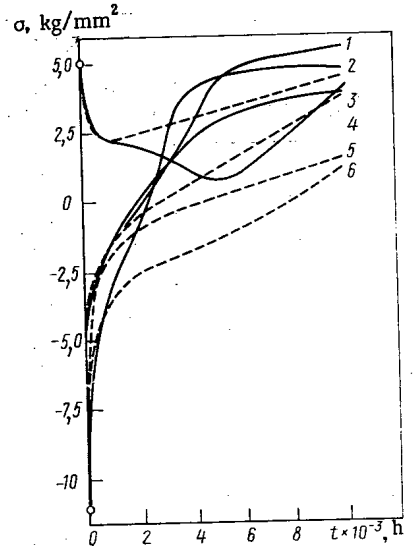

Fig. 18

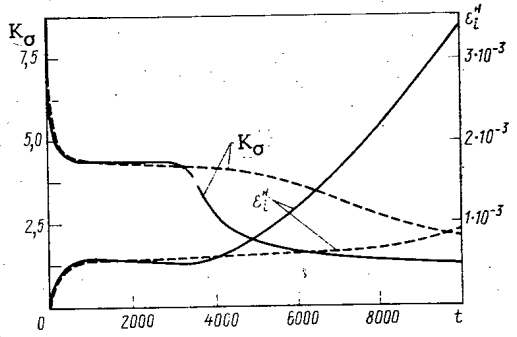

Fig. 19

Fig. 18. Time dependence of the axial and circumferential stresses in the "hot" section of the can belonging to a fuel element close to the wall of a fast power reactor: 1, 2, 5, 6) $\sigma_z Z = 0.5$; -0.5; 0.5; -0.5; 3, 4) $\sigma_0 Z = 0.5$; -0.5 respectively; broken lines, without allowing for swelling; continuous lines, after allowing for the swelling of the steel.

Fig. 19. Time dependence of the long-term strength reserve coefficient and the accumulated inelastic deformation in the "hot" section of the can belonging to a fuel element close to the wall (see Fig. 18).

of deformation laws under reactor conditions in the plane-stressed state.

On using the method of variable elastic parameters the problem reduces to the consideration of an anisotropic elastic solid with variable elastic parameters and additional deformations. The process of loading the can is divided (in time) into a series of brief stages, and for each stage the increments in the stress and strain components are determined, making use of the equations of equilibrium and deformation compatibility, the boundary conditions, and the physical relationships:

$$\Delta\varepsilon_x = \langle c_{11}\rangle \Delta\sigma_x + \langle c_{12}\rangle \Delta\sigma_y + \quad \ldots + \langle\varphi_{xT}\rangle \Delta T + \langle\varphi_{xH}\rangle \Delta H^p + \langle\varphi_{xc}\rangle \Delta t + 1/3\Delta S, \tag{3}$$

where the elasticity parameters take the form $c_{11} = (1/E) + (3F_\sigma/2\sigma_i)(\sigma_x - \sigma)^2$; $c_{12} = -(\mu/E) + (3F_\sigma/2\sigma_i)(\sigma_x - \sigma)(\sigma_y - \sigma)$, while the functions of the additional deformations may be expressed as follows:

$$\varphi_{xT} = \frac{d(\alpha T)}{dT} - \frac{1}{E^2}[\sigma_x - \mu(\sigma_y + \sigma_z)]\frac{dE}{dT} - \frac{1}{E}(\sigma_y + \sigma_z)\frac{d\mu}{dT} + F_T(\sigma_x - \sigma);\ \varphi_{xH} = F_H(\sigma_x - \sigma);\quad \varphi_{xc} = F_c(\sigma_x - \sigma).$$

The plasticity functions for active loading take the form

$$F_\sigma = \frac{3}{2\sigma_i}\left(\frac{1}{E_\kappa} - \frac{1}{E}\right);$$

$$F_T = \frac{3}{2\sigma_i}\left(\beta + \frac{1}{E^2}\frac{dE}{dT}\sigma_i\right);$$

$$F_H = \frac{3}{2\sigma_i}\gamma,$$

while for unloading and neutral loading $F_\sigma = F_T = F_H = 0$.

The coefficients $1/E_K = \partial\varepsilon_0/\partial\sigma_0$; $\beta = \partial\varepsilon_0/\partial T$ and $\gamma = \partial\varepsilon_0/\partial H$ may easily be found if we are able to deduce the relationship $\varepsilon_0 = \varepsilon_0(\sigma_0, T, H^p)$ from a set of tensile-test curves plotted at various T and H^p; ε_0 and σ_0 are the deformation and stress associated with uniaxial extension, and the creep function $F_c = (3/2)(\xi_i^c/\sigma_i)$. The increment in the swelling of the can material ΔS is found from certain well-known empirical relationships of the form [23]:

$$S = A(T)(\Phi)^{\lambda(T)}, \tag{4}$$

where $\Phi = \int \varphi dt$ is the integrated neutron flux with $E > 0.1$ MeV (or the number of displacements per

atom). Of the several problems associated with steel swelling which largely determine the validity of any prediction of fuel-element serviceability, and therefore require special consideration, we may mention the following: 1) extrapolation of the swelling to large integrated fast-neutron fluxes, approaching $3 \cdot 10^{23}$ neutrons/cm^2 (with E > 0.1 MeV), and possible swelling saturation effects; 2) the influence of cold deformation and stresses; 3) the influence of transient reactor operating conditions, such as a sudden change in the irradiation temperature or the neutron flux intensity. For each stage of loading the systems of equations characterizing an anisotropic elastic solid are solved, and the increments in the stress components are determined, using the values assumed by the latter at the end of the previous stage; the elastic parameters are refined by the method of successive approximations [17].

The nonuniformity of the temperature around the perimeter of the can in the central fuel elements of the fuel assembly is usually very slight ($T_{max} - T_{min} < 15°C$ [24, 25]), and for the fuel elements under consideration the problem may be regarded as axisymmetrical. The can is assumed to be thin-walled, and the deformation of the fuel element is regarded as plane, since the axial gradients of the temperature and neutron fields are usually slight, and individual cross sections of the fuel element may be considered independently.

For the gas model we accordingly have to execute the numerical solution of a system consisting of the physical relationships, the condition of equilibrium, and the deformation-compatibility condition of the can only. For the contact model the system is further supplemented by the physical relationships, equilibrium equation, and deformation-compatibility equation of the fuel, as well as the matching conditions (for the oxide fuel three structural zones are taken into account).

The nonuniformity of the temperature distribution around the perimeter is especially substantial for the fuel elements close to the wall and in the corners. The circumferential nonuniformity of the temperature fields of the fuel element has been considered in a large number of theoretical and experimental investigations (the experiments being executed on models of fuel-element assemblies) [23-25]. We may note that the nonuniform temperature distribution around the perimeter has a considerable influence on the serviceability of the fuel element for large doses of fast neutrons, since a nonuniform swelling of the steel around the perimeter under conditions of restricted deformation of the fuel elements (resulting from small gaps) creates additional stresses in the can.

The warping of the fuel element within the limits of dimensional tolerance is usually many times smaller than the free warping of the can due to the circumferential nonuniformity in the temperature and swelling of the steel; we may therefore regard the can axis as straight and consider individual cross sections of the fuel element separately. For the fuel-element can we use the physical relationships and equilibrium and deformation — compatibility relationships derived from the moment theory of a thin anisotropic cylindrical shell [26]. For the contact model we also allow for the physical relationships and equilibrium and deformation — compatibility relationships associated with the fuel itself, as well as the matching conditions, the fuel being regarded as having been deformed symmetrically. The temperature functions are represented by Fourier series, so that simple algorithms may be obtained for the numerical solution of the systems of equations [17, 27].

Knowing the kinetic characteristics of the stress/strained state of the fuel element during the operation of the reactor, we may estimate the serviceability of the fuel element. In general the damaged state of the can material may be written in the following form after allowing for the prolonged action of varying stresses at high temperatures (in the steady state) and reversing plastic deformations (in transient processes):

$$a_\sigma^{\alpha_1} + a_N^{\alpha_2} = 1, \tag{5}$$

where α_1, α_2 are experimental coefficients determined from tests inside the reactor. Quasistatic damage due to the prolonged action of stress may be determined from the condition of linear damage accumulation of:

$$a_\sigma = \int \frac{dt}{t_b}, \tag{6}$$

where t_b is the time to failure, determined from tests on the long-term strength of the can material carried out inside the reactor, using the relationship $D(T) = \sigma_e^\gamma t_b$,

$$\sigma_e = \chi\sigma_i + (1-\chi)\sigma_1 A^{1-\beta}, \tag{7}$$

where $\beta = 3(\sigma_1 + \sigma_2 + \sigma_3)\sigma_i^{-1}$, A and χ are experimental constants.

Here σ_e is the equivalent stress characterizing the rupture process in the complex-stressed state. Usually we use the maximum principal stress (σ_1), the stress intensity (σ_i), or some combination of these, such as, for example, the criterion of V. P. Sdobyrev [28] $\sigma_e = (\sigma_1 + \sigma_i)/2$ of the generalized A. A. Lebedev criterion [29, 30] as equivalent stress. We note that this latter criterion agrees closely with experimental data for nonirradiated materials.

A study of the long-term strength of austenitic Kh16N15M3B steel in a plane-stressed state (torsion plus tension of thin-walled tubes) carried out in "Neutron" test systems under the conditions of the SM-2 reactor showed [31, 32] that none of the existing criteria adequately described the rupture of the irradiated material, as clearly seen from Figs. 14 and 15. The stressed state may change the time to failure very substantially (Fig. 16). A new criterion was proposed in [33] for the long-term strength of irradiated austenitic steel

$$\sigma_e = [f_1(\beta) + f_2(\beta) \lg t](\sigma_i - \sigma_1) + \sigma_1,$$

where $\beta = \operatorname{arctg} |\sigma_3/\sigma_1|$ is a parameter characterizing the form of the stressed state, and in order to find the functions f_1 and f_2 the results of tests with three forms of stressed state are required. The use of V. N. Kiselevskii's criterion is indicated in Fig. 17.

If the deformation taking place during the reactor stopping periods is restricted to the elastic limits, the fatigue damage of the can material may be neglected, and by using Eq. (6) we may obtain the following expression for the nominal reserve-of-strength coefficient with respect to the stresses:

$$K_\sigma = \left[\int_0^t \frac{Da_0\, dt}{\sigma_e^\gamma}\right]^{1/\gamma}, \tag{7a}$$

where a_0 is the experimental damage coefficient. Of course the law of linear damage summation (6) is frequently not satisfied, especially for thin-walled constructions such as the fuel-element can [34].

In these cases we should use the relationships of the theory of nonlinear damage accumulation, for example, the following kinetic equation:

$$\frac{da_\sigma}{dt} = f(\delta, \sigma_e, T, \eta^\sigma, H^\sigma, a_\sigma, q), \tag{8}$$

where δ is the thickness of the can; η^σ and H^σ are the accumulation intensity and number of the radiation defects, which determine the influence of irradiation on the long-term strength. The increment dq in the damage parameter is calculated thus:

$$dq = R_1(\sigma_e)\, d\sigma_e + R_2(T)\, dT + R_3(\eta^\sigma)\, d\eta^\sigma + R_4(t)\, dt. \tag{9}$$

The functions R_1, R_2, R_3 are determined from long-term strength tests carried out inside the reactor under conditions as close as possible to those encountered in actual service (in respect of the wall thickness, irradiation spectrum and intensity, action of the ambient, and so on), with a gradual change in the individual parameters σ_e, T and η^σ.

In determining the quasistatic damage we may take the inelastic viscoplastic unilateral deformations (ε_i^H) as a criterion. After linear summation we obtain the following equation:

$$a_\varepsilon = \int_{\varepsilon_{ic}^H} \frac{d\varepsilon_{ic}^H}{\varepsilon_{B\eta}^H} + \int_{\varepsilon_{in}^H} \frac{d\varepsilon_{in}^H}{\varepsilon_{BH}^H}, \tag{10}$$

where $\varepsilon_{B\eta}^H(T, \zeta_i^H, \eta^\varepsilon)$ and $\varepsilon_{BH}^H(T, \zeta_i^H, H^\varepsilon)$ are the breaking inelastic deformations respectively obtained from prolonged reactor tests and brief tests at a specified rate of deformation carried out on ζ_i^H samples irradiated so as to obtain a specified level of radiation damage H^ε. Here ε_{ic}^H and ε_{in}^H are the intensities of the deformations respectively accumulated in the prolonged steady-state and brief transient reactor operating conditions. The damage due to the deformation may be summed by analogy with Eq. (8).

Fatigue damage includes low-cycle fatigue due to reversing plastic deformations during the heat exchanges and many-cycle fatigue due, for example, to vibrating loads.

Figures 18 and 19 show the calculated time variation of the stresses, the long-term strength reserve coefficient (K_σ), and the accumulated inelastic deformation (ε^H) in the can of a fuel element close to the wall (circumferential temperature deviation ~50°C), from which it follows that the circumferentially

nonuniform swelling of the steel has a considerable influence on the serviceability of the fuel element. Nonuniform swelling of the steel over the thickness of the can may also exert a substantial influence.

LITERATURE CITED

1. I. S. Golovnin, O. K. Bibilashvili, and T. S. Men'shikova, At. Énerg., 34, No. 3, 147 (1973).
2. I. S. Golovnin, in: Transactions of the International Agency for Atomic Energy Symposium on Fast-Reactor Fuel and Fuel Elements [in Russian], Brussels, July 2-6 (1973), Paper No. 173/69.
3. A. I. Leipunskii et al., 4th Geneva Conf. (1971), Paper No. 49/709.
4. V. V. Orlov, M. F. Troyanov, and V. B. Lytkin, At. Énerg., 30, No. 2, 170 (1971).
5. O. D. Kazachkovskii et al., ibid., p. 174.
6. A. I. Leipunskii et al., in: Transactions of the Comecon Symposium "Present state of operations in the creation of nuclear power stations with fast neutron reactors," [in Russian], Vol. 1, Izd. FÉI, Obninsk (1967), p. 151.
7. I. S. Golovnin et al., [4], p. 216.
8. I. S. Golovnin et al., Anglo—Soviet Symposium (1975).
9. J. Holmes [2], Paper 173/54.
10. J. Ratier [2], Paper 173/9.
11. H. Baily [2], Paper 173/74.
12. K. Eickhoff et al., [2], Paper 173/61.
13. F. Anselin and C. Mercier, Paper at the Franco—Soviet Symposium, Cadarache (1970).
14. O. D. Kazachkovskii et al., in: Transactions of the Comecon Symposium "Present state of operations in the creation of nuclear power stations with fast neutron reactors," [in Russian], Vol. 2, Izd. FÉI, Obninsk (1967), p. 425.
15. I. G. Lebedev et al., Preprint P-166, Scientific-Research Institute of Nuclear Reactors (1972).
16. R. V. Kotel'nikov et al., High-Temperature Nuclear Fuel [in Russian], Atomizdat, Moscow (1969), p. 87).
17. Yu. I. Likhachev and V. Ya. Pupko, Strength of Nuclear-Reactor Fuel Elements [in Russian], Atomizdat, Moscow (1975).
18. I. A. Birger, Izv. Akad. Nauk SSSR, Ser. Mekhan., No. 2, 113 (1965).
19. I. A. Birger and I. V. Dem'yanushko, Mekhan. Tverd. Tela, No. 6, 70 (1968).
20. Yu. I. Likhachev and V. V. Popov, At. Énerg., 32, No. 1, 3 (1972).
21. V. N. Kiselevskii et al., Paper at the All-Union Conf. on "Radiation effects leading to a change in the mechanical properties of construction materials and methods of studying these" [in Russian], Inst. of Strength Problems, Academy of Sciences, Ukrainian SSR, Kiev (1974).
22. E. Gilbert and I. Straalsund, Nucl. Engng. and Design, 12, 421 (1970).
23. V. I. Subbotin et al., Third Geneva Conf., Paper No. 328 (1964).
24. Liquid Metals [in Russian], Atomizdat, Moscow (1967), p. 137.
25. P. A. Ushakov et al., At. Énerg., 13, No. 2, 162 (1962).
26. I. A. Birger, Circular Plates and Shells of Revolution [in Russian], Oborongiz, Moscow (1961).
27. Yu. I. Likhachev, A. A. Proshkin, and Zh. N. Shcherbakov, At. Énerg. [4], p. 206.
28. V. P. Sdobyrev, Izv. Akad. Nauk SSSR, Mekhan. i Mashinostr., No. 6, 93 (1959).
29. G. S. Pisarenko and A. A. Lebedev, Resistance of Materials to Deformation and Rupture in the Complex-Stressed State [in Russian], Naukova Dumka, Kiev (1969).
30. A. A. Lebedev and B. I. Koval'chuk, Probl. Prochnosti, No. 8, 12 (1970).
31. V. N. Kiselevskii et al., Probl. Prochnosti, No. 9, 39 (1974).
32. V. N. Kiselevskii et al., Probl. Prochnosti, No. 12, 48 (1974).
33. V. N. Kiselevskii et al., ibid., p. 48.
34. V. D. Kurov and V. D. Tokarev, Probl. Prochnosti, No. 2 (1969), No. 1, 31 (1970).

IN-REACTOR MEASUREMENTS OF THE MODULUS OF ELASTICITY OF URANIUM DIOXIDE

V. M. Baranov, Yu. K. Bibilashvili, I. S. Golovnin, V. N. Kakurin, T. S. Men'shikova, Yu. V. Miloserdin, and A. V. Rimashevskii

UDC 620.179.16:621.039

The measurement of the modulus of elasticity allows valuable information to be obtained on the strength, the degree of imperfection, and the changes occurring in the material lattice. The knowledge of this property of the material is also very important for engineering calculations. The determination of the modulus of elasticity directly in the irradiation process is of the greatest scientific and practical interest; however, the experimental difficulties which arise usually make it necessary to restrict oneself to postradiation measurements.

In this connection, a study has been undertaken by the ultrasonic spectroscopic method [1, 2] of the properties of the fissionable materials in conditions of reactor irradiation. The method is based on the dependence of the characteristics of the resonance ultrasonic oscillations of small samples on the properties of the material, and their alteration under the influence of external factors.

The working principle of the apparatus to measure the modulus of elasticity of materials under irradiation in one of the central vertical experimental channels of the IRT-2000 reactor is illustrated by a structural scheme (Fig. 1). The high-frequency pulse generator excites the piezoemitter, which transforms the electrical pulses into ultrasonic oscillations and transmits them to the studied sample through a wire sound conductor. The oscillations of the latter reach the piezoreceiver through the sound conductor. The piezoreceiver signal is amplified and recorded on the screen of an electron-ray oscillograph, or on the diagram of a loop oscillograph. When the generator frequency varies with the increase of the recorded signal, resonance frequencies are determined, according to the values of which the modulus of elasticity is calculated. The internal friction of the material may be obtained from the decrement of the oscillations or the width of the resonance curve.

The transmission of oscillations from the piezoemitter to the sample, and from the sample to the receiver, is accomplished with sound conductors of 3-mm-diameter aluminum wire, whose quality was previously checked with a defectoscope by the echo method. Each sound conductor was 2.5 m long, securing the normal working of the piezotransformers. The electronic apparatus was housed in a room that provided normal working conditions.

Figure 2 shows the construction of the measurement capsule. On one sound conductor, an upper supporting disk is fixed, rigidly attached with three guides to the lower disk. The other sound conductor passes freely through the central opening in the lower disk and is attached in the mobile disk by means of a Teflon bushing. The sample is placed between the tapered ends of the sound conductors and is compressed with a spring, fixed between the mobile and immobile disks. The sound conductors are brought out of the capsule through the lid by means of multilayer sound isolators, consisting of a Teflon bushing and aluminum and rubber disks. To regulate the irradiation temperature, a heater is provided, containing a nichrome spiral placed inside porcelain tubes.

To check the temperature in the capsule, a control sample is provided with a chromel—alumel thermocouple sealed in it. The conductors of the thermocouple are brought out through the capsule lid

Translated from Atomnaya Énergiya, Vol. 40, No. 1, pp. 37-40, January, 1976. Original article submitted May 12, 1975.

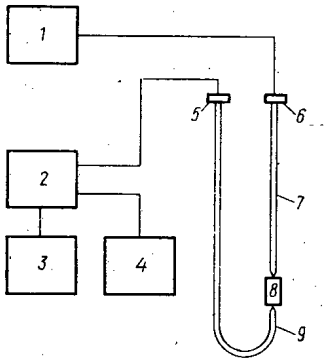

Fig. 1

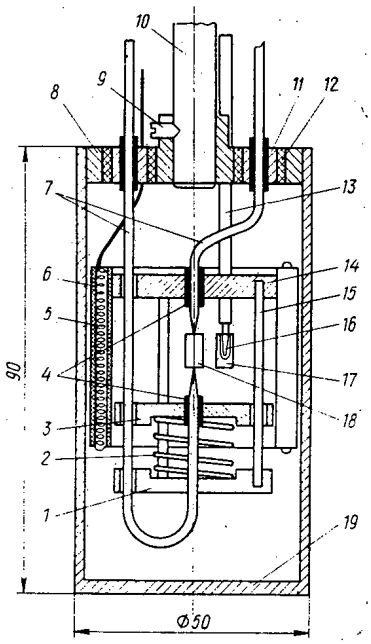

Fig. 2

Fig. 1. Structural scheme for the measurement of the modulus of elasticity for samples irradiated in a nuclear reactor: 1) high-frequency pulse generator; 2) amplifier; 3) electron-ray oscillograph; 4) bifilar oscillograph; 5) piezoreceiver; 6) piezoemitter; 7, 9) sound conductors; 8) sample.

Fig. 2. Construction of the capsule to measure the modulus of elasticity of a sample irradiated in a nuclear reactor: 1) lower immobile supporting disk; 2) spring; 3) mobile disk; 4) Teflon bushings; 5) heater spiral; 6) porcelain bush; 7) sound conductors; 8) capsule lid; 9) fixing screw; 10) bearing rod; 11,12) aluminum and rubber disks; 13) porcelain tube; 14) upper immobile supporting disk; 15) guide; 16) thermocouple; 17,18) control and samples; 19) aluminum vessel.

with a two-channel porcelain tube. The parts of the capsule are enclosed in an aluminum body attached on the lid. After assembly, the capsule is fixed with a screw on an aluminum rod, which is used to load the capsule in the experimental channel; on it are placed, moreover, sound conductors with piezotransformers and the conductors of the heater and thermocouple.

TsTS-19 piezoceramic plates of diameter 10 mm and 2 mm thick were used as piezotransformers. During the experiment, the transformers are exposed to a neutron flux of 10^5-10^6 neutrons/($cm^2 \cdot sec$) density, which did not disturb their normal operation.

To determine the possible influence of ultrasonic oscillations on the movement of defects of the structure, the amplitude of the oscillations of the samples was measured beforehand. The maximum value of the dynamic stresses in the sample caused by its oscillations is nearly $3 \cdot 10^{-3}$ kgf/mm^2, which is $\sim 1.5 \cdot 10^{-7}$ G (G is the shear modulus). The latter is much lower than the Peierls stresses, whose value is about $5 \cdot 10^{-4}$ G [3]. Hence it may be considered that there is no shift in the dislocations under the effect of ultrasonic oscillations.

In the course of careful pre-reactor measurements, the following maximum errors were obtained for the measurement apparatus: 2% for the absolute value of the modulus of elasticity, 0.1% for the variation of the modulus of elasticity through irradiation, 12% for the internal friction, and, for the temperature, 2.5% of the difference between irradiation temperature and that of the laboratory measurements.

Samples of natural enrichment of 4 mm diameter and 6.5 mm height were studied. The UO_2 density was 10.33 ± 0.05 g/cm^3, the oxygen coefficient 2.01, the mean grain dimensions 12-15 μm, and the lattice constant a = 5.475 ± 0.002. The modulus of elasticity before irradiation is 20,200 kgf/mm^2.

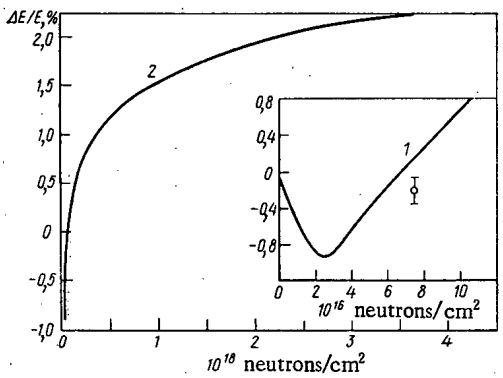

Fig. 3. Variation of the modulus of elasticity of uranium dioxide under the effect of neutron flux of density $1.7 \cdot 10^{11}$ (1) and $5 \cdot 10^{12}$ (2) neutrons/(cm^2·sec), respectively, at T = 90 and 300°C.

The capsule with the samples was loaded in the vertical experimental channel of 52 mm diameter, which was evacuated and then filled with helium before starting irradiation. To obtain fluxes of different intensity, the channel with the capsule was shifted vertically. The samples were exposed to the effect of the neutron flux of the reactor, the fast neutron component being nearly 4%.

During the interruptions in the reactor operations, the samples were at a temperature 22-25°C. To take into account the change in the modulus of elasticity caused by self-heating of the sample under the effect of neutron irradiation, the temperature dependence of resonance frequencies was first obtained in laboratory conditions, according to which the data from in-reactor measurements were corrected. The necessary temperature correction was obtained from the indications of the thermocouple fixed in the control sample.

Figure 3 shows how the modulus of elasticity varies under radiation. The flow (integral neutron flux) was $1 \cdot 10^{17}$ and $4 \cdot 10^{18}$ neutrons/cm^2, respectively, for the first and second samples. In the first approximation, the initial section of curve 2 coincides with curve 1, i.e., the irradiation intensity and the temperature do not influence greatly the initial changes of the modulus. At the beginning of irradiation, the modulus of elasticity decreases by approximately 1% for a flow of the order $2.5 \cdot 10^{16}$ neutrons/cm^2, after which it starts to increase again. The starting value is increased for a flow $\sim 7 \cdot 10^{16}$ neutrons/cm^2, after which the modulus of elasticity tends monotonically to a stationary value. The general form of the curve of variation of the modulus of elasticity may be explained with the known data on the radiation damages of uranium dioxide, if the presence of two competing processes of radiation damage is assumed. As is known [4], the UO_2 lattice constant increases under irradiation, reaching saturation for a flow of $2 \cdot 10^{17}$ neutron/cm^2. This increase, related to the presence of point defects, should weaken the bonds of atoms in the crystal lattice, which is apparently also reflected in the decrease in the modulus of elasticity in the starting period of irradiation. Simultaneously with the increase of the number of point defects, the probability of dislocation being fixed on these defects also increases, which should lead to an increase of the modulus of elasticity through the decrease of the dislocation component of the deformation in the range of elastic stresses [3]. Inasmuch as the indicated effect is related to the migration of the point defects formed, whose probability increases after the lattice is saturated with defects, it is natural to expect its delay with respect to the beginning of irradiation.

A comparison of the results of pre-reactor and in-reactor measurements shows that, for one and the same testing temperature, the measurements in the reactor lead to somewhat higher (up to 0.5%) values of the modulus of elasticity. Hence it may be assumed that the neutron flux induces a change in the modulus of elasticity, eliminated after the flux stops. However, it should be noted that the errors in the determination of the temperature did not allow exact quantitative measurements of this effect. The internal friction of uranium dioxide in the irradiation process varies very irregularly, and there are considerable spreads on the curve of the dependence of internal friction on the flow. Inasmuch as this type of behavior of internal friction is absent in the pre-reactor experiments, it may be assumed that this effect is due to the influence of radiation. Its most probable mechanism is the effect of internal microstresses, propagating sporadically in the sample during irradiation. The mean value of internal friction tends to increase slightly.

It follows from the indicated results that, for small burnups, the radiation changes in the modulus of elasticity are slight and need not be considered in engineering works.

LITERATURE CITED

1. V. M. Baranov, V. N. Kakurin, and A. V. Rimashevskii, Methods and Means of Investigating Materials and Machines Operating under Radiation [in Russian], Vol. 1, Atomizdat, Moscow (1973), p. 62.
2. Yu. V. Miloserdin et al., At. Énerg., 35, No. 2, p. 101 (1973).
3. V. S. Postnikov, Internal Friction in Metals [in Russian], Metallurgiya, Moscow (1969).
4. B. Lastman, Radiation Phenomena in Uranium Dioxide [in Russian], Atomizdat, Moscow (1964).

HYDROGEN EMBRITTLEMENT OF VESSEL STEELS

V. V. Gerasimova and E. Yu. Rivkin

UDC 621.039.53:539.56:546.11

Hydrogen arising by corrosion dissolves in the metal of the containment vessel during the operation of a nuclear reactor; this hydrogen can produce embrittlement. The tendency to this form of failure can be evaluated from the change in the mechanical characteristics after electrolytic hydrogenation at room temperature [1]. It is then assumed that the processes are identical with those during the operation of the reactor. To check this it is necessary to have a model for the process that one could use to estimate quantitatively the strength changes in the metal in relation to the method of hydrogenation. Some concepts on the causes of hydrogen embrittlement [2-5] give only qualitative descriptions.

Hydrogen embrittlement can be reversible or irreversible [2, 3]; in the reversible case, the mechanical characteristics tend to the values corresponding to the initial state when the hydrogenation is stopped [5]. Another distinctive feature of reversible hydrogen embrittlement is that the hydrogenated and initial specimens show similar mechanical characteristics on rapid plastic deformation [2, 3]. In the irreversible case, the plasticity of the hydrogenated metal is less than that of the initial material not only after prolonged rest in air but also on rapid plastic strain. In existing views [4] the hydrogen embrittlement is due in the main to micropores with elevated pressures of molecular hydrogen, which produce elevated stresses and facilitate a crack nucleation. Dislocations either act as crack nuclei on account of dislocation fusion [6] or else facilitate the transport of hydrogen to collectors [4]. A defect of all these explanations of hydrogen embrittlement is that they fail to distinguish the conditions that result in reversible or irreversible embrittlement, while also not giving any quantitative evaluation.

Here we present a model for hydrogen embrittlement that can define the differences in the two processes and the conditions for occurrence, while also giving quantitative evaluation. The model is applied to materials electrolytically hydrogenated at room temperature and also under working conditions, where the hydrogenation may occur by corrosion at elevated temperatures.

In the first case we consider a plastically deformed metal with a perfect structure (to facilitate distinction of the reversible and irreversible cases). In the second case, we consider a metal under a stress that does not exceed the yield point, and the lattice may contain defects, including ones produced by irradiation.

We thus consider reversible hydrogen embrittlement. Plastic strain is accompanied by formation and motion of dislocations [6]; hydrogenation of a plastically deformed metal leads to the hydrogen being trapped by dislocations [7], around which it forms Cottrell atmospheres [2], which retard the dislocation motion [6], which facilitates the formation of planar accumulations, which in turn may be the cause of crack nucleation and growth. The loss of plasticity in the reversible case is due to the restricted dislocation mobility on account of the Cottrell atmospheres. If the strain and hydrogenation are stopped before a crack is formed, the mechanical characteristics gradually recover to the values for the original material [5]. This recovery is due to dissipation of the Cottrell atmospheres and dislocation release, the dislocations thus regaining their initial mobility. This means that the time to crack nucleation on account of a planar accumulation of dislocations is determined by the ratio of the dislocation mean free path from the instant of generation to the instant of blocking on hydrogenation taken with respect to the dislocation speed:

$$\tau_d = L/v. \tag{1}$$

In the limiting case, the dislocation speed in the presence of a Cottrell atmosphere equals the

Translated from Atomnaya Énergiya, Vol. 40, No. 1, pp. 40-45, January, 1976. Original article submitted January 3, 1975; revision submitted December 21, 1975.

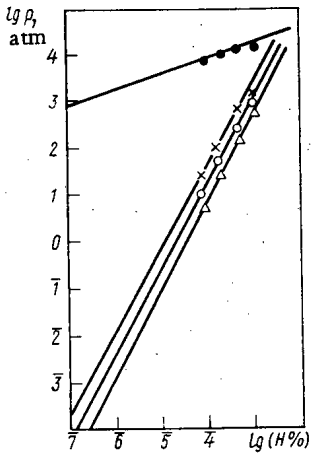

Fig. 1

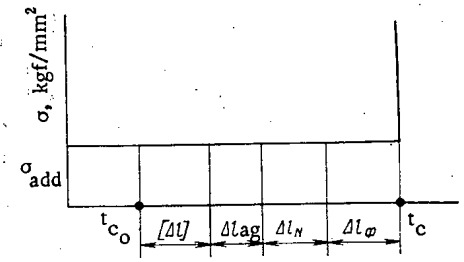

Fig. 2

Fig. 1. Hydrogen pressure in collector as a function of hydrogen concentration in metal [17]: ●) 20; ×) 200; ○) 300; △) 400°C.

Fig. 2. Resistance to brittle fracture (explanation in text).

hydrogen diffusion rate in the metal [6], and the latter is [18]

$$v = fu, \tag{2}$$

where f is the force generating the motion and u is the mobility, i.e., the speed in response to unit force.

In turn we have [8]

$$f = \frac{RT}{C}\frac{dC}{dx}, \tag{3}$$

where R is the gas constant, T is the temperature in °K, C is the hydrogen concentration in the metal, and dC/dx is the concentration gradient.

The mobility is [8]

$$u = D/RT, \tag{4}$$

where D is the diffusion coefficient. Then (2)-(4) give

$$\tau_d = \frac{LC}{D}\frac{1}{dC/dx}. \tag{5}$$

In the reversible case, the crack nucleus cannot develop, but the microcavity begins to operate as a collector. The accumulation of molecular hydrogen may result in pressures of k atm [9], which then produce irreversible hydrogen embrittlement. It is virtually impossible to remove the molecular hydrogen from the collector at 20°C, since only atomic hydrogen can penetrate into the lattice, and the dissociation constant is $1.2 \cdot 10^{-71}$, i.e., extremely small. At 300°C, the dissociation is increased, and the constant is $7.6 \cdot 10^{-41}$ [10]. Consequently, the hydrogen will accumulate in the micropores until the stress in the surrounding material becomes sufficient to produce a crack of critical size (C_{cr}). Griffith's [11] relationship is

$$\sigma + P \geqslant \sqrt{4E\gamma/\pi C_{cr}}, \tag{6}$$

where P is the hydrogen pressure, σ is the external applied stress, E is Young's modulus, and γ is the surface energy. The pressure in a micropore is

$$P = (nRT)/3V, \tag{7}$$

where n is the number of moles of hydrogen in a micropore and V is the volume.

The crack volume is [12]

$$V = (\pi C_{cr}^3)/8. \tag{8}$$

The number of moles of hydrogen in a crack is

$$n = M/N \tag{9}$$

TABLE 1. Failure Stress as a Function of Defect Length, Distance between Defects, and Hydrogen Pressure within a Defect

Press. in defect, kgf/cm²	Defect length, mm	Distance between defects, mm	Failure stress, kgf/mm²
0	5	30	35,5
	10	40	24,5
1000	5	30	31,7
	10	40	21,2

(here N is the weight of 1 mole, and M is the amount of hydrogen in a pore). The amount of hydrogen in a micropore is determined from Fick's equation [8]:

$$M = DS\tau_a \frac{dC}{dx}, \tag{10}$$

where S is the area of the crack and τ_a is the hydrogen accumulation time.

If the conditions favor crack growth, we have

$$\sigma_\Sigma = \sigma + P = \sqrt{4E\gamma/\pi C_{cr}}. \tag{11}$$

From (7), (8), and (10) we have

$$\frac{2D\tau_a RT}{3NC_{cr}} \frac{dC}{dx} = \sqrt{\frac{4E\gamma}{\pi C_{cr}}} - \sigma. \tag{12}$$

Then the time needed for the hydrogen to accumulate to an extent sufficient to meet (6) is

$$\tau_a = \frac{3NC_{cr}}{2DRT}\left(\sqrt{\frac{4E\gamma}{\pi C_{cr}}} - \sigma\right)\frac{1}{dC/dx}. \tag{13}$$

Comparison of (5) and (13) can define the failure mechanism; if $\tau_a/\tau_d > 1$, a crack is formed by the reversible mechanism; if $\tau_a/\tau_d < 1$, by the irreversible one.

In the second case, the reversible embrittlement cannot be realized for elastically deformed metal with the actual crystal structure on account of the absence of plastic deformation, which requires dislocation movement. The dislocations are blocked by the hydrogen that has penetrated the metal, which reduces the plasticity, and this is the definitive stage in the reversible embrittlement. Therefore, in that case (6) will be realized if

$$\sigma_\Sigma \geqslant \sqrt{4E\gamma/\pi C_{cr}}. \tag{14}$$

In the case of a cylindrical pore [13] we may have $p = \sigma_\Sigma$; the time needed for the hydrogen pressure to reach the level to produce a crack of critical size is given by

$$\tau_a = \frac{3NC_{cr}}{2DRT}\sqrt{\frac{4E\gamma}{\pi C_{cr}}}\frac{1}{dC/dx}. \tag{15}$$

These arguments are applicable to hydrogenation in the center of the containment vessel, since in that zone, which is subject to the heaviest irradiation, the stresses do not exceed the yield point, so the reversible stage should be absent. The structure defects due to radiation damage can attain $\sim 10^2 - 5\cdot 10^2$ Å [14], and they can act as collectors for the molecular hydrogen.

This model enables one to evaluate the behavior of materials electrolytically hydrogenated at room temperature and on account of corrosion at 316°C. The amount of hydrogen defusing through steel on electrolytic hydrogenation at 20°C is known [1, 15], and the same is known for corrosion in water at pH 10 and 316°C [16], which gives the maximum hydrogen concentration in the metal. The hydrogen concentration at the surface in contact with the air is virtually zero, and then $C = C_{met.max}$; in electrolytic hydrogenation of perlitic steel in sulfuric acid containing stimulators, the value of $C_{met.max}$ varies from $4.48\cdot 10^{-5}$ to $7.05\cdot 10^{-4}$ atm %; the equilibrium hydrogen pressure in a collector is [17] $(5.25\text{–}9.13)\cdot 10^{13}$ atm (Fig. 1). The hydrogen concentration in the metal derived from corrosion in water at pH 10 at 316°C is $4.67\cdot 10^{-7}$ atm %, while the equilibrium hydrogen pressure in a collector at 300°C is $3.8\cdot 10^{-4}$ atm.

Such pressures are completely safe for use at elevated temperatures; the hazard for hydrogen embrittlement occurs when the body is cooled rapidly to 20°C. Figure 1 shows that the transition from 316 to 20°C produces a marked increase in the hydrogen pressure in the collector, viz., to $1.15\cdot 10^3$ atm, which is probably related to marked reductions in the dissociation of the molecular hydrogen. There may also be a considerable increase in the hydrogen pressure in the micropores on account of accelerated diffusion to the surface layers, since the atomic-hydrogen concentration at the surface falls to zero. The hydrogen concentration in the metal as a function of time is described by

$$\ln\frac{C_0}{C} = \frac{\tau D}{\delta}, \tag{16}$$

where C_0 is the initial concentration, C is the value at time τ, and δ is the thickness of a layer or the distance of a defect from the surface.

If $\delta = 10^{-3}$ cm, while the thickness of a defect itself is 10^{-5} cm, the time needed to fill a defect with hydrogen to a pressure of 10^3 atm is $1.65 \cdot 10^2$ sec. The hydrogen concentration in the metal does not change substantially during this time, so the metal should have zones hazardous as regards irreversible hydrogen embrittlement.

The metal may also be embrittled by the irradiation, thermal ageing, and strain ageing, in conjunction with cyclic loading. The diagram representing resistance to brittle failure[18] (Fig. 2) defines the acceptable conditions for operating such a vessel in the brittle state; the material is in a brittle state if it is operated at temperatures below the critical embrittlement temperature t_c, which equals the sum of the critical embrittlement temperature in the initial state (t_{c_0}), the temperature safety margin [Δt] = 30°C, and the shifts in the critical embrittlement temperature on account of ageing Δt_{ag}, cyclic loading Δt_N, and irradiation Δt_Φ. In constructing the diagram it has been assumed that all these factors operate additively. If the hydrogenation is also additive, one can introduce an additional shift in the critical temperature as the result of hydrogenation Δt_F, which enables one to estimate the reduction in the permissible stresses in the brittle region on account of the hydrogen pressure within the material, and so the brittle-failure resistance diagram can be modified suitably.

To establish how hydrogen embrittlement affects the carrying capacity we examined the body of a water-cooled and water-moderated reactor made of 15Kh2MFA steel. The calculation is performed within the framework of linear-elastic failure mechanics, the following being the basic assumptions: the minimum failure viscosity of irradiated and hydrogenated metal is $K_{I_c} = 100$ kgf/mm$^{3/2}$ in the working temperature range, while the pressure in a defect is $p = 10^3$ kgf/cm^2; further, a defect is a sharp crack passing completely through the thickness of the wall.

First we consider the wall of the reactor vessel as a continuous medium uniformly penetrated by through cracks of maximum size $2l = 5 \cdot 10^{-5}$ mm and mutual separation $2b = 1 \cdot 10^{-4}$ mm; the tensile stress σ is given by

$$K_{I_c} = \sigma \sqrt{\pi l}\, f_{1c}, \tag{17}$$

where

$$f_{1c} = \sqrt{\frac{1}{4\pi l \cos\left(\frac{\pi}{2}\frac{l}{b}\right)}}\left[\sqrt{8b \sin\left(\frac{\pi}{2}\frac{l}{b}\right)} + \frac{P \cdot 2l}{\sigma\sqrt{2b \sin\left(\frac{\pi}{2}\frac{l}{b}\right)}}\right]. \tag{18}$$

The theoretical value is 10^4 kgf/mm^2; this stress is more than 100 times the actual strength of 15Kh2MFA steel. The calculation shows that hydrogenation has virtually no effect on the carrying capacity when the body is considered as a continuous medium with microdefects.

A real reactor vessel may contain macroscopic defects; for instance, welded joints may have hollow defects of size up to $2l = 5$ mm with distances apart not less than $2b = 30$ mm, as well as slag inclusions of length up to $2l = 10$ mm and distances apart not less than $2b = 40$ mm [19]. Table 1 gives the stresses calculated from (17); it is clear that hydrogenation can reduce the failure stresses in the body by 10-13%, which is a comparatively small reduction, and can be incorporated by correcting the brittle-failure resistance diagram simply by reducing the permissible stresses.

It is also very important to establish the precise effects of hydrogenation on the critical embrittlement temperature, which can be done by testing specimens in shock bending.

It has been shown [20] that retarded failure in A-542, A-543, and A-302 V steels does not occur for a neutron fluence up to 10^{20} n/cm^2 and hydrogen concentration in the steel up to 0.0004%.

These figures indicate that it is unlikely that failure will occur in hydrogenated reactor steels, although the conclusion requires additional confirmation.

CONCLUSIONS

1. A model has been proposed for hydrogen embrittlement that provides a quantitative evaluation of the resistance of steel to this form of failure.

2. There is found to be no correlation between the state of the metal electrolytically hydrogenated at 20°C and hydrogenated by corrosion at 300°C; it would appear impossible to judge the susceptibility to hydrogen embrittlement at 300°C from the change in the mechanical characteristics of specimens electrolytically hydrogenated at room temperature.

3. If the temperature is reduced from 300 to 20°C, specimens of vessel steel electrolytically hydrogenated or hydrogenated by corrosion at 300°C behave identically, so the resistance to hydrogen embrittlement can be estimated on specimens electrolytically hydrogenated at room temperature.

4. Hydrogenation can reduce the failure stress in the vessels of water-cooled and water-moderated reactors by 10-13%; the effects of hydrogenation can be incorporated by correcting the corresponding brittle-failure resistance calculation schemes and estimating the acceptable safety margin for vessel operation.

LITERATURE CITED

1. A. Rossin, T. Beewitt, and A. Troiano, Nucl. Eng. and Design, 4, No. 5, p. 446 (1966).
2. P. Cotterill, Hydrogen Embrittlement of Metals [Russian translation], Vol. 3, Metallurgiya, Moscow (1963).
3. G. V. Karpenko and R. I. Kripyakevich, The Effects of Hydrogen on the Properties of Steel [in Russian], Metallurgiya, Moscow (1962).
4. Failure in Solids [in Russian], Metallurgiya, Moscow (1967).
5. Yu. A. Rozhdestvenskii, Korroziya i Zashchita v Neftegazovoi Prom., No. 3, 30 (1972).
6. J. P. Hirth and J. Lothe, Theory of Dislocations [Russian translation], Atomizdat, Moscow (1971).
7. R. Bouraou, M. Cornet, and S. Talbot-Besnard, Comp. Rend. Acad. Sci., 277c, No. 5, p. 231 (1973).
8. A. A. Zhukhovitskii and L. A. Shvartsman, Physical Chemistry [in Russian], Metallurgiya, Moscow (1964).
9. M. Raczyshki, Bull. Acad. Pol. Sci., Ser. Chim., 15, 15 (1966).
10. W. Gianque, J. Amer. Chem. Soc., 52, No. 12, 4916 (1930).
11. Failure [Russian translation], Vol. 1, Mir, Moscow (1973).
12. Physical Metallography [Russian translation], Vol. 3, Mir, Moscow (1968).
13. V. N. Sedov, Mechanics of Continuous Media [in Russian], Vol. 2, Nauka, Moscow (1970).
14. V. N. Bykov et al., At. Énergiya, 36, No. 1, 24 (1974).
15. W. Bankloh and G. Zimmerman, Arch. Eisenhüttenwesen, No. 9, p. 459 (1936).
16. M. Bloom and M. Krulfeld, J. Electrochem. Soc., 104, No. 5, p. 264 (1957).
17. A. Corney et al., in: Proc. Electric Furnace Steel, AJME, 6, p. 38 (1948).
18. Rules for Testing Welded Joints and Corners in Nuclear Power Stations and Experimental and Research Reactors PK1514-72 [in Russian], Metallurgiya, Moscow (1973).
19. Standards for Strength Calculations on Parts of Reactors, Boilers, Vessels, and Pipes in Nuclear Power Stations and Experimental and Research Reactors [in Russian], Metallurgiya, Moscow (1973).
20. C. Brinkman and J. Beeston, IN-1359, Idano Falls, Feb., 1970.

NONSTEADY-STATE SPACE-ENERGY SPECTRUM OF NEUTRONS IN A HEAVY, WEAKLY INHOMOGENEOUS MEDIUM, ALLOWING FOR NEUTRON CAPTURE

E. V. Metelkin

UDC 539.125.52;621.039.51.12

The study of the transmission of neutrons from a nonsteady-state source is of considerable interest and has quite a wide range of applications [1]. Nonsteady-state neutron transmission is used to measure the neutron-physics constants of various media, and also to analyze the structure and composition of media that are not accessible for direct investigation (as in nuclear geophysics, for example). Moreover, a knowledge of the evolution through time of neutron spectra is necessary for the solution of a whole series of problems in neutron physics, radiation—protection physics, and many other fields.

An analytical investigation of nonsteady-state elastic retardation of neutrons in a heavy homogeneous medium was conducted in [2]. Nonsteady-state space-energy spectra of neutrons from a pulsed, monochromatic point source were calculated in [3] for important particular cases of elastic retardation in a heavy, weakly inhomogeneous medium. It was assumed in the calculations that neutron capture was absent. In an inhomogeneous medium, the maximum density of neutron collisions is shifted (in comparison with a homogeneous medium) toward increased density of the retarding medium [3].

However, in most cases that arise in practice, neutron capture is very substantial and cannot be neglected. Increase in the density of the retarding medium leads to intense neutron capture, causing additional redistribution of the neutrons in space.

In the present paper, the results of [3] are generalized for retarding media in which neutron capture occurs. It is everywhere assumed [3] that the spatial dependence of the macroscopic scattering and capture cross sections is produced by the changing density of the medium and, in view of its weak inhomogeneity, is of the form

$$\Sigma_{s,\,a}(\mathbf{r},\,v)=\Sigma_{s,\,a}(v)\,\Sigma(\mathbf{r}),\qquad \Sigma(\mathbf{r})=1-\mathbf{r}\nabla l. \tag{1}$$

It is assumed also that

$$\Sigma_s(v)=\text{const};\quad \Sigma_a(v)=\frac{\Sigma_a^{(0)}}{v};\quad \Sigma_a^{(0)}=\text{const}, \tag{2}$$

which is found to hold for the majority of retarding media [2, 4].

The equation describing the nonsteady-state elastic retardation in an inhomogeneous medium of neutrons from a pulsed, monochromatic source has the following form [4]:

$$\frac{l_s(u,\,\mathbf{r})}{v}\frac{\partial\Psi(u,\,\mathbf{r},\,\Omega,\,t)}{\partial t}+\Omega\nabla\left[l_s(u,\,\mathbf{r})\,\Psi(u,\,\mathbf{r},\,\Omega,\,t)\right]+\left(1+\frac{\Sigma_a}{\Sigma_s}\right)\Psi(u,\,\mathbf{r},\,\Omega,\,t)=$$
$$=\int_0^u du'\int d\Omega' f(\mu_0,\,u-u')\,\Psi(u',\,\mathbf{r},\,\Omega',\,t)+\frac{1}{4\pi}\,\delta(u)\,\delta(\mathbf{r})\,\delta(t), \tag{3}$$

where $\Psi(u, \mathbf{r}, \Omega, t) = [v/l_S(u, \mathbf{r})]N(u, \mathbf{r}, \Omega, t)$ is the density of elastic collisions of the neutrons, referred to unit interval of $\mathbf{r}$, Ω, u; $\mathbf{r}$ is the radius vector of the point in space; Ω is the unit vector in the direction

Translated from Atomnaya Énergiya, Vol. 40, No. 1, pp. 45-48, January, 1976. Original article submitted March 31, 1975; revision submitted June 30, 1975.

of the velocity v; $u = \ln(E^+/E)$ is the lethargy (E^+ is the energy of the source); $l_S(u, \mathbf{r}) = 1/\Sigma_S(u, \mathbf{r})$ is the free path length of the neutrons with respect to scattering; $f(\mu_0, u)$ is the elastic scattering index of the neutrons [2-4].

The solution of Eq. (3) will be sought in the form

$$\Psi = \Psi'(u, \mathbf{r}, \Omega, t)\exp(-\Sigma_a^0 t). \tag{4}$$

Substituting (4) into Eq. (3), we obtain the following equation for the function $\Psi'(u, \mathbf{r}, \Omega, t)$:

$$\frac{l_s(u, \mathbf{r})}{v}\frac{\partial\Psi'(u, \mathbf{r}, \Omega, t)}{\partial t} + \Omega\nabla[l_s(u, \mathbf{r})\Psi'(u, \mathbf{r}, \Omega, t)] + \left[1 - \frac{g}{v}(\mathbf{r}\nabla l)\right]\times\Psi'(u, \mathbf{r}; \Omega, t)$$
$$= \int_0^u du'\int d\Omega' f(\mu_0, u-u')\Psi'(u', \mathbf{r}, \Omega', t) + \frac{1}{4\pi}\delta(u)\delta(t)\delta(\mathbf{r}), \tag{5}$$

where $g = v\Sigma_a(v, \mathbf{r})/\Sigma_S(v, \mathbf{r}) = \text{const}$ [see (1), (2)].

As in [3], the solution of Eq. (5) will be sought in the diffusion approximation. Transforming to the variables $\tilde{\chi}_0$, $\tilde{\chi}_1$ (see (12) in [3]) and repeating the procedure described in detail in [3], we obtain the following system of equations for determining the form of the functions $\tilde{\chi}_0$, $\tilde{\chi}_1$:

$$\chi_1 = \left(\frac{ll_0}{3}\right)\frac{\nabla\tilde{\chi}_0 + \tilde{\chi}_0\frac{\nabla\Psi}{\Psi}}{\frac{1}{2}M\Phi + \frac{g}{v}(\mathbf{r}\nabla l)}; \tag{6}$$

$$\frac{l_0}{v}\frac{\partial\tilde{\chi}_0}{\partial t} + \frac{l_0^2}{3}\operatorname{div}\left[l\frac{\nabla\tilde{\chi}_0 + \tilde{\chi}_0\frac{\nabla\Psi}{\Psi}}{\frac{1}{2}M\Phi + \frac{g}{v}(\mathbf{r}\nabla l)}\right] + \frac{l_0^2}{3}l\frac{\nabla\tilde{\chi}_0 + \tilde{\chi}_0\frac{\nabla\Psi}{\Psi}}{\frac{1}{2}M\Phi + \frac{g}{v}(\mathbf{r}\nabla l)}\frac{\nabla\Psi}{\Psi} - \frac{g}{v}\frac{(\mathbf{r}\nabla l)}{l}\tilde{\chi}_0 = \frac{\Phi}{l}\frac{\partial\tilde{\chi}_0}{\partial u}; \tag{7}$$

$$l(\mathbf{r}) = \frac{\Sigma_s(v)}{\Sigma_s(v, \mathbf{r})} = \frac{1}{\Sigma(\mathbf{r})} \simeq 1 + \mathbf{r}\nabla l;$$
$$l_0 = \frac{1}{\Sigma_s(v)} = \text{const},$$

where M is the mass number of the retarding material nuclei, and the expressions for Φ and Ψ can be found in [3].

The solution of the system (6), (7) should satisfy the following initial conditions [3]:

$$\lim\tilde{\chi}_0 = \delta(\mathbf{r}) \quad \text{as} \quad u \to 0, \text{ and } t \to 0. \tag{8}$$

Since neutron capture in the medium is proportional to 1/v, neutrons with different velocities are captured equally. In this case, capture has no effect on the form of the energy spectrum [2], but leads to a decrease in the total number of neutrons with time. Therefore in the given case, as also in the absence of capture [2-3], the distribution function for the neutrons differs from zero in the region of velocities close to the mean $v_m(t, \mathbf{r})$. Taking this into account, we find the solution of Eq. (7) in the form of a series:

$$\tilde{\chi}_0 = \sum_i \tilde{\chi}_i'\xi^i; \quad \xi = \frac{v_m(t, \mathbf{r}) - v}{v}, \tag{9}$$

in which all but the first few terms may be neglected.

If we substitute (9) into (7), expand the terms appearing in it into series in powers of ξ (expressions for $\Phi(u, t, \mathbf{r})$, $v_m(t, \mathbf{r})$, and $\nabla\Psi/\Psi$ are given in [3]), and equate terms of identical order in ξ we obtain a system of equations for determining the form of the functions $\tilde{\chi}_0'$, $\tilde{\chi}_1'$, $\tilde{\chi}_2'$, etc.

Equating terms of zero order in ξ, we obtain the following equation:

$$\frac{l_0}{v_m}\frac{\partial\tilde{\chi}_0'}{\partial t} = \frac{l_0^2}{3}l(\mathbf{r})\Delta\chi_0' - \frac{l_0^2}{3}\nabla l[\nabla\tilde{\chi}_0' - 2\nabla\tilde{\chi}_1'] + \frac{ll_0^2}{3}\frac{g}{v_m}[\nabla\tilde{\chi}_0'\nabla l + (\mathbf{r}\nabla l)\Delta\tilde{\chi}_0'] + \frac{g}{v_m}(\mathbf{r}\nabla l)\tilde{\chi}_0'. \tag{10}$$

Since the medium is weakly inhomogeneous, in deriving Eq. (10) we retained only terms of first order [3] in (∇l). In deriving subsequent equations of the system, it is necessary to retain only terms of order $(\nabla l/\eta)$, $(\nabla l/\eta)^2$ [3]. Since terms containing the cross section for neutron capture (g) are of order (∇l), they will not appear in the remaining equations of the system, except for Eq. (10). In this case, the equations that are obtained by equating terms of first order in ξ and above coincide with the analogous equations (18b, c) in [3].

Since the medium is weakly inhomogeneous, i.e.,

$$l(\mathbf{r}) = 1 + \mathbf{r}\nabla l, \tag{11}$$

we find the solution of Eq. (10) in the form of a series in powers of ∇l:

$$\tilde{\chi}_0' = \chi_0^{(0)} + (\chi_0^{(1)}\nabla l). \tag{12}$$

Substituting (12) into (10), we obtain

$$\frac{\partial \chi_0^{(0)}}{\partial \tau} = \Delta \chi_0^{(0)}; \tag{13a}$$

$$\frac{\partial \chi_0^{(1)}}{\partial \tau} = \Delta \chi_0^{(1)} - \nabla \chi_0^{(0)} + 2\nabla \tilde{\chi}_1' + 2\mathbf{r}\Delta \chi_0^{(0)} - \frac{2}{a}\frac{\partial}{\partial \tau}\nabla \chi_0^{(0)} + \frac{g}{v^+} e^{a\tau}\left\{\nabla \chi_0^{(0)} + \mathbf{r}\Delta \chi_0^{(0)} + \frac{3}{l_0^2}\mathbf{r}\chi_0^{(0)}\right\}, \tag{13b}$$

where $\tau = (2l_0^2/3\eta)\ln[v^+/v_m(t, \mathbf{r})]$ is the age of the neutrons; $\eta = 2/(M+1)$; $a = 3/Ml_0^2$. For a point source, the solution of (13a) is of the form

$$\chi_0^{(0)} = \frac{1}{(4\pi\tau)^{3/2}} \exp\left\{-\frac{r^2}{4\tau}\right\}. \tag{14}$$

The solution of the remaining equations, as in [3], is found for a medium in which $l(\mathbf{r}) = l(z) = 1 + z\nabla l$ (here $\nabla l = \frac{dl}{dz}\Big|_{z=0}$).

Using Eq. (14), and also expression (29) for the function $\tilde{\chi}_1^1$ from [3], we find the solution of (13b) in the form

$$\chi_0^{(1)} = [zf(\tau) + zr^2\varphi(\tau) + \alpha(\tau) + z^2\beta(\tau)]. \tag{15}$$

Substituting (15) into (13b) and equating terms of equal order in the coordinates, we obtain the following system of equations:

$$\begin{gathered}
\frac{d\varphi}{d\tau} + \frac{3\varphi}{\tau} - \frac{3(1-e^{-a\tau})}{4a\tau^3} - \frac{1}{2\tau^2} - \frac{1}{4a\tau^3} - \frac{g}{v^+}\frac{e^{a\tau}}{4\tau^2} = 0; \\
\frac{\partial f}{\partial \tau} - 10\varphi + \frac{1}{\tau}f + \frac{15(1-e^{-a\tau}) - 2a\tau^2}{2a\tau^2} + \frac{7}{2\tau} + \frac{5}{2a\tau^2} - \frac{g}{v^+}e^{a\tau}\left(\frac{3}{l_0^2} - \frac{2}{\tau}\right) = 0; \\
\frac{d\alpha}{d\tau} - 2\beta - \frac{6\nabla l}{\eta a\tau}(1-e^{-a\tau}) = 0; \\
\frac{d\beta}{d\tau} + \frac{2\beta}{\tau} + \frac{3\nabla l}{\eta a\tau^2}(1-e^{-a\tau}) = 0.
\end{gathered} \tag{16}$$

Solving this system with the corresponding initial conditions [2, 3], and using Eq. (15), we obtain

$$\begin{aligned}
\chi_0^{(1)} = \frac{\exp\left\{-\frac{r^2}{4\tau}\right\}}{(4\pi\tau)^{3/2}}\Bigg\{ & -z\left[\frac{15}{2(a\tau)^2}\times\right. \\
& \left.\times(e^{-a\tau} + a\tau - 1)\right]\left(1 - \frac{r^2}{10\tau}\right) - \frac{r^2}{4a\tau^2}(1 + a\tau) - \\
& - \frac{5g}{2v^+(a\tau)^2}(e^{a\tau} - 1)\left(1 - \frac{4}{5}a\tau\right) + \frac{5g}{2v^+(a\tau)} + \\
& + \frac{g}{v^+a\tau}\left(\frac{2}{\eta}\right)[e^{a\tau}(1-a\tau) - 1]\left[\left(1 + \frac{r^2}{4a\tau^2}\frac{\eta}{2}\right)\right] + \\
& + \frac{6(\nabla l)\tau}{\eta(a\tau)^2}\left(1 - \frac{z^2}{2\tau}\right)(e^{-a\tau} + a\tau - 1)\Bigg\}.
\end{aligned} \tag{17}$$

As a result, the final expression for the function $\chi_0(\mathbf{r}, u, t)$ [3] takes the form

$$\chi_0(\mathbf{r}, u, t) = \frac{\exp\left\{-\frac{r^2}{4\tau}\right\}}{(4\pi\tau)^{3/2}}\{1 + \nabla l[-z + C(\tau, \mathbf{r})] + \xi D(\tau, \mathbf{r}) + \xi^2 F(\tau, \mathbf{r})\}, \tag{18}$$

where $C(\tau, \mathbf{r}) = \chi_0^{(1)}(4\pi\tau)^{3/2}e^{r^2/4\tau}$, while $D(\tau, \mathbf{r})$ and $F(\tau, \mathbf{r})$ coincide with the corresponding terms of expression (32) of [3].

From Eq. (18) it follows that in an inhomogeneous medium the maximum of the function $\chi_0(\mathbf{r}, u, t)$ occurs at the point

$$z_{max} = -\frac{2\nabla l}{a}\left\{a\tau + \frac{15}{2a\tau}(e^{-a\tau} + a\tau - 1) -\right.$$

$$-\frac{9}{2}\left(\frac{4}{3}-e^{-a\tau}\right)-\frac{5g}{2v^{+}(a\tau)}(e^{a\tau}-1)\left(1-\frac{4}{5}a\tau\right)+$$
$$+\frac{5g}{2v^{+}}+\frac{g}{v^{+}}\frac{2}{\eta}\tau[e^{a\tau}(1-a\tau)-1]\Big\}, \tag{19}$$

where the last term in the curly brackets is the largest of the terms determined by neutron capture.

For g = 0, Eq. (19) evidently coincides with the analogous result of [3]. For $a\tau \gg 1$, i.e., for $t \to \infty$, Eq. (19) yields

$$z_{max} = -2\nabla l\tau\left\{1+\frac{3}{2a\tau}-\frac{2}{\eta}\frac{\Sigma_a(v_m)}{\Sigma_s}\right\}. \tag{20}$$

The last term in (20) is easily transformed to give

$$\frac{2}{\eta}\frac{\Sigma_a(v_m)}{\Sigma_s}=\Sigma_a^0 t, \tag{21}$$

which means that it coincides with the exponent characterizing the decline in the total number of neutrons with time (4). It is evident from Eq. (20) that for $(2/\eta)(\Sigma_a(v_m)/\Sigma_s) > 1$, when the decrease in neutrons in the system due to capture is large (since $1-\Sigma_a^0 t \ll 1$), the maximum density of neutron collisions is shifted toward a lower density of the retarding medium ($z_{max} > 0$). This explains the lower rate of neutron capture in this part of space. Comparing (20) with the analogous result in [3], it is easy to establish that the occurrence of neutron capture significantly affects the spatial distribution of the neutrons.

The results obtained in the present paper allow the space-time distribution of the neutron capture density to be determined. The number of neutrons captured in unit time at time t and in unit volume close to the point **r** is

$$q(\mathbf{r}, t)=e^{-\Sigma_a^0 t}\int_0^\infty dv\,\frac{\Sigma_a(\mathbf{r}, v)}{\Sigma_s(\mathbf{r})}\Psi(u, \mathbf{r}, t)\chi_0(u, \mathbf{r}, t). \tag{22}$$

Using the expression for $\Psi(u, \mathbf{r}, t)$ [3] and Eq. (18), we obtain

$$q(\mathbf{r}, t)=\Sigma_a e^{-\Sigma_a^0 t}\frac{\exp\left\{-\frac{r^2}{4\tau}\right\}}{(4\pi\tau)^{3/2}}\left\{1+\nabla l[-z+C(\tau, \mathbf{r})]+\frac{1}{3}\eta F(\tau, \mathbf{r})\right\}. \tag{23}$$

If neutron capture occurs up to the last emission of a γ quantum, then $q(\mathbf{r}, t)$ is also the density of the source of secondary γ radiation, information on which is necessary for the solution of a whole series of problems [5].

From (23) it is easily shown that the maximum density of the number of captured neutrons occurs at the point

$$z_{max}=-\frac{2\nabla l}{a}\left\{a\tau+\frac{15}{2a\tau}[3e^{-a\tau}+a\tau-e^{-2a\tau}-2]+\frac{1}{4}[1-3e^{-a\tau}-4e^{-2a\tau}]-\right.$$
$$\left.-\frac{5g}{2v^{+}a\tau}(e^{a\tau}-1)\left(1-\frac{4}{5}a\tau\right)+\frac{5g}{v^{+}}+\frac{g}{v^{+}}\frac{2}{\eta}[e^{a\tau}(1-a\tau)-1]\right\}. \tag{24}$$

For $a\tau \gg 1$, i.e., for $t \to \infty$, Eq. (24) can be written as follows:

$$z_{max} = -2\nabla l\tau\left\{1+\frac{7.75}{a\tau}-\frac{2}{\eta}\frac{\Sigma_a(v_m)}{\Sigma_s}\right\}. \tag{25}$$

Subtracting the value of (24) from (19), we obtain the distance between the maximum density of collisions and the maximum density of the number of captured neutrons:

$$\Delta z=\frac{2\nabla l}{a}\left\{6.25-5.25e^{-a\tau}-4e^{-2a\tau}-\frac{15}{2a\tau}(2-2e^{-a\tau}+e^{-2a\tau})\right\}, \tag{26}$$

or, for $a\tau \gg 1$,

$$\Delta z=4.17\cdot Ml_0^2\nabla l\left\{1-\frac{1,2}{a\tau}\right\}. \tag{27}$$

Hence, with respect to the maximum density of neutron collisions, the maximum density of captured neutrons is displaced toward increased density of the retarding medium by a constant value (for large times) given by Eq. (27).

LITERATURE CITED

1. Theoretical and Experimental Problems of Nonsteady-State Neutron Transmission [in Russian], Atomizdat, Moscow (1972).
2. M. V. Kazarnovskii, Tr. Fiz. Inst. Akad. Nauk SSSR, 11, 176 (1959).
3. E. V. Metelkin and G. Ya. Trukhanov, At. Énerg., 37, No. 6, 466 (1974).
4. A. Vainberg and E. Wigner, Physical Theory of Nuclear Reactors [Russian translation], IL, Moscow (1961).
5. A. V. Zhemer et al., At. Énerg., 38, No. 3, 174 (1975).

EXPERIMENTS ON COOLING BY ELECTRONS*

G. I. Budker, Ya. S. Derbenev,
N. S. Dikanskii, V. I. Kudelainen,
I. N. Meshkov, V. V. Parkhomchuk,
D. V. Pestrikov, A. N. Skrinskii,
and B. N. Sukhina

UDC 539.107

Cooling by electrons was proposed in the early 1960's; the principle of the method was discussed in 1966 publications [1]. We assume that in one of the straight gap sections of a storage ring for heavy particles, e.g., protons, there exists a beam of electrons whose average velocity has the same magnitude and direction as the average velocity of the protons. In the area of the coinciding particle trajectories, the two beams are equivalent to a two-component plasma which is at rest in the coordinate system moving with the average velocity of the particles. If the effective temperature of the electrons is rather low, the temperature of the protons must decrease until it is comparable with the temperature of the electrons (provided that multiple scattering at the residual gas can be disregarded). This means that the angular spread θ_p of the proton beam decreases to

$$\theta_p \sim \sqrt{\frac{m}{M}}\,\theta_e, \tag{1}$$

where θ_e denotes the relative "temperature-equivalent" velocity of the electrons; and m and M denote the mass of the electron and the mass of the proton, respectively. The characteristic time within which the "temperatures" are balanced is given by the formula

$$\tau = \frac{3}{2\sqrt{2\pi}}\,\frac{M}{m}\,\frac{1}{cr_e^2 n_e \eta L}\begin{cases}\gamma^2\left(\dfrac{T'_e}{mc^2}\right)^{3/2}, & \theta_p \ll \theta_e;\\ \beta^3\gamma^5\theta_p^3, & \theta_p \gg \theta_e.\end{cases} \tag{2}$$

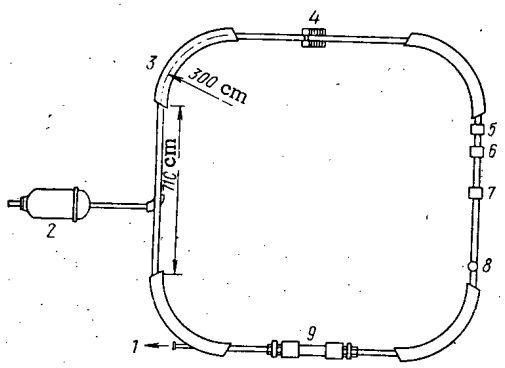

Fig. 1. Scheme of the NAP-M proton storage device: 1) neutral hydrogen atoms; 2) electrostatic injector (1.5 MeV); 3) deflecting magnet; 4) accelerating station; 5) slow sampler; 6) 3-μ quartz filament; 7) scanning magnesium jet; 8) scintillation counter; 9) section with electron beam.

The notation is interpreted as follows: n_e denotes the density of the electrons in the laboratory system; T'_e denotes the temperature of the electrons in the moving coordinate system; e and r_e denote the charge and the classical radius of the electron, respectively; η denotes the ratio of the length of the orbital section covered by the electron beam to the perimeter of this orbital section; and $L \approx 20$ is the Coulomb logarithm.

The kinetics of the real cooling process is more complicated. The considerations must include the specific features of the proton motion in the storage device, the influence of errors for the combination of the average velocities of protons and electrons, the inhomogeneities of the electron beam, coherent fluctuations in it, etc. These problems were theoretically treated in [2, 3], modelled on a computer in [3], and experimentally checked.

*Report presented to the National Conference on Accelerators (USA, Washington, March 1975).

Translated from Atomnaya Énergiya, Vol. 40, No. 1, pp. 49-52, January, 1976. Original article submitted June 2, 1975.

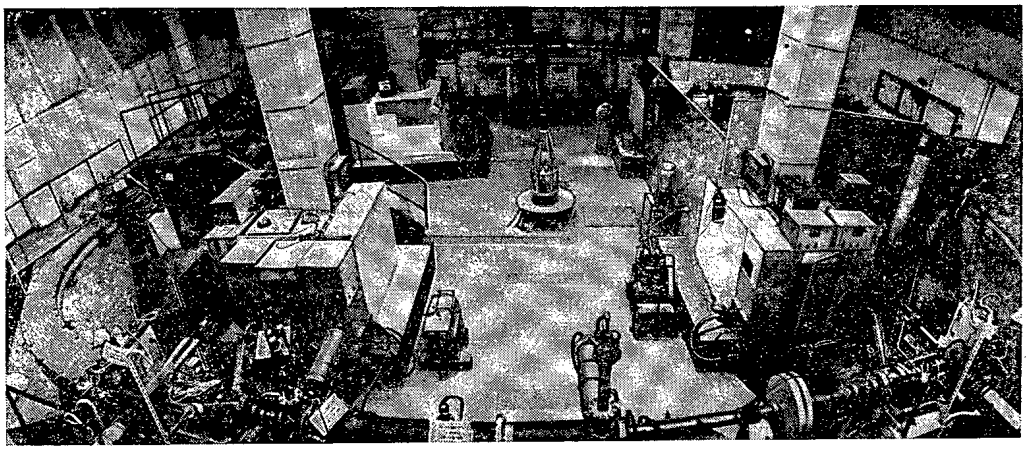

Fig. 2. View of the NAP-M proton storage device.

The experiments were made on the special NAP-M setup [4, 5] which is a model of the NAP anti-proton storage device from the "oppositely directed proton—anti-proton beam" project of the Institute of Nuclear Physics of the Siberian Division of the Academy of Sciences of the USSR [6] (Figs. 1 and 2). The basic parameters of the NAP-M storage device are as follows:

Proton energy, MeV	up to 150
Injection energy, MeV	1.5
Multiplicity factor	1
Radius of curvature of trajectories within magnets, m	3
Length of rectilinear gaps, m	7.1
Aperture of deflecting magnets, cm:	
vertical	7
radial	10
Aperture on cooling section, cm	6
Freq. of betatron oscillations:	
ν_z	1.24
ν_r	1.34
Coefficient of spatial contraction of orbits	0.8
Critical energy, MeV	110
Length of acceleration cycle, sec	30
Av. vacuum, torr	$(2\text{-}5)\cdot 10^{-10}$

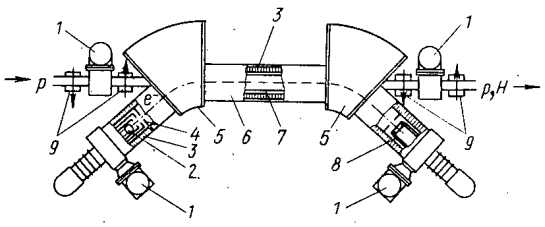

Fig. 3.

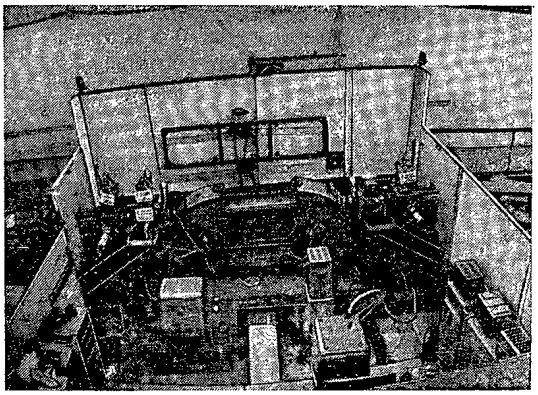

Fig. 4

Fig. 3. Scheme of the section with the electron beam: 1) magnetic discharge pumps; 2) electron gun; 3) solenoid coil; 4) anodes; 5) sections of beam deflection; 6) section of oppositely directed beams; 7) vacuum chamber; 8) collector; 9) adjusting magnets.

Fig. 4. View of the section with the electron beam.

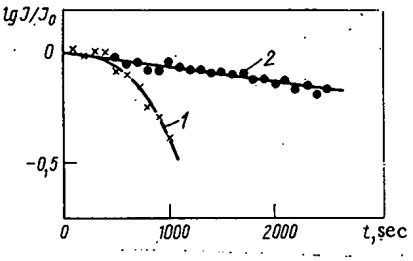

Fig. 5. Time dependence of the current represented by the proton beam.

The section with the electron beam (Figs. 3 and 4) is inserted in one of the rectilinear gaps of the storage device and has the following parameters:

Length of cooling section, m	1
Electron energy, keV	up to 100
Electron current, A	up to 1
Rel. transverse velocity of electrons	$2 \cdot 10^{-3}$
Stability of energy	$1 \cdot 10^{-4}$
Associated magnetic field, kG	1

An intensive electron beam with low transverse velocities is obtained with a special gun having three anodes; the gun is inserted into a uniform longitudinal magnetic field [6]. The energy of the electrons is recuperated in this section (this is very important at high energies): the potential of the collector differs from the potential of the cathode by 1-2 kV.

The typical parameters and the main results which to date have been obtained in an experiment are as follows:

Current of 50-MeV protons, μA	50
Current of 27-keV electrons, A	0.1
Diam. of electron beam, mm	10
Vacuum, torr	$5 \cdot 10^{-10}$

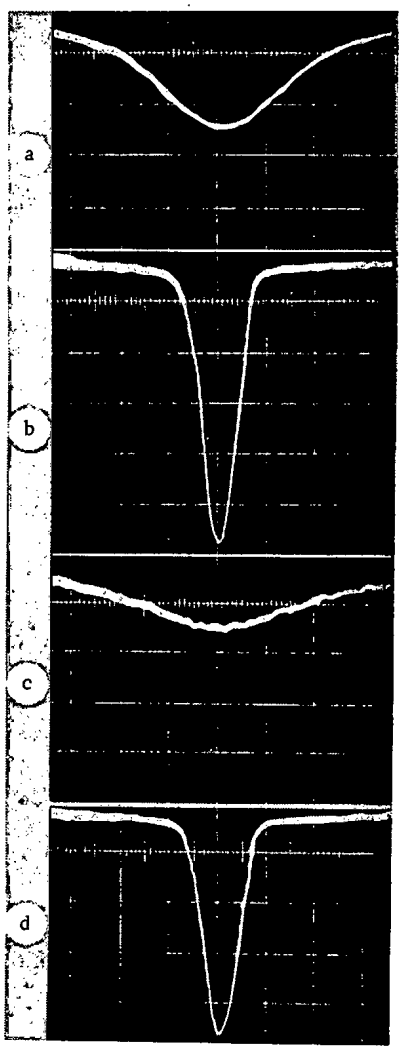

Fig. 6. Oscillogram of the vertical distribution of the protons: a) proton beam immediately after the acceleration, electron beam switched off; b) proton beam, 10 sec after switching on the electron beam; c) initially cooled proton beam, 200 sec after switching off the electron beam; d) the same beam, 10 sec after switching on again the electron beam.

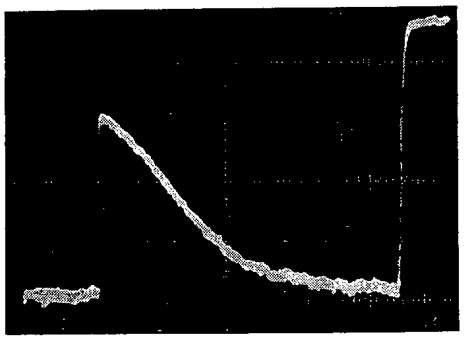

Fig. 7. Oscillogram of the time dependence of the density at the center of the proton beam.

Cooling time τ, sec	3
Stationary diam. of proton beam, mm	<1
Energy spread $\Delta E_p/E_p$ of proton beam	$<5\cdot10^{-5}$
Temp. T'_e of electrons, eV	0.2
Life time of protons, sec:	
without cooling by electrons	900
with cooling by electrons	5000

In the experiments under consideration, the high-frequency system was switched off after the acceleration and the protons could freely circulate in the constant magnetic field of the storage device. Then the longitudinal magnetic field was switched on and the cathode of the section with the electron beam was heated.

It was observed that the proton lifetime increases substantially when a beam of electrons having optimum energy is present. Figure 5 shows the time dependence of the proton current without cooling by electrons (curve 1) and with cooling by electrons (curve 2). There are two characteristic sections on curve 1: a plateau and an exponential drop. Immediately after the acceleration, multiple scattering only broadens the beam without causing losses (the protons lose their energy only by single scattering). From the time at which the boundary of the beam has reached the walls of the chamber, further broadening of the beam by multiple scattering eliminates the particles, so that the total losses increase approximately like the Coulomb logarithm (approximately 5 times in our case). When the cooling by electrons is switched on (curve 2), the multiple scattering is completely suppressed and an equilibrium diameter of the beam much smaller than the chamber diameter is reached. As in the first case, the lifetime is given by single-scattering events involving large angles. The process of cooling by electrons is accompanied by the formation of neutral hydrogen atoms resulting from the recombination of protons and electrons and having the energy of the protons [5]. The above temperature of the electrons was calculated disregarding the time of cooling; the above electron temperature was obtained from the stationary diameter of the proton beam and amounted to 0.2 eV.

Several methods were used to measure the diameter of the proton beam. The method in which a thin jet of magnesium vapor scans the beam over a single transverse diameter is the most convenient method; the secondary electrons are collected on a luminophor with the aid of an electrostatic field and recorded with a photomultiplier. In the experiment, a band-like jet with a cross section of 1×20 mm was shifted in vertical direction; the plane "of the band" was parallel to the beam. The magnesium vapor pressure in the jet was 10^{-6} torr. The signal was proportional to the vertical distribution of the protons. Figure 6 shows the signal obtained from the proton beam before and after cooling (a and b). When the electron beam is switched off, the peak is "smeared" by multiple scattering after a sufficiently long time; when cooling by electrons is switched on again, the same peak occurs, i.e., the diameter of the proton beam is reduced to 1 mm after the time required for cooling (c and d).

The above method can be used to determine the time dependence of the current density at a particular point in the chamber. To do this, the jet is kept fixed and the oscilloscope is triggered at the beginning of the acceleration. Figure 7 is an oscillogram of the time-dependent change of the density at the center of the beam after its impact on the inward-deflector: the signal amplitude at point 1 corresponds to the increased beam diameter; section 2 illustrates the beam compression and the increase in the particle density at the center of the beam; and point 3 corresponds to the signal amplitude outside the beam. All effects associated with cooling by electrons can be observed only if the proton velocity after acceleration and the electron velocity coincide in both magnitude and direction with an accuracy better than 10^{-3}. The effect disappears when the velocity differences are greater.

Some words on the application of cooling by electrons are in place. Of greatest interest is the possibility of storing intensive, compressed anti-proton beams for various purposes. Some classes of physics experiments which can be made since the cooling by electrons has been invented are listed below.

1. Research on proton—anti-proton interactions at high and superhigh energies involving oppositely directed beams with high brightness [7].

2. Using highly monochromatic cooled proton—anti-proton beams for investigations of narrow resonances.

3. Spectrometric experiments made with cooled beams of heavy particles on superfine internal targets (a target is considered superfine in this case, if multiple scattering in the target is smaller than the attenuation caused by cooling by electrons).

4. Generation (storage) of anti-proton beams of high intensity at low (of the order of MeV) energies. In this case, the bound proton—anti-proton (protonium) state can be investigated (under very well-defined conditions). The very efficient conversion (~1) of anti-protons into protonium can be obtained when one makes an anti-proton beam parallel to a moving beam of hydrogen atoms of the same average velocity as the anti-proton beam.

5. Generation and investigation of the properties (spectrum, etc.) of anti-atoms, i.e., of anti-hydrogen atoms which are generated by recombination of parallel beams of anti-protons and positrons stored in a special storage device. Experiments and calculations have shown that when a stored anti-proton beam is available, the beam can be fully converted into an anti-hydrogen jet. This means that we are not concerned with individual anti-atoms but rather with a dense, intense (of the order of 10^8–10^9 atoms/sec) jet of anti-hydrogen with a cross section of 1 mm^2 and a divergence angle of less 10^{-4}.

The authors take this opportunity to express their gratitude to all co-workers of the Institute who made possible the successful execution of the present work.

LITERATURE CITED

1. G. Budker, in: Proc. Intern. Symp. on Electron and Positron Storage Rings, Saclay, Sept. 26-30, 1966, Rep. II-1-1; G. I. Budker, At. Énerg., 22, No. 5, 346 (1967).
2. Ya. S. Derbenev and A. N. Skrinskii, Preprint [in Russian], IYaF SO Akad. Nauk SSSR, No. 225, Novosibirsk (1968).
3. G. I. Budker et al., 4th All-Union Conference on Accelerators of Charged Particles [in Russian], Moscow, November 18-20, 1974; Report No. XIII-2.
4. V. V. Anashin et al., 4th All-Union Conference on Accelerators of Charged Particles [in Russian], Moscow, November 18-20, 1974; Report No. XIII-3.
5. G. I. Budker et al., 4th All-Union Conference on Accelerators of Charged Particles [in Russian], Moscow, November 18-20, 1974; Report XIII-4.
6. V. I. Kudelainen, I. N. Meshkov, and R. A. Salimov, Zh. Tekh. Fiz., 41, 2294 (1971).
7. Proc. 8th Intern. Conf. on High-Energy Accelerators, Geneva, Sept. 20-24, 1971, p. 72.

THE USE OF MICROWAVE METHODS IN THE DOSIMETRY OF IMPULSE FLUXES OF IONIZING RADIATION

Yu. A. Medvedev, N. N. Morozov, B. M. Stepanov, and V. D. Khokhlov

UDC 621.387.422:533.9

At the present time, high-power pulsed sources of ionizing radiation are widely employed in physical investigations. Under these circumstances, dosimetrical monitoring during the radiation pulses is of particular interest from the point of view of obtaining correct solutions to physical problems.

In the case of dosimetry involving single pulses of ionizing radiation, we have to ensure a wide dynamic range and a high temporal resolution. These requirements are sufficiently well met by the shf method of plasma diagonostics. With the aid of microwave radiation, it is possible to determine the imaginary part of the complex high-frequency conductivity of ionized air σ_i which, when the condition $\nu_{eff} \ll \omega$ is observed (where ν_{eff} is the effective frequency of collision of electrons; ω is the cyclic frequency of the probe field), is proportional to the concentration of electrons [1] and must depend little on the distribution function of the electrons with respect to energy. We should note that for a nonsteady-state source of radiation at low air pressures, where the thermalization time of the fast electrons is comparable with the characteristic time of measurement of the ionizing-radiation flux, the distribution function of the electrons with respect to energy [2, 3] can differ considerably from an equilibrium distribution.

With sufficiently short pulses of ionizing radiation, i.e., when the loss of electrons due to deionization processes is insignificant during the pulse, the imaginary part of the conductivity can be linked by a linear relationship to the exposure dose, which is defined by

$$D = \frac{n}{2.08 \cdot 10^9} \frac{\rho_0}{\rho},$$

where n is the number of electron—ion pairs per cm^3, ρ_0 is the air density under normal conditions, ρ is the air density in the transducer.

For metrological determination of the exposure dose from the parameters of the air plasma, the authors carried out experimental and theoretical studies of the effect of a nonequilibrium state in the spectrum of the secondary electrons, formed in the final stages of the development of electron avalanches, on the conducting properties of the air subject to the nonsteady-state flux of ionizing radiation.

The air was ionized by pulsed beams of relativistic electrons from a linear accelerator having the following parameters: electron energy 4 MeV, duration of square-wave pulse of electrons 2.7 μsec, transmission frequency 400 Hz, maximum current in pulse 10^{-1} A. The complex conductivity of the plasma was measured by the resonator method. A three-dimensional cylindrical resonator with a Q of about 1600, in which E^0_{010} electromagnetic oscillations are excited at a frequency of $2.815 \cdot 10^{-9}$ Hz, provides us with a temporal resolution of not less than 10^{-7} sec. The end wall of the resonator at the electron-beam end is a grid of radial copper wires which is transparent to electrons.

When employed to create plasma, the electron beam is capable of ensuring a sufficiently uniform distribution of plasma within the plasma cavity of the resonator. For a resonator uniformly filled with plasma, the relative displacement of resonant frequency $\Delta\omega/\omega$ and the variation of the reciprocal of the factor of merit $\Delta(1/Q)$ are related to the real component of the complex conductivity σ_r and the imaginary

Translated from Atomnaya Énergiya, Vol. 40, No. 1, pp. 53-55, January, 1976. Original article submitted March 13, 1975.

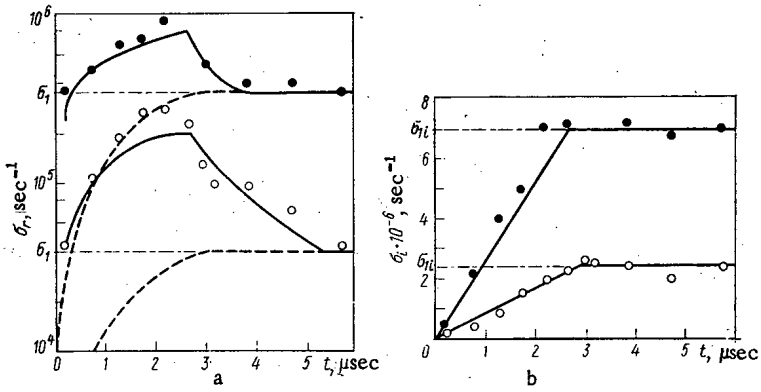

Fig. 1. The real (a) and imaginary (b) parts of the complex conductivity of air ionized by a pulsed electron beam, torr: ○) 1; ●) 3.

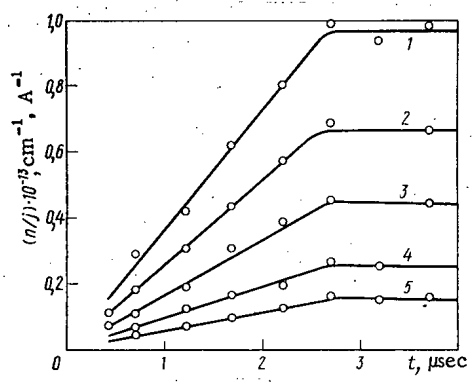

Fig. 2. Temporal relationship of the relative concentrations of electrons in the cavity of the resonator to the amplitude value of the density of the electron-beam current, torr: 1) 15; 2) 10; 3) 6; 4) 3; 5) 2.

part of the conductivity σ_i, respectively [3]

$$\frac{\Delta\omega}{\omega} = -\frac{2\pi\sigma_i}{\omega}; \quad \Delta\left(\frac{1}{Q}\right) = \frac{2\pi\sigma_r}{\omega}.$$

The method of measurement and the schematic of the measuring equipment are described in [4].

The measurements were carried out at an air pressure of 2 torr. Under these circumstances, the life of the electrons in air is significantly greater than the duration of the electron pulse and the time during which the parameters of the plasma are measured, which enables us to make some judgement regarding the development of nonequilibrium effects from the nonsteady-state features of the temporal relationship $\sigma_r(t)$ and $\sigma_i(t)$.

Figures 1a and 1b give the results of measurements at pressures of 1 and 3 torr. At the end of the electron pulse, after an interval $\tau \approx 3$ μsec at a pressure of 1 torr, $\sigma_r(t)$ reduces from its maximum value, existing at the end of the pulse, to some constant value σ_1. If the reduction in the number of electrons at this instant in time is taken into consideration, then the observed nonsteady-state condition can be related to the development of nonequilibrium effects, while σ_1 in this case corresponds to the conductivity of the thermalized electrons. A similar effect is not observed in the relationship $\sigma_i(t)$, however.

The influence of nonequilibrium effects on the plasma parameters can be estimated, assuming that the movement of a secondary electron in the energy gap is continuous and can be described by the relaxation equation [5]

$$dE = -\alpha(E)\,\nu(E)\,(E - E_0)\,dt, \tag{1}$$

where E is the energy of the electron; $\alpha(E)$ is the relative energy lost by the electron during one collision; $\nu(E)$ is the frequency of electron collisions; E_0 is the thermal energy of the molecule, which at the same time characterizes the extent of the Maxwellian distribution of thermalized electrons. Let us assume that the rate of formation of secondary electrons $q(t, E)$ in the interval of energy from E to E + dE per unit volume is known. Tracing the deceleration process of these electrons with the aid of Eq. (1) for the distribution function of the secondary electrons according to energy at that instant in time, we obtain an expression for the life of the electron

$$F(t, E) = \frac{1}{E(\alpha)\,\nu(E)\,(E - E_0)} \int_E^\infty q(t - t', E)\,dE', \tag{2}$$

where

$$t' = \int_E^{E'} \frac{dE''}{\alpha(E'')\,\nu(E'')\,(E'' - E_0)}.$$

From the experimental data [6, 7], on the relationships $\alpha(E)$ and $\nu(E)$ (1), we can satisfy ourselves that the deceleration time of an electron

$$\tau = \int_{2E_0}^{E_1} \frac{dE}{\alpha(E)\,\nu(E)\,(E-E_0)}$$

does not depend on its initial energy E_1 in the case where $\sqrt{E_1} \gg \sqrt{E_0}$. In this case, we can ignore the presence in the plasma of electrons for which $\sqrt{E} \gg \sqrt{E_0}$, while for parameters only slightly dependent on energy, we can assume a constant value of $\alpha = 1.7 \cdot 10^{-3}$ [6], the collision cross-section of the electrons with air molecules being $6 \cdot 10^{-16}$ cm^2 [7].

As we know from [3], the real part σ_r and imaginary part σ_i of the conductivity of a nonequilibrium plasma can be found from the expressions:

$$\sigma_r = -\frac{4\pi}{3}\frac{ne^2}{m}\int_0^\infty \frac{\nu}{\omega^2+\nu^2}\frac{\partial F(v)}{\partial v}v^3\,dv;$$

$$\sigma_i = \frac{4\pi}{3}\frac{ne^2}{m}\int_0^\infty \frac{\omega}{\omega^2+\nu^2}\frac{\partial F(v)}{\partial v}v^3\,dv,$$

where m, e, and v are the mass, charge, and speed of the electron, respectively; F(v) is the distribution function of the electrons with respect to speed.

To calculate the conductivity of the plasma, we use distribution function (2). In this case, we assume that $q(t, E) = N\delta(E - E_1)$, where $E_1 = 10$ eV (a monochromatic source of electrons). The rate of formation of the secondary electrons per unit volume can be found by measuring σ_i, corresponding to a uniform distribution of electrons with respect to energy (Fig. 2). The results of the calculation do not depend on E_1, provided that $\sqrt{E_1} \gg \sqrt{E_0}$; therefore, when E varies from 1 to 10 eV, the conductivity of the plasma varies within the range of 5%.

Comparing the results of numerical calculations of σ_r using the distribution function given (the continuous curve of Fig. 1a) with the results obtained on the assumption of a Maxwellian distribution of electrons (dashed curves) shows that when $t < \tau$, the high-frequency conductivity is roughly one order of magnitude greater than the uniform value. The imaginary part of the plasma conductivity σ_i under the conditions $\omega \gg \nu_{eff}$ does not depend on the form of the distribution function of the electrons with respect to energy, and can be described by the uniform equation.

This is in close accord with the results of experiments. The relationship n(t) was found from the experimental relationship $\sigma_i(t)$ by means of the expression obtained on the assumption of an equilibrium plasma [1], and this coincides in form (see Fig. 2) with the integral of the radiation intensity.

Consequently, from the relationship $\sigma_i(t)$ during a pulse of radiation of duration $T \ll \theta$, (where θ is the life of an electron in air), we can determine the exposure dose

$$D(t) = -\frac{m\omega}{2.08 \cdot 10^9 e^2}\frac{\rho_0}{\rho}\sigma_i(t).$$

From the data given in [4] within the range of concentrations of electrons $n \leqslant 10^{10}$ cm^{-3}, where electron—ion recombination does not take place, the life of the electrons in air has a maximum value of $\theta \approx 10^{-4}$ sec at an air pressure of 1-10 torr. When $p \leqslant 1$ torr, the life of the electrons is reduced, due to the loss of electrons by diffusion.

The shf method of plasma diagnosis is used in the range of electron concentrations 10^7-10^{13} cm^{-3}, which for an atmospheric pressure of ~10 torr corresponds to the range of exposure doses 1-10^6 R. However the upper limit of application of such a method with air-filled transducers is really 10^4-10^5 R. This limitation is due to the reduction in the life of the electrons in air at electron concentrations > 10^{10} cm^{-3} arising out of the fact that the predominant process of electron loss in this case is electron—ion recombination. The use of this method when $D \geqslant 10^4$ R is permissible only when the condition that the duration of the radiation pulse $T \ll 1/(10D)$ is observed.

We should note that the range of recording times and the range of measured doses can be extended considerably by employing gases for which the electron lives are significantly greater than is the case in air: The inert gases, for example.

Many present-day sources of pulsed ionizing radiation flux (x-ray tubes, accelerators, impulsed

reactors, etc.) operate in the range $1-10^4$ R in pulses with characteristic times of dosage measurement of $10^{-5}-10^{-7}$ sec, so that the proposed method is suitable for widespread use in studies concerned with the employment of such equipment.

LITERATURE CITED

1. V. E. Golant, Superhigh-Frequency Methods of Investigating Plasma [in Russian], Nauka, Moscow (1968).
2. Yu. A. Medvedev and B. M. Stepanov, Prikl. Matem. i Teor. Fiz., No. 4, 3 (1970).
3. L. L. Mar'yanovskaya and Yu. A. Medvedev, Geomagn. i Aeronom., 11, 290 (1970).
4. G. L. Kabanov et al., Zh. Tekh. Fiz., 43, No. 6, 1275 (1973).
5. V. L. Ginzburg, The Propagation of Electromagnetic Waves in Plasma [in Russian], Nauka, Moscow (1967).
6. Ya. B. Zel'dovich and Yu. P. Raizer, The Physics of Impulse Waves and High-Temperature Hydrodynamic Phenomena [in Russian], Nauka, Moscow (1966).
7. I. Shkarovskii, T. Johnstone, and M. Bachinskii, The Kinetics of Plasma Particles [Russian translation], Atomizdat, Moscow (1969).

UNIVERSAL ABSORPTION CURVES FOR A SINUSOIDALLY MODULATED ELECTRON BEAM

R. Ya. Strakovskaya, I. R. Entinzon, and G. N. P'yankov

UDC 539.171.4

Curves have been computed for the absorption of a sinusoidally modulated electron beam for various materials and for electron spectra of maximum energies 0.4, 0.35, 0.30, and 0.25 MeV [1]. It has been assumed that the overall effect on the absorber from electrons of different energies is the superposition of the result from monoenergetic beams.

The calculations were performed for the following materials: cellulose triacetate, cellophane, polymethylmethacrylate, polyethylene, polyester resin, atmospheric oxygen, boron, sodium, aluminum, titanium, lead, barium titanate, silica, and borosilicate glass. Differential curves were calculated (Fig. 1) showing the dose rate as a function of depth in the absorber, and also integral curves (Fig. 2) for the total absorbed dose as a function of depth. The calculations for the sinusoidally modulated beam F_{sm} were also accompanied by ones for a monoenergetic beam F_m. We also calculated the stopping power averaged over all energies in the spectrum and the mean electron energies for the sinusoidal-modulation case.

We found that the differential and integral absorption curves could be represented by a universal curve for the various substances and energies.

An appendix gives results on the stopping powers, ranges, and average stopping powers for this series and these energies. An ALGOL-60 program is also appended.

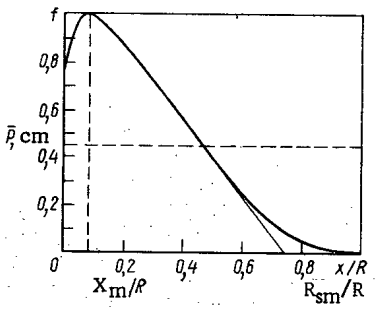

Fig. 1

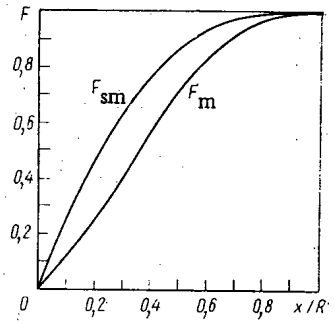

Fig. 2

Fig. 1. Depth distribution of dose rate from a sinusoidally modulated x-ray beam: (f) absorbed dose in relative units; x/R) absorber depth as a fraction of range of most energetic electrons in beam; $\bar{P}_{sm}$) dose rate averaged over range; R_{sm}/R) practical range of sinusoidally modulated beam in relative terms).

Fig. 2. Integral absorbed dose rates F_m and F_{sm} for monenergetic and sinusoidally modulated electron beams against x/R (absorber depth in relative units).

Translated from Atomnaya Énergiya, Vol. 40, No. 1, p. 56, January, 1976. Original article submitted April 7, 1975.

DOSIMETRY ON AN OBJECT ROTATING IN AN ELECTRON BEAM

R. Ya. Strakovskaya, G. N. P'yankov, and Yu. F. Golodnyi

UDC 539.171.4

We have determined the absorbed dose for a cylindrical rotating object exposed to a collimated electron beam.

The dose received in one turn is dependent on the shape of the dose-rate curve, the distance between the object and the accelerator window, and also on the radius of the object and the period of rotation.

Approximate solutions for use in dosimetry are given in view of the complexity of the calculations.

Two limiting cases are discussed:

1. Object Radius Much Less Than Beam Width. In this case one can assume that the object rotates in a uniform radiation field giving a dose rate P_0, which corresponds to the peak in the distribution; the dose in one turn is given by

$$D_1 = 2\int_0^{T/4} P_0 \cos \omega t \, dt = \frac{P_0 T}{\pi},$$

where P_0 is the dose rate, T is the rotation period, and $\omega = 2\pi/T$; then the dose received by the object in such a field is less by a factor π than that for an immobile object. It has been shown [1] that the dose in a rotating object is one-third of that in an immobile one.

2. Size of Object Much Greater Than Beam Width ($r \gg a$, where a is the beam half-width). If $D_1 = \int_0^T P_1(t)dt$, then after replacing the variable t by x we get

$$D_1 = \frac{T}{2\pi r}\int_{-\infty}^{\infty} P(x)\, dx.$$

The area under the dose-rate distribution curve for the beam cross section is proportional to the accelerator current, and the coefficient of proportionality is dependent on the distance between the object and the window:

$$\int_{-\infty}^{\infty} P(x)\, dx = K_H I_{acc}.$$

In this case

$$D_1 = \frac{K_H I_{acc} T}{2\pi r},$$

where H is the distance between the object and the window, P_X is the peak in the distribution, I_{acc} is the accelerator current, P(x) is the shape of the dose-rate in the beam cross section.

The result for the dose applies for $r \gg a$, i.e., when the irradiation is as for a planar object moving uniformly along the x coordinate. The coefficient of proportionality K_H can be determined fairly accurately by experiment by moving a dose meter along the x coordinate at a constant speed.

Translated from Atomnaya Énergiya, Vol. 40, No. 1, p. 57, January, 1976. Original article submitted April 7, 1975.

In intermediate cases, the radius of the object is comparable with the beam size, and then one can assume that the object is exposed to a beam of rectangular cross section of height P_0 and equivalent width $2\bar{a}$, which is determined from the area of the cross section at P_0. If the size of the component is greater than the equivalent beam width, we have

$$D_1 = 2\int_0^{\arcsin(\bar{a}/r)} P_0 \cos \omega t \, dt = \frac{P_0 T}{\pi} \frac{\bar{a}}{r} .$$

If these formulas are used, one has to incorporate also the depth dose distribution in the rotating object, which is very similar to that for isotropic incidence of an electron beam [2].

Tests were performed on cylindrical objects of various radii with the ELT-1.5 accelerator [3] and showed that these approximate formulas are suitable for dose calculation.

LITERATURE CITED

1. K. Chadwick, Intern. Symp. on Food Irradiation, Wageningen, Netherlands (1966), p. 91.
2. R. Ya. Strakovskaya, G. N. P'yankov, and I. R. Entinzon, At. Énerg., 36, No. 4, 302 (1974).
3. E. A. Abramyan and V. A. Gaponov, At. Énerg., 20, No. 5, 385 (1966).

CALCULATIONS ON WEAKLY INTERACTING SYSTEMS

V. P. Ginkin

UDC 517.9:621.039.5

The paper by R. Avery, in: Physics of Nuclear Reactors, A. I. Leipunskii and V. S. Fursov (editors), Vol. 3, Pt. 2, Atomizdat, Moscow (1959), p. 321 gave a matrix equation for the reactivity of a system of interacting breeding assemblies in terms of integral parameters, which themselves give an exhaustive characterization of the individual assemblies and the coupling between them. These parameters are the effective multiplication factor for one assembly k_{ef}^{1} for $\nu = 0$ in all assemblies apart from the given one, together with the interaction parameter g for two assemblies, which is defined as the probability that a neutron generated in one assembly produces a neutron of the next generation in the other assembly. An analytical solution is given to this equation for line, planar, and spatial lattices of identical assemblies, for the case where each assembly interacts with the first layer of assemblies surrounding it. The solution is based on approximate replacement of the matrix equation for the boundary-value problem of the first kind; formulas are derived for the effective multiplication factor for a lattice with an arbitrary number of assemblies. In the linear case

$$k_{ef}^{(m)} = k_{ef}^{(1)} + q\left[2 - \frac{\pi^2}{(m+1)^2}\right],$$

where m is the number of assemblies and q is the interaction parameter. For the planar case:

$$k_{ef}^{(m,n)} = k_{ef}^{(1)} + 2(q_{1,0} + q_{0,1} + 2q_{1,1}) - \pi^2\left[\frac{q_{1,0} + 2q_{1,1}}{(m+1)^2} + \frac{q_{0,1} + 2q_{1,1}}{(n+1)^2}\right],$$

where $q_{\alpha,\beta}(\alpha, \beta = 0,1)$ are the interaction parameters for assemblies (i, j) and $(i \pm \alpha, j \pm \beta)$, with m and n the numbers of assemblies along the X and Y axes. For the three-dimensional case

$$K_{ef}^{(m,n,l)} = K_{ef}^{(1)} + 2(q_{1,0,0} + q_{0,1,0} + 2a) - \pi^2\left[\frac{q_{1,0,0} + 2a}{(m+1)^2} + \frac{q_{0,1,0} + 2a}{(n+1)^2} + \frac{q_{0,0,1} + 2a}{(l+1)^2}\right],$$

where $a = q_{1,1,0} + q_{1,0,1} + 2q_{1,1,1}$; $q_{\alpha,\beta,\gamma}(\alpha, \beta, \gamma = 0,1)$ are the parameters for the interaction between assemblies (i, j, k) and $(i \pm \alpha, j \pm \beta, k \pm \gamma)$, with m, n, and l the numbers of assemblies along the X, Y, and Z axes.

The errors of these formulas are comparatively small, and they decrease rapidly as the number of assemblies increases. In particular, the error in $k_{ef} \approx 0.5\%$ for the linear case with 5 assemblies.

The paper also gives the theoretical or experimental method of finding the interaction parameters for two assemblies. Criteria are given for evaluating the nuclear safety conditions.

Translated from Atomnaya Énergiya, Vol. 40, No. 1, pp. 57-58, January, 1976. Original article submitted April 9, 1975.

LETTERS TO THE EDITOR

SELF-ACCELERATION EXPERIMENT OF A STRONG ELECTRON BEAM IN A FERRITE ACCELERATING STRUCTURE

V. V. Zakutin, N. N. Nasonov,
A. A. Rakityanskii, and A. M. Shenderovich

UDC 621.384.6:621.384.364.3

It has been suggested that a strong electron beam can be self-accelerated as a result of either the betatron effect [1, 2] or by magnetic moment precession [3]. As proved by theoretical analysis [4], the increment in beam energy in the latter case is

$$\Delta\varepsilon = 2\cdot 10^{-9} l \Delta I \ln\frac{r_1}{r^2}\frac{\gamma^2 B^2}{\omega_p\,(1+\omega_p^2\tau^2)}\,[\sin\omega_p t+\omega_p\tau^{-t/\tau}(e-\cos\omega_p t)],$$

where l, r_1, and r_2 are the length and the outside and inside radii of the ferrite in cm, ΔI is the beam current drop in A, τ is the beam current drop time constant in sec, and $\omega_p = \gamma\sqrt{BH_z}$ (here γ is the gyromagnetic ratio, H_z is the longitudinal magnetic field, and B is the saturation induction of the ferrite).

However, no pertinent data are available on electron-beam acceleration by such methods. Here we describe an experiment on electron-beam acceleration with the aid of a ferrite structure.

The electron source was a cold-cathode electron gun EG (see Fig. 1). A voltage pulse U_g = 150 kV, provided by pulse generator PG with 100-Ω internal resistance, was applied to the gun. The voltage U_g was measured with a resistive voltage divider R_3R_2 (R_3 = 1500 Ω, R_2 = 5 Ω); the beam current (up to 1 kA), with the aid of a resistance ring (R_1 = 1 Ω). The beam has been transported for a distance of 2 m within a vacuum ceramic tube with a 35-mm aperture by means of a longitudinal magnetic-field pulse H_p produced by solenoid S_1. The magnetic field intensity was varied between 100 and 5000 Oe. The pressure in the tube was 10^{-3}-10^{-5} torr. At the exit of the ceramic tube, the beam current was calculated from the voltage drop it produces across R_4 (3 Ω) connected to the foil F. The experiments were carried out with a beam current of 100 to 200 A at the exit of the ceramic tube.

The accelerating system consisted of a set of type 60 NN ferrite rings FR with l, r_1, and r_2 equal to 200, 9, and 2 cm, respectively. The particle energy was determined by measuring the intensity of the beam passing through a replaceable foil F at the ceramic tube exit; the foil thickness varied from 20 to 200 μ. The current of the beam which passed the foil was measured from the voltage drop produced across

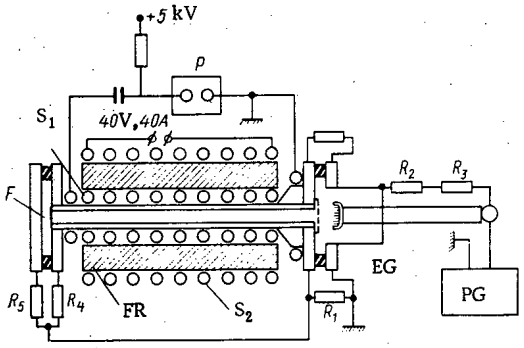

Fig. 1. Experimental setup.

Translated from Atomnaya Énergiya, Vol. 40, No. 1, pp. 59-60, January, 1976. Original article submitted March 17, 1975.

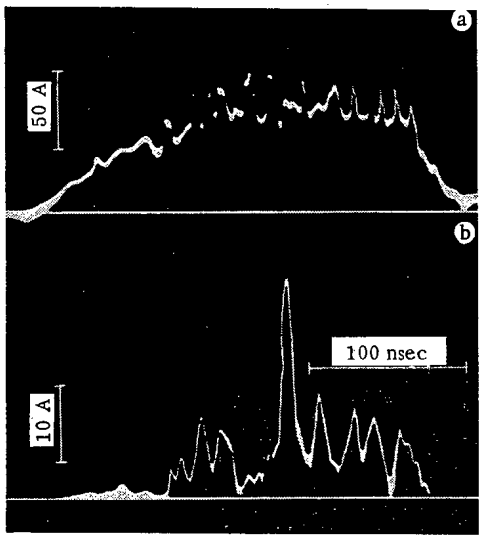

Fig. 2

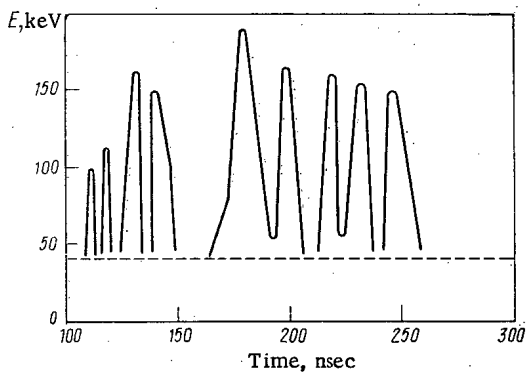

Fig. 3

Fig. 2. Oscillograms of current pulse at the ceramic tube exit (a) and of the current pulse that passed through a 100-μ foil (b).

Fig. 3. Beam energy as a function of time. Time is reckoned from the start of the beam current pulse. E_0 = 100 keV.

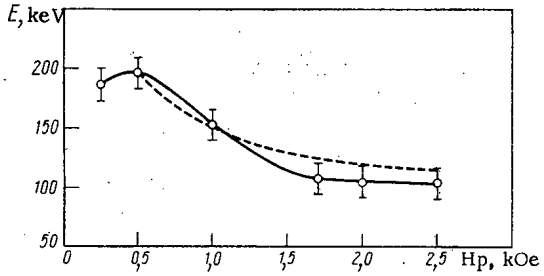

Fig. 4. Accelerated beam energy as a function of focussing magnetic field for E_0 = 100 keV: experimental and theoretical curves shown by solid and broken lines respectively (experimental and theoretical data are assumed to be the same at H_p = 500 Oe).

R_5. All measurements (R_1, R_2R_3, R_4, and R_5) were made with nanosecond resolution.

The experiments confirmed that a beam traveling along the axis of ferrite cores is self-accelerated. Measurement of absorption in the foil proved that a beam with an initial energy equal to 110 keV is accelerated to a maximum energy of 220 keV. The beam energy has been thus doubled.

Figure 2 shows typical oscillograms of a beam current pulse at the ceramic tube exit and of a current pulse that passed through foil F. The position of the accelerated particle peaks in oscillogram b coincides with neither the leading nor trailing edge of the total current pulse. It can be thus assumed that the effect of self-acceleration is due to abrupt changes in the azimuthal magnetic field H_φ caused by rapid fluctuations of beam intensity on the pulse top (see Fig. 2a). Since the input current to the accelerating system is unmodulated, these fluctuations are excited by the development of a longitudinal instability (the mechanism of the development of such an instability in an unsaturated ferrite has been discussed in [5]).

Figure 3 shows the energy of accelerated particles as a function of time calculated from absorption factors in the foil. The figure shows that the energy varies in time in an oscillatory manner (no data are given for energies below 40 keV because of very high errors). The total energy increment of all accelerated particles is 0.25 J amounting to 15% of the total starting beam energy of 1.7 J. The charge on the accelerated particles is 30% of the total charge of particles before acceleration.

In the course of measurements we have observed a significant dependence of the acceleration effect on magnitude of the focussing field H_p produced by the inner solenoid S_1 (Fig. 4). The energy increment decreases with increasing H_p (> 500 Oe). This behavior is associated with the fact that the focussing field of solenoid S_1 penetrates the ferrite and saturates it when H_p = 500 Oe. Measurements proved that no acceleration effect took place without the ferrite. It can be thus assumed that self-acceleration is associated with precession of the magnetic moment in saturated ferrite. The drop in ε at H_p < 500 Oe can then be explained by the decrease in the total magnetic moment of the precessing ferrite. As seen in Fig. 4, experimental data agree with theoretical calculations. However, the expression corresponds to shock excitation

of the magnetic moment precession, whereas the effect of self-acceleration is, as noted above, probably associated with the development of a longitudinal nonstability. Thus, a comprehensive understanding of the mechanism of self-acceleration requires a theoretical analysis of the instability of a beam interacting with gyrotropic ferrite.

LITERATURE CITED

1. B. N. Rodimov, Dissertation [in Russian], Izd. Tomsk. Polytekhn. In-ta, Tomsk (1967).
2. Yu. A. Bashmakov et al., Brief Communications in Physics [in Russian], No. 5 (1971), p. 10.
3. A. A. Rakityanskii and A. M. Shenderovich, in: Proceedings of the Symposium on Collective Acceleration Methods [in Russian], Izd. JINR, Dubna (1972), p. 129.
4. N. N. Nasonov and A. M. Shenderovich, Izv. Vyssh. Uchebn. Zaved., Radiofiz., 17, No. 6, 909 (1974).
5. V. K. Grishin, Zh. Tekh. Fiz., 42, 9 (1972).

DETERMINATION OF THE HALF-LIFE OF ^{238}Pu

V. G. Polyukhov, G. A. Timofeev,
P. A. Privalova, V. Ya. Gabeskiriya,
and A. P. Chetverikov

UDC 546.799.4:539.163

Up to 1950, several determinations were made of the half life of ^{238}Pu ($T_{\alpha 238}$). The values obtained range from 30 to 99 yr [1]. In 1950 Jaffey and Lerner [2] found $T_{\alpha 238}$ = 89.59 ± 0.37 yr, and in 1957 Hoffman et al. [3] published the value 86.41 ± 0.30 yr. In 1972, Hastings and Strohm, in determining the period of spontaneous fission of ^{238}Pu, used the value 87.77 ± 0.03 yr, with a reference to a private communication from Jordan [4]. Thus at present there is some uncertainty in the value of the half life of ^{238}Pu.

In this article we give the results of a determination of $T_{\alpha 238}$. In our experiments we used ^{238}Pu formed by the decay of ^{242}Cm and subjected to careful radiochemical purification. The isotopic composition of the plutonium, found by means of an MI-1311 mass spectrometer, was as follows: ^{238}Pu (99.82 ± 0.02); ^{239}Pu (0.08 ± 0.02); ^{240}Pu (0.10 ± 0.02) atm %. (Here and below, all the experimental errors are quoted for the 95% confidence interval.)

The radiochemical purity of the plutonium was monitored by α and γ spectrometry. No foreign alpha emitters were found in the plutonium preparation.

Plutonium dioxide, which according to the spectral analysis data contained about 1 mass % of inert impurities, was dissolved and subjected to additional purification by precipitation of the hydroxide and then the oxalate of plutonium (IV) which was heated for 4 h at 850°C. The resulting plutonium dioxide was redissolved in concentrated nitric acid and the solution diluted to 1 M with respect to HNO_3. The concentration of ^{238}Pu in this initial solution was found by automatic coulommetric titration [5] and isotopic dilution [6]. As a tracer for the isotopic dilution we used a standard solution of ^{239}Pu prepared by dissolving a weighed portion of 1.1832 g of metallic plutonium in hydrochloric acid. Before measuring the mass spectra (before and after mixing with the tracer solutions) we treated the ^{238}Pu solutions with hydrogen peroxide with heating to bring the plutonium into the same chemical state. In each determination we measured at least 20 mass spectra. The mass concentrations were calculated by the method in [6].

In all we made 17 coulommetric and 11 mass-spectrometric determinations of the mass concentration of ^{238}Pu in the initial solution. From the results of the coulommetric analysis we found that the concentration of ^{238}Pu was 0.28282 ± 0.00299 mg ^{238}Pu/g; for the mass-spectrometric analysis the corresponding figure was 0.28280 ± 0.00241 mg ^{238}Pu/g. In the calculations we used the weighted mean of 0.28281 ± 0.00030 mg ^{238}Pu/g solution.

The absolute value of the specific α activity of ^{238}Pu ($Q_{\alpha 238}$) was determined by measuring the α activity of an aliquot solution with a flow-type proportional $4\pi\alpha$ counter and with a small-solid-angle counter operating according to the principles described in [7]. The method of determining the specific α activity by the method of $4\pi\alpha$ measurement and the method of processing the experimental results were similar to those described in [8].

The collimator diameter of the small-solid-angle counter was 10.000 ± 0.002 mm, the cylindrical part was 0.030 ± 0.002 mm long. As the alpha-ray detector we used a Si(Au) surface barrier detector. The preparations for the alpha measurements were disks of stainless steel Grade Kh18N9T, 0.50 ± 0.05 mm thick and 25.00 ± 0.05 mm in diameter. The diameter of the active spot in the center of the disk was 10.0 ± 0.5 mm. To obtain uniform distribution of the plutonium over the area of the substrate, before

Translated from Atomnaya Énergiya, Vol. 40, No. 1, pp. 61-62, January, 1976. Original article submitted March 18, 1975.

TABLE 1. Results of Determination of $\bar{\bar{Q}}_{\alpha 238}$

$4\pi\alpha$ measurements						Small-solid-angle counter			
							H_1	H_2	H_3
n*	$Q_{\alpha 238}$	n	$Q_{\alpha 238}$	n	$Q_{\alpha 238}$	n	$Q_{\alpha 238}$	$Q_{\alpha 238}$	$Q_{\alpha 238}$
1	6,2686	21	6,3347	41	6,3451	1	6,5376	6,6173	6,6427
2	6,5932	22	6,2735	42	6,3442	2	6,4557	6,4716	6,4741
3	6,3006	23	6,5248	43	6,3744	3	6,2254	6,2029	6,3167
4	6,3734	24	6,5598	44	6,5494	4	6,2781	6,2656	6,3126
5	6,4988	25	6,4496	45	6,4765	5	6,4159	6,4766	6,4444
6	6,3285	26	6,4201	46	6,3705	6	6,1986	6,2832	6,1610
7	6,5558	27	6,4230	47	6,4857	7	6,3694	6,4664	6,3063
8	6,3173	28	6,2029	48	6,3788	8	6,3922	6,4359	6,4917
9	6,3100	29	6,3306	49	6,1502	9	6,4274	6,4446	6,4639
10	6,3254	30	6,3911	50	6,3983	10	6,3106	6,3846	6,4941
11	6,5180	31	6,3507	51	6,3746	11	6,4526	6,5455	6,4442
12	6,4753	32	6,3280	52	6,5677	12	6,3708	6,4162	6,4589
13	6,3669	33	6,4405	53	6,3944	13	6,2360	6,1636	6,0338
14	6,6954	34	6,3632	54	6,2138	14	6,4192	6,4217	6,4415
15	6,5554	35	6,3171	55	6,1338	15	6,4424	6,5250	6,5026
16	6,5991	36	6,2790	56	6,5362	16	6,3711	6,4326	6,2686
17	6,3956	37	6,4811	57	6,2309	17	6,3023	6,3399	6,2305
18	6,5066	38	6,3709			18	6,3100	6,3409	6,3483
19	6,2228	39	6,4106			19	6,3572	6,4320	6,4650
20	6,5991	40	6,2165			20	6,4041	6,4401	6,4152
	$\bar{Q}_{\alpha 238}\times 10^{-11} = 6,3965 \pm \pm 0,0326$		$\bar{\bar{Q}}_{\alpha 238} = (6,389 \pm 0,029) \times 10^{11}$ counts $\cdot$ sec$^{-1} \cdot$ g^{-1}				6,3638± 0,0458	6,4053± 0,0551	6,3858± 0,0664

*Preparation number.

adding the aliquot solution the spot was treated with insulin solution. The measurements were made in a vacuum of $2 \cdot 10^{-2}$ mm Hg. The design of the counter permitted us to make absolute measurements of the α activity of the preparations with three different, accurately known distances between the active spot on the preparation and the upper plane of the collimator: $H_1 = 80.40 \pm 0.05$ mm, $H_2 = 100.15 \pm 0.05$ mm, $H_3 = 120.22 \pm 0.05$ mm. The corresponding solid angles Ω, calculated by means of the expressions in [9], were (in fractions of the complete sphere): $\Omega_1 = (9.613 \pm 0.020) \cdot 10^{-4}$; $\Omega_2 = (6.2080 \pm 0.0077) \cdot 10^{-4}$, and $\Omega_3 = (4.3132 \pm 0.0043) \cdot 10^{-4}$. The errors in the determination of the solid angle were limiting and are due to errors in measuring the geometrical dimensions of the small-solid-angle counter and the diameter of the active spot of α preparations.

From the initial solution, by a gravimetric method based on the number of dilutions, we prepared eight series of α preparations for $4\pi\alpha$ measurements and four for measurement with the small-solid-angle counter. Each series consisted of at least five α preparations. Each preparation was measured at three points on the alpha plateau and five times at each point. The statistical error of the separate measurements was not worse than ±2%.

The results of our determination of the specific α activity of ^{238}Pu, calculated from the results of the $4\pi\alpha$ measurements and the measurements with the small-solid-angle counter, are listed in Table 1. In calculating the values of $Q_{\alpha 238}$ from the measurements, we made corrections for the decay of ^{238}Pu during the time between the moment of determination of the mass concentration of ^{238}Pu in the initial solution and the time of the α measurements. For this purpose we used a preliminary value of the half-life, 87 yr, found from the $4\pi\alpha$ count. In our case the maximum correction for decay did not exceed 0.72%. Calculations revealed that the uncertainty in the value of the half-life, equal to ±5 yr, led to an error of ±0.04% in the final result.

The rms errors in the results of determination of $\bar{Q}_{\alpha 238}$ given in Table 1, as well as errors due to the preparation and measurement of the specimens, contain the limiting errors of determination of the solid angle (for measurements on the small-solid-angle counter) and errors due to inaccuracies in the error for decay (0.04%).

The value $\bar{\bar{Q}}_{\alpha 238}$, equal to $(6.389 \pm 0.029) \cdot 10^{11}$ counts $\cdot$ sec$^{-1} \cdot$ g^{-1}, is the weighted mean. The final error of its determination includes the errors of determination of the concentration of ^{238}Pu in the initial solution (0.11%) and of determination of the isotopic composition of the plutonium (0.02%). The half-life $T_{\alpha 238}$, calculated from the value found for $\bar{\bar{Q}}_{\alpha 238}$, is 86.98 ± 0.39 yr (P = 0.95). In this calculation we have

assumed the following values: 1 yr = $3.15576 \cdot 10^7$ sec; ln 2 = 0.693147; $N_0 = 6.02252 \cdot 10^{23}$ mole^{-1}; atomic weight of ^{238}Pu, 238.0495 (on the ^{12}C scale) [10]. The value found for $T_{\alpha 238}$ is closest to that published in [3], and is 3% lower than that in [2].

LITERATURE CITED

1. G. Seaborg, in: The Actinides [Russian translation], IL, Moscow (1955), p. 173.
2. A. Jaffey and J. Lerner, ANL-411, 13 Feb., 1950 (cited in [1]).
3. D. Hoffman, G. Ford, and F. Laurence, J. Inorg. and Nucl. Chem., 5, 6 (1957).
4. K. Jordan, in: J. Hastings and W. Strohm, J. Inorg. and Nucl. Chem., 34, 25 (1972).
5. G. A. Simakin et al., Zh. Analiticheskoi Khim., 29, No. 8, 1385 (1974).
6. R. Webster, in: Progress in Mass Spectrometry [Russian translation], IL, Moscow (1963), p. 107.
7. A. Jaffey [1], p. 519.
8. V. G. Polyukhov et al., At. Énerg., 36, No. 4, 319 (1974).
9. K. A. Petrzhak and M. A. Bak, Zh. Tekh. Fiz., 25, No. 4, 636 (1955).
10. V. A. Kravtsov, The Masses of Atoms and the Binding Energies of Nuclei [in Russian], Atomizdat, Moscow (1965), p. 359.

THE HIGH-TEMPERATURE THERMAL DIFFUSIVITY AND ELECTRICAL RESISTIVITY OF YTTRIUM AND GADOLINIUM

I. I. Novikov and I. P. Mardykin

UDC 669.854.536.2

The results of an investigation of the specific heats of yttrium and gadolinium at high temperatures (> 1000°K) were published in [1]. In this report we give data on the thermal diffusivity of Y and Gd and the electrical resistivity of gadolinium at T > 1100°K.

These investigations were prompted by the small number of published data, their large discrepancies, and the narrowness of their temperature range.

The thermal diffusivity was measured by the method of radial temperature waves based on one variety of regular thermal field of the third order. The thermal diffusivity can be determined either by means of the phase of the first harmonic of the temperature oscillations, or by means of the difference between the times corresponding to the maximum temperature and the moment of switching on the periodic electronic heating of the specimen [2].

We investigated yttrium of 99.8% purity and gadolinium of 99.75% purity, in the form of hollow cylinders 7 cm long with external diameters of 15 mm and internal diameters of 6 mm. The impurity content of the yttrium was as follows (in percent): Gd, Tb, Dy, Ho < 0.1; Fe < 0.01; Ca < 0.03; Cu < 0.05; Ta ~ 0.06; that of the gadolinium was: Y ~ 0.08; Tb ~ 0.07; Eu ~ 0.04; Cu ~ 0.025; Fe ~ 0.02; Ca < 0.004. The systematic error of the reslts on the thermal diffusivity was about 5%.

Data on the dc electrical resistivity ρ were obtained by the four-probe method. We used heating by electron bombardment of the internal surface of the hollow cylindrical specimens (external diameter 15 mm, internal 6 mm, length 7 cm). We also measured ρ by heating in a resistance furnace on solid cylinders, 6 mm in diameter and 7 cm long [3]. The systematic error of the results on ρ was about 2% for the solid phase and about 3% for the liquid.

Figure 1 plots the results of measurements of the thermal diffusivity of yttrium and gadolinium between 1100 and 1700°K. The rms deviation of the individual points from the smoothed values is about 3%.

The results for Gd are close to those in [4]. The discrepancy is about 6% at T ~ 1400°K or higher, i.e., close to the total systematic error.

TABLE 1. High-Temperature Thermal Conductivities of Y and Gd [$\lambda \cdot 10^2$ W/(m·deg K)]

Element	T,°K			
	1100	1300	1500	1700
Y	0,17	0,18	0,19	0,20
Gd	0,17	0,19	0,21	0,20*

*Estimated from data for ρ on the basis of the Wiedemann–Franz law.

Translated from Atomnaya Énergiya, Vol. 40, No. 1, pp. 63-64, January, 1976. Original article submitted March 31, 1975.

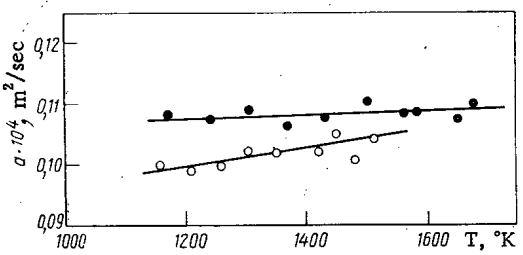

Fig.1

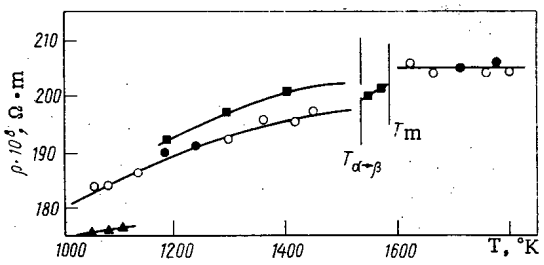

Fig. 2

Fig. 1. High-temperature thermal diffusivity of Y and Gd. ●) Yttrium; ○) gadolinium.

Fig. 2. High-temperature electrical resistivity of Gd. ▲) Data from [4]; ■) data from [5]; ○) present authors' data for solid cylinders; ●) for hollow cylinders.

The results of measurements of the electrical resistivity of gadolinium are plotted in Fig. 2. Between 1100 and 1500°K they are comparatively close to the data in [4, 5].

At the phase transition point $T_{\alpha \rightarrow \beta} = 1537$°K [5], the structure of gadolinium changes from hcp to bcc, but there is little change in the electrical resistivity. According to Dennison et al. [6] there is a marked change in the specific heat.

For the β phase, $\rho \sim 200$ $\mu\Omega \cdot$cm. The random errors are rather larger than for the α phase at $T \sim 1500$°K, so that one could only conclude that there is a singularity in the behavior of ρ in this region after a marked improvement in the accuracy. We can note a deviation from linearity in $\rho(T)$ which is typical of the lanthanides [3].

The electrical resistivity of liquid gadolinium is about 205 $\mu\Omega \cdot$cm, and between the melting point T_{mp} and 1800°K it is independent of the temperature, $\rho_l/\rho_s \sim 1.04$. A slight change of ρ on melting has been observed [7] for transition metals.

The data in [1] on the volumetric specific heat of gadolinium and yttrium, together with our results on the thermal diffusivity, were used to obtain values for the thermal conductivities of these elements (Table 1).

The published information on the thermal conductivities of Y and Gd at about 1200°K or higher is very limited: we know only the results in [4, 8] on the thermal conductivities of Y and Gd at 900-1500°K, and the data given in [9] concerning the thermal conductivity of Y at 350-1150°K. It is difficult to compare these results, because the thermal conductivity of Y depends on the hydrogen content [9].

The thermal conductivites of Y and Ga increase with rise of temperature. The data obtained for ρ and λ were used to estimate the Lorenz numbers L. The results for L are higher than the theoretical values, possibly owing to the phonon contribution to the thermal conductivity. A high value of this component is one feature of the lanthanides. Using the data in [10] between 90 and 310°K and in [4] between 900 and 1400°K, as a result of our experiments we can infer that there is a monotonic rise in the thermal conductivity of gadolinium in the paramagnetic region (270-1500°K). Similar inferences were drawn for the specific heat and electrical resistivity. Similar behavior of the thermal properties was noted for yttrium [1, 8].

Our discussion of the data on ρ was based on the assumption that elastic scattering processes play a leading role above the Curie and Néel points (and the Debye temperature), and that Matthiessen's rule applies. The observed behavior of ρ in the paramagnetic region is largely governed by scattering of electrons by disordered spins [11].

Analysis of the thermal conductivity is based on the assumption that the Wiedemann — Franz law holds and that the thermal conductivity can be expressed in the form of a sum of the phonon and electron components. This approach to the transition elements meets objections in [12].

We must also reckon with the existence of other contributions to the thermal conductvity [10], including that of magnetic ordering in the high-temperature region.

A complete examination of the behavior of the properties of the lanthanide elements is made difficult by the lack of complete information on the structures and energy spectra of these elements.

LITERATURE CITED

1. I. I. Novikov and I. P. Mardykin, At. Énerg., 37, No. 4, 348 (1974).
2. L. P. Filippov, Investigation of the Thermal Properties of Solid and Liquid Metals at High Temperatures [in Russian], Izd. MGU (1967).
3. I. P. Mardykin, Teplofiz. Vys. Temp., 13, No. 1, 211 (1975).
4. V. E. Zinov'ev et al., Fiz. Tverd. Tela, 14, 2747 (1972).
5. F. Spedding, J. Hanak, and A. Daane, J. Less. Comm. Met., 3, 110 (1961).
6. D. Dennison, K. Gschneidner, and A. Daane, J. Phys. Chem., 44, 4273 (1966).
7. A. R. Regel', in: The Structures and Properties of Liquid Metals [in Russian], Izd-vo Akad. Nauk SSSR, 3 (1959).
8. V. E. Zinov'ev and P. V. Gel'd, Fiz. Tverd. Tel., 13, 2261 (1971).
9. Y. S. Touloukian (editor), Thermophysical Properties of High Temperature Materials, Vol. 1, Macmillan, New York — London (1967).
10. D. Chuah and R. Ratnalingam, J. Low Temper. Phys., 14, 257 (1974).
11. T. Kasuya, Progr. Theor. Phys., 16, 45 (1956).
12. M. Laubitz, High Temper. — High Press., 4, 379 (1972).

EFFECT OF IMPLANTED SPACE CHARGE ON PARTICLE RANGE DISTRIBUTION

V. S. Remizovich and A. I. Rudenko

UDC 539.124.17

If the thickness of a layer of matter is sufficiently great, heavy charged particles (ions, protons) are decelerated because of interactions with atoms of the material and then are stopped, forming a distributed space charge. The amount of this charge increases as the radiation time increases and the intensity of the electric field created by the implanted charge can reach significant values (of the order of 10^6 V/cm) [1]. There is evidence [2, 3] that the macroscopic electrostatic field can have a significant effect both on the penetration of charged particles into matter and on the mechanical properties of the material itself. At the same time, because of the presently important problem of ion implantation in materials, there is interest in a calculation of the depth distribution of the implanted particles for various irradiation times.

In this paper, a solution of the transport equation is obtained for heavy charged particles including the effect of the self-consistent field of the space charge produced in the target in the case of plane geometry.

Let a broad beam of monoenergetic, nonrelativistic particles having a velocity v_0 directed along the normal to the surface of a plane-parallel plate (along the x axis) be incident on this plate, which is made of a nonmetallic homogeneous material, starting at the time t = 0. For heavy particles, one can neglect velocity deviations from the original direction and fluctuations in energy loss during deceleration [4]. The transport equation for the distribution function is then written in the form

$$\frac{\partial f(x, v, t)}{\partial t}+v\frac{\partial f}{\partial x}+\frac{F_x(x, t)}{m}\frac{\partial f}{\partial v}-\frac{1}{m}\frac{\partial}{\partial v}[\bar{\varepsilon}(v) f(x, v, t)]=0, \quad (1)$$

where $\bar{\varepsilon}(v)$ is the average energy lost per unit path length by a particle with velocity v; m is the mass of a particle; F_x is the projection of the force acting on a moving particle. In a number of cases the specific energy loss $\bar{\varepsilon}$ depends very slightly on particle velocity so that in first approximation it can be assumed constant — $\bar{\varepsilon} \approx \varepsilon_0$, where $\varepsilon_0 = mv_0^2R_0^{-1}/2$ (here, R_0 is the range of particles with an initial velocity v_0 in the absence of space charge). The boundary condition for Eq. (1) takes the form

$$f(0, v, t)=\frac{I_0}{v_0}\delta(v-v_0)\theta(t), \quad (2)$$

where I_0 is the incident particle flux density.

The time from entrance to a complete stop is $t_0 = mv_0(\varepsilon_0)^{-1}$ in the absence of electrostatic interactions between particles. In actual cases, $t_0 \approx 10^{-10}$–10^{-13} sec. The electrostatic force produced by the presence of an implanted space charge decreases the stopping time. Therefore the total number of particles (per unit surface area) moving in the material at any time is no greater than $I_0t_0 = I_0mv_0(\varepsilon_0)^{-1}$. The moving particles create a field which acts on a particle entering the medium with a force not greater than $F = 2\pi I_0(ze)^2mv_0(\varkappa\varepsilon_0)^{-1}$ (here, ze is the charge of the incident particles and $\varkappa$ is the dielectric constant of the material). The magnitude of this force even for the most intense continuous sources is many orders of magnitude less than the stopping power of the medium, i.e.,

$$\alpha=\frac{F}{\varepsilon_0}=2\pi\frac{I_0(ze)^2mv_0}{\varkappa e_0^2}\ll 1. \quad (3)$$

Translated from Atomnaya Énergiya, Vol. 40, No. 1, pp. 64-66, January, 1976. Original article submitted August 7, 1975.

This circumstance makes it possible to neglect the interaction between moving particles and to assume that the decelerating electric field is created only by the stopped particles, i.e., by the implanted charge. It is impossible to neglect the contribution of the latter to the field since their number increases with time.

Since the mobility of the stopped particles in a dielectric is very small [5], one can neglect a slight displacement of these particles after stopping because of the forces of electrostatic repulsion. Then the force F_x in Eq. (1) describes only the effect of implanted charge on the moving particles.

The presence of a decelerating electric field leads to the fact that particles entering the material at later times experience greater deceleration than particles entering earlier. Therefore the total stopping range R(t) decreases as t increases. Thus at the time t the stopped particles are distributed with a certain density over the range of depths $R(t) \leq x \leq R_0$ and the moving particles are found in the region $0 < x < R(t)$. If the time dependence R(t) of the range is known, the distribution of the implanted charge, $\rho(x, t)$, can be calculated in the following manner: in the time interval from t to t+dt, $dN = I_0 dt$ particles enter the material which stop in the layer $dx = -(dR/dt)dt$ at the depth $x = R(t)$. Therefore

$$\rho(x, t) = \begin{cases} -I_0 \left(\frac{dR}{dt}\right)^{-1}_{t=t(x)}; & R(t) \leqslant x \leqslant R_0; \\ 0; & x < R(t), \end{cases} \tag{4}$$

where t(x) is determined from the equation $x = R(t)$.

For plane geometry, the decelerating force acting on a moving particle from the direction of the implanted space charge is $F_x = -2\pi(ze)^2 \varkappa^{-1} \sigma(t)$ ($\sigma(t)$ is the total charge of stopped particles per unit area at the time t). The effect of space charge on range becomes noticeable for an irradiation time $t \sim t_* = \varkappa \varepsilon_0 (2\pi I_0 (ze)^2)^{-1}$, when the electric decelerating force is comparable to the stopping power ε_0 of the medium. In actual situations, $t_* \approx 1\text{-}10^4$ sec, i.e., $t_* \gg t_0$. Therefore in the time range $t \gg t_0$ of interest to us, $\sigma(t) \approx I_0 t$, since the stopped particles outnumber the moving particles. As a result, F_x is written in the form

$$F_x = -2\pi (ze)^2 \varkappa^{-1} I_0 t. \tag{5}$$

The solution of Eq. (1) with Eqs. (2) and (5) taken into consideration takes the form

$$f(\xi, u, \tau) = \frac{2I_0}{v_0^2} \theta(\tau_0) \theta(\tau - \tau_0) \delta \left\{ (\tau - \tau_0) \left[2 - (\tau - \tau_0) + \frac{2\alpha}{3} (\tau_0 - \tau) \left(\tau_0 + \frac{\tau}{2} \right) \right] - \xi \right\}, \tag{6}$$

where

$$\xi = \frac{x}{R_0}; \quad u = \frac{v}{v_0}; \quad \tau = \frac{t}{t_0}; \quad \tau_0(\tau) = \tau - \frac{1+\alpha\tau}{\alpha} \left[1 - \left(1 - \frac{2\alpha(1-u)}{(1+\alpha\tau)^2} \right)^{\frac{1}{2}} \right], \tag{7}$$

and the parameter α is defined by Eq. (3). In the limiting case ($\alpha = 0$), we obtain from Eq. (6) an expression for the distribution function

$$f_0(\xi, u, \tau) = \frac{2I_0}{v_0^2} \theta(1-u) \theta(\tau + u - 1) \delta(1 - u^2 - \xi). \tag{8}$$

Equation (8) represents a solution of the transport equation (1) in the absence of the decelerating force F_x. Since $\alpha \ll 1$, Eq. (6) is considerably simplified:

$$f(\xi, u, \tau) \approx \frac{2I_0}{v_0^2} \theta(1-u) \delta \left[\frac{1-u^2}{1+\alpha\tau} - \xi \right]; \quad \tau \gg 1. \tag{9}$$

Setting u = 0 in Eq. (9) we find the time dependence of particle range:

$$R(t) = \frac{R_0}{1+\alpha\tau} = \frac{R_0}{1+\alpha\frac{t}{t_0}} = \frac{R_0}{1+\frac{t}{t_*}}. \tag{10}$$

The particle range decreases as the time increases. We find $R = (1/2)R_0$ when $t = t_* = t_0/\alpha$. Now using Eqs. (4) and (10), we find the density of implanted charge:

$$\rho(x, t)=\begin{cases}\dfrac{mv_0^2\varkappa}{4\pi(ze)^2}\dfrac{1}{x^2}; & \dfrac{R_0}{1+\dfrac{t}{t_*}}\leqslant x\leqslant R_0;\\ 0; & x<\dfrac{R_0}{1+\dfrac{t}{t_*}}.\end{cases} \tag{11}$$

For example, the expression obtained for $\rho(x, t)$ makes it possible to calculate the electric field produced by an implanted charge in an irradiated sample.

LITERATURE CITED

1. B. Gross and S. Nablo, J. Appl. Phys., 38, 2272 (1967).
2. V. I. Veretel'nik and O. B. Evdokimov, Izv. Vyssh. Uchebn. Zaved., Fiz., 4, 167 (1972).
3. O. B. Evdokimov and A. P. Yalovets, Izv. Vyssh. Uchebn. Zaved., Fiz., 10, 32 (1973).
4. B. Rossi, High-Energy Particles, Prentice-Hall (1952).
5. Hiroaka Furuto, J. Appl. Phys., 37, 4 (1966).

YIELDS OF ^{95m}Tc, ^{96}Tc, AND ^{97m}Tc FROM IRRADIATION OF MOLYBDENUM AND NIOBIUM

P. P. Dmitriev, G. A. Molin,
Z. P. Dmitrieva, and M. V. Panarin

UDC 539.172.12

In the irradiation of molybdenum by protons, deuterons, and α particles, and of niobium by α particles, technetium isotopes are formed with half lives suitable for use in applied and basic research: ^{95m}Tc ($T_{1/2}$ = 61 days), ^{96}Tc ($T_{1/2}$ = 4.3 days), ^{97m}Tc ($T_{1/2}$ = 90.5 days). Stable isotopes of technetium do not exist in nature and therefore its radioactive isotopes can be obtained with exceptionally high specific activity.

In the present work we measured the dependence of ^{95m}Tc, ^{96}Tc, and ^{97m}Tc yields on the energy of bombarding particles for irradiation of thick molybdenum targets with protons and deuterons and also the yields of ^{95m}Tc and ^{96}Tc for irradiation of niobium and molybdenum with α particles.

Metallic samples of molybdenum and niobium were irradiated and the energy of the bombarding particles was varied by means of copper stopping foils. The techniques for sample irradiation and measurement of total irradiation current and isotope activity were basically the same as those described previously [1]. The values of the gamma-ray and K x-ray quantum yields used for measurements of isotope activity are given in Table 1.

The K x-ray yields were obtained in the present work. According to calculations made, the K x-ray quantum yield in the decay of ^{95m}Tc, which is 70%, results from K capture (67%) and the internal conversion of gamma transitions, mainly of the 204.12 keV γ ray, in the K shell (3%). The probability of K capture was calculated from formulas and data given in [4]; the K-shell internal conversion coefficient for the 204.12 keV γ ray was taken from [2]. Since ^{95m}Tc has an intense γ line at 204.12 keV along with the K x ray, having a pure ^{95m}Tc emitter provides an opportunity to subtract the ^{95m}Tc x ray from the total photopeak for the K x rays from a ^{95m}Tc + ^{97m}Tc mixture and also to calibrate an NaI(Tl) detector with respect to photoefficiency for K x rays, as is necessary for measurement of ^{97m}Tc activity.

^{97m}Tc decays only by isomeric transition from the 96.5 keV level to the ground state ^{97}Tc ($T_{1/2}$ = $2.6 \cdot 10^6$ yr) and the multipole order of the transition is M4. The energy and multipole order of the transition were taken from [5], and the theoretical internal conversion coefficient from [6] was used for the calculation of the quantum yields of 96.5-keV γ rays and K x rays. As is well known, K x radiation

TABLE 1. Energies and Quantum Yields for Gamma Rays and K X Rays

Isotope	γ-ray and K x-ray energy, keV	Quantum yield of gamma rays and K x rays	Reference
^{95m}Tc	204,12	66,2	[2]
	KX 17,79	70	Present work
^{96}Tc	1126,8	15,2	[3]
	1091,2	1,10	
	96,5	0,29	Present work
^{97m}Tc	*KX* 18,66	49	

Translated from Atomnaya Énergiya, Vol. 40, No. 1, pp. 66-68, January, 1976. Original article submitted April 28, 1975.

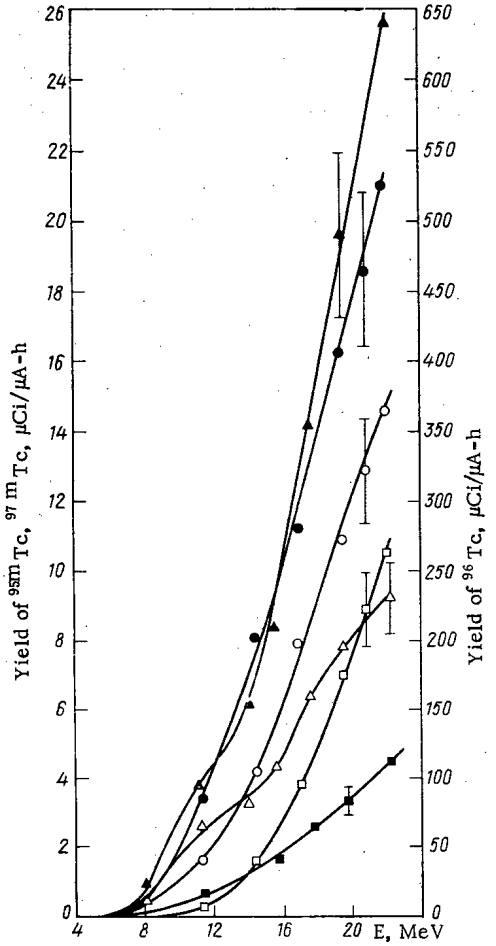

Fig. 1

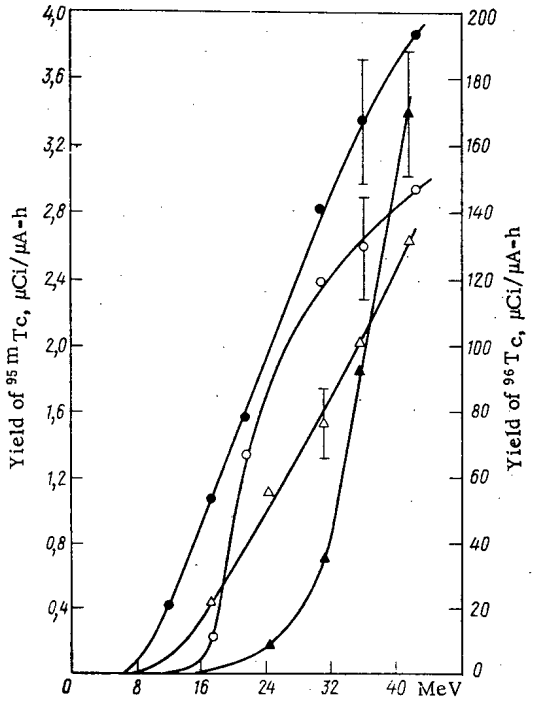

Fig. 2

Fig. 1. Dependence of ^{95m}Tc, ^{96}Tc, and ^{97m}Tc yields on energy of bombarding particles for irradiation of thick molybdenum targets by protons and deuterons: ○) (Mo + p) → ^{95m}Tc; ●) (Mo + p) → ^{96}Tc; □) (Mo + p) → ^{97m}Tc; Δ) (Mo + d) → ^{95m}Tc; ▲) (Mo + d) → ^{96}Tc; ■) (Mo + d) → ^{97m}Tc.

Fig. 2. Dependence of ^{95m}Tc and ^{96}Tc yields on energy of bombarding particles for irradiation of thick niobium and molybdenum targets by α particles: ○) (Nb + α) → ^{95m}Tc; ●) (Nb + α) → ^{96}Tc (×2); Δ) (Mo + α) → ^{95m}Tc (×5); ▲) (Mo + α) → ^{96}Tc.

includes the $K_{\alpha 1}$, $K_{\alpha 2}$, $K_{\beta 1}$, and $K_{\beta 2}$ components. Table 1 gives the average energy of the K x radiation according to [7] where the intensities of the components and the fluorescence yields ω_k are also given. Measurements of ^{95m}Tc and ^{97m}Tc activities were made 50-60 days after irradiation when the ^{96}Tc had decayed out. The activity of ^{96}Tc was measured by means of the total photopeak for the two γ lines (see Table 1) 1-2 days after irradiation. In this case, the contribution from hard γ lines in ^{95m}Tc was taken into account.

Table 2 gives the reactions resulting in the formation of ^{95m}Tc, ^{96}Tc, and ^{97m}Tc, and also the isotopic yields measured at maximum energy of the bombarding particles. Experimental curves for the dependence of ^{95m}Tc, ^{96}Tc, and ^{97m}Tc yields on particle energy are given in Figs. 1 and 2 for the ten production methods studied. The errors in the yield measurements are ±12% and are mainly caused by systematic errors in measurement of isotope activity and of the total sample irradiation current. In the irradiation of molybdenum by α particles, ^{97m}Tc is also formed but its yield was not measured in the present work.

Published results on the cross sections of reactions in which the specified technetium isotopes are formed are limited to [8] where the excitation function was measured for the ^{96}Mo(pn)^{96}Tc reaction (using the compound MoO_4 enriched to 96.8% ^{96}Mo) in the proton energy range from 10 to 65 MeV and to [9] where the excitation function was measured for the ^{93}Nb(αn)^{96}Tc and ^{93}Nb(α2n)^{95m}Tc reactions. We performed a

TABLE 2. Production Reactions and Yields for ^{95m}Tc, ^{96}Tc, and ^{97m}Tc

Production reaction	Reaction threshold, MeV	Content of initial isotope, %	Yield data		
			particle energy, MeV	yield, μCi/μA-h	reference
^{95}Mo $(p\ n)$ ^{95m}Tc ^{96}Mo $(p\ 2n)$ ^{95m}Tc ^{97}Mo $(p\ 3n)$ ^{95m}Tc	2,51 11,76 18,64	15,70 16,50 9,45	22,1±0,2	14,6±1,8	Present work
^{96}Mo $(p\ n)$ ^{96}Tc ^{97}Mo $(p\ 2n)$ ^{96}Tc ^{98}Mo $(p\ 3n)$ ^{96}Tc	3,76 10,65 19,38	16,50 9,45 23,75	22,1±0,2 22	527±63 458*	The same [8]
^{97}Mo $(p\ n)$ ^{97m}Tc ^{98}Mo $(p\ 2n)$ ^{97m}Tc	1,14 9,87	9,45 23,75	22,1±0,2	10,5±1.3	Present work
^{94}Mo $(d\ n)$ ^{95m}Tc ^{95}Mo $(d\ 2n)$ ^{95m}Tc ^{96}Mo $(d\ 3n)$ ^{95m}Tc	— 4,81 14,15	9,10 15,70 16,50	22,3±0,2	9,3±1,1	The same
^{95}Mo $(d\ n)$ ^{96}Tc ^{96}Mo $(d\ 2n)$ ^{96}Tc ^{97}Mo $(d\ 3n)$ ^{96}Tc	— 6,07 13,03	15,70 16,50 9,45	22,3±0,2	638±76	» »
^{96}Mo $(d\ n)$ ^{97m}Tc ^{97}Mo $(d\ 2n)$ ^{97m}Tc ^{98}Mo $(d\ 3n)$ ^{97m}Tc	— 3,42 12,24	16,50 9,45 23,75	22,3±0,2	4,6±0,6	» »
^{92}Mo $(\alpha\ p)$ ^{95m}Tc ^{94}Mo $(\alpha\ p\ 2n)$ ^{95m}Tc	5,9 24,40	15,85 9,10	42±0,5	0,53±0,06	» »
^{94}Mo $(\alpha\ p\ n)$ ^{96}Tc ^{95}Mo $(\alpha\ p\ 2n)$ ^{96}Tc	16,15 23,83	9,10 15,70	42±0,5	170±20	» »
^{93}Nb $(\alpha\ 2n)$ ^{95m}Tc	15,55	100	42,8±0,5 44	2,95±0,35 3,1†	» » [8]
^{93}Nb $(\alpha\ n)$ ^{96}T	7,3	100	42,8±0,5 30	97±12 110†	Present work [8]

*Obtained by integration of the excitation function for the $^{96}Mo(p, n)^{96}Tc$ reaction.
†Obtained by integration of the excitation function for the $^{93}Nb(\alpha, 2n)^{95m}Tc$ and $^{93}Nb(\alpha, n)^{96}Tc$ reactions.

numerical integration over the range of the excitation functions mentioned and the resultant values of ^{95m}Tc and ^{96}Tc yields for a thick target are given in Table 2.

The results show that one can obtain ^{95m}Tc free of ^{96}Tc and ^{97m}Tc impurities by α-particle irradiation of niobium. To obtain radioisotopically pure ^{95m}Tc, ^{96}Tc, and ^{97m}Tc by irradiation of molybdenum with protons or deuterons, it is necessary to use enriched molybdenum isotopes. It should be noted that the irradiation of molybdenum also produces the long-lived isotopes ^{97}Tc ($T_{1/2} = 2.6 \cdot 10^6$ yr), ^{98}Tc ($T_{1/2} = 1.5 \cdot 10^6$ yr), and ^{99}Tc ($T_{1/2} = 2.12 \cdot 10^5$ yr). However, because of the long half-lives, the activities of these isotopes relative to the activity of ^{95m}Tc, e.g., will be 10^{-4}-10^{-5}%.

The authors thank G. N. Grinenko for assistance.

LITERATURE CITED

1. P. P. Dmitriev et al., At. Énerg., 31, No. 2, 157 (1971); 32, No. 5, 426 (1972).
2. N. M. Anton'eva et al., Izv. Akad. Nauk SSSR, Ser. Fiz., 38, 48 (1974).
3. W. Bowman and K. MacMurdo, Atom. Data and Nucl. Data Tables, 13, 204 (1974).
4. M. Martin and P. Blichert-Toft, Nucl. Data Tables, A8, 156 (1970).
5. C. Lederer, J. Hollander, and J. Perlman, Tables of Isotopes, Wiley, New York (1967).
6. R. Hager and E. Seltzer, Nucl. Data, 4, Nos. 1-2 (1968).
7. A. Wapstra, G. Nijgh, and R. Van Lieshout, Nuclear Spectroscopic Tables, Interscience (1959).
8. J. Hogan, Inorg. and Nucl. Chem., 35, 1429 (1973).
9. T. Matsuo et al., Phys. Rev., 139, 886 (1965).

STIMULATING ISOTOPICALLY SELECTIVE HETEROGENEOUS REACTIONS WITH LASER LIGHT

V. D. Borman, B. I. Nikolaev, and V. I. Troyan

UDC 539.196.5:541.128

Isotope separation by stimulation of gaseous-phase chemical reactions with laser light [1-8] is being studied intensively. In particular, by selectively exciting molecules containing a given isotope it is possible to predissociate the molecule and to have a chemical reaction involving this isotope [3, 4, 7], or to use photodissociation of excited molecules by ultraviolet light [1, 2, 5]. In this article we consider isotope separation as a result of a selective interaction of laser light with gas molecules which are participating in an heterogeneous chemical reaction. When a molecule is irradiated with infrared light, it acquires additional energy, considerably exceeding the room temperature thermal energy. Catalytic reactions are known which proceed sufficiently rapidly at temperatures of about 400 to 600°K and for which the reaction rate increases exponentially with temperature [9].

To stimulate a heterogeneous chemical reaction it is practical to choose a temperature at which the reaction proceeds slowly. A molecule, in absorbing an infrared quantum, receives excess energy $h\nu \gg kT$ lumped in a particular bond. If an excited molecule hits the surface of a catalyst so that the longitudinal vibrations of the excited bond are parallel to the surface, then its lifetime in this state will be comparable to the adsorption time [10]. In this case the excess excitation energy of the molecule may be sufficient to overcome the reaction barrier at the surface of the catalyst. This also causes an increase in the rate of the heterogeneous reaction (e.g., disintegration of the molecule).

Processes which reduce the isotope separation coefficient for stimulated heterogeneous chemical reactions include transfer of vibrational excitation to molecules containing another isotope during gaseous-phase collisions and heating of the gas due to transfer of excitation energy into translational degrees of freedom. It is possible to reduce the effect of these processes on isotope separation if the distance between the surface of the catalyst and the laser beam is chosen to satisfy the conditions

$$l \ll \tau_{VV} v; \quad l \ll \tau_{Vt} v, \tag{1}$$

where τ_{VV} and τ_{Vt} are the characteristic times for vibrational — vibrational and vibrational — translational relaxation, respectively, and v is the average speed of the molecules.

We shall examine the possibility of stimulating the disintegration of ammonia in an heterogeneous reaction at the surface of a platinum catalyst. The mechanism of this reaction is described by the following equations [11]:

$$\begin{aligned} NH_3 &\longrightarrow (NH_2)_{ads} + H_{ads}; \\ H_{ads} &\longrightarrow \frac{1}{2} H_2; \\ (NH_2)_{ads} &\longrightarrow \frac{1}{2} N_2 + H_2. \end{aligned} \tag{2}$$

The probability of disintegration of NH_3 on the surface of platinum activated with trimethylpentane at T = 500°K is about 10^{-5}. Molecules of ammonia $^{15}NH_3$ can be selectively excited by CO_2 laser light ($\lambda = 10.6$ μ) [5].

For NH_3 the relaxation times are $\tau_{VV} \simeq 10^{-5}$ and $\tau_{Vt} \simeq 2 \cdot 10^{-6}$ sec at p = 1 torr [12]. Thus, already

Translated from Atomnaya Énergiya, Vol. 40, No. 1, p. 69, January, 1976. Original article submitted April 29, 1975.

at T = 300°K and p = $5 \cdot 10^{-2}$ torr, for l = 3 mm the inequalities (1) hold: $l/\tau_{VV} \cdot v = 0.037$ and $l/\tau_{VT} \cdot v = 0.19$. If we assume that the cross section for resonant absorption of CO_2 laser light by ammonia molecules is $\sigma \simeq 10^{-17}$-10^{-16} cm^2, then the length of a chemical reactor at a pressure of $5 \cdot 10^{-2}$ torr must be L ≃ 5-50 cm.

When $^{15}NH_3$ molecules are excited by CO_2 laser light they gain a vibrational energy $h\nu = 10^{-13}$ erg which is comparable to the thermal energy at T ≃ 1300°K. At this temperature, the probability of disintegration of ammonia molecules increases by four orders of magnitude and becomes about 10^{-1} [11]. Thus, under these conditions the rate of disintegration of $^{14}NH_3$ and $^{15}NH_3$ molecules will differ by four orders of magnitude. This results in concentration of the ^{15}N isotope in the form of molecular nitrogen (Eq. (2)).

In conclusion, we note that it is also possible to separate isotpes by use of laser light to stimulate heterogeneous reactions which take place by an impact mechanism (e.g., oxidation of ferric oxide).

The authors thank A. P. Senchenkov and L. P. Kudrin for fruitful discussions and useful advice.

LITERATURE CITED

1. R. Ambartzumian and V. Letokhov, IEEE J. Quant. Electr., QE-7, 305 (1971).
2. N. V. Karlov, Yu. B. Konev, and A. M. Prokhorov, Pis'ma v Zh. Éksperim. i Teor. Fiz., 14, 178 (1971).
3. V. Letokhov, Chem. Phys. Letters, 15, 221 (1972).
4. E. Yeung and C. Moore, Appl. Phys. Lett., 21, 109 (1972).
5. R. V. Ambartsumyan et al., Pis'ma v. Zh. Éksperim. i Teor. Fiz., 17, 91 (1973).
6. É. Sh. Belenov et al., ibid., 18, p. 196.
7. S. Leone and C. Moore, Phys. Rev. Lett., 33, 269 (1974).
8. R. V. Ambartsumyan et al., Pis'ma v Zh. Éksperim. i Teor. Fiz., 20, 597 (1974).
9. G. Thomas and W. Thomas, Heterogenous Catalysts [Russian translation], Mir, Moscow (1968).
10. A. M. Prokhorov and V. K. Konyukhov, Pis'ma v Zh. Éksperim. i Teor. Fiz., 13, 216 (1971).
11. A. Robertson and E. Willhoft, Trans. of Farad. Soc., 13, 476 (1967).
12. R. V. Ambartsumyan et al., in: Proceedings of the 1st International Conference on Laser Spectroscopy, Vail, Colorado, USA (1973).

EFFICIENCY FOR CONVERSION OF ELECTRONS INTO POSITRONS AT 20-70 MeV

V. A. Tayurskii

UDC 539.124.6

Positrons are produced by conversion of electrons in a solid target. In the target of a converter, electrons emit bremsstrahlung γ rays which create positrons in the pair production process. Electron beams with energies of hundreds of MeV are used for the purpose of producing positions for e^- and e^+ clashing beams. The efficiency for conversion of electrons into positrons is very low at energies of

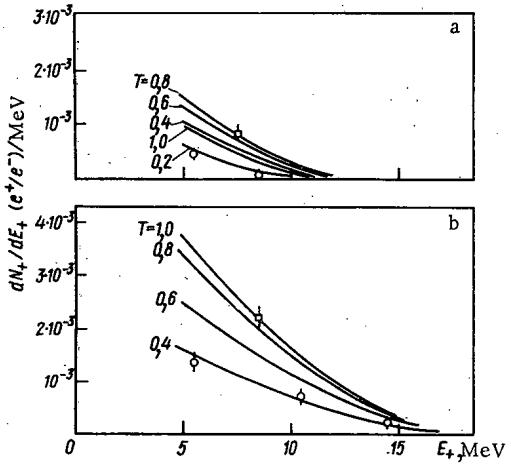

Fig. 1

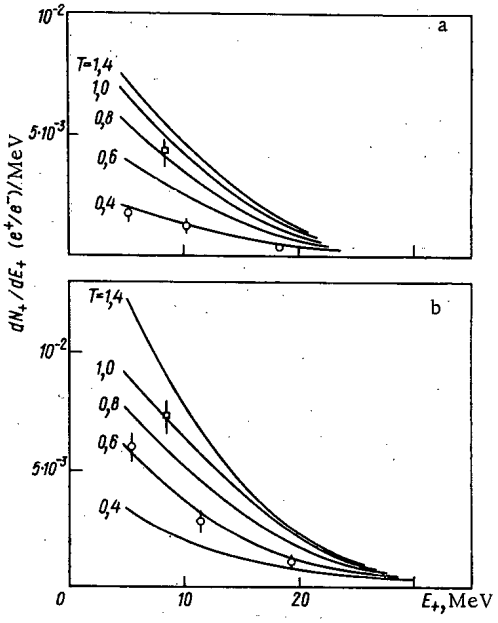

Fig. 2

Fig. 1. Energy spectra of positrons emerging from a converter in the forward direction in the solid angle $\Omega = 2\pi$. a) $E_- = 20$ MeV; T = 0.2, 0.4, 0.6, 0.8, and 1.0 radiation lengths; ○) individual calculated points for T = 0.2; □) the same for T = 0.8; b) $E_- = 30$ MeV; T = 0.4, 0.6, 0.8, and 1.0 radiation lengths; ○) individual calculated points for T = 0.4; □) the same for T = 1.0.

Fig. 2. Energy spectra of positrons emerging from a converter in the forward direction in the solid angle $\Omega = 2\pi$. a) $E_- = 50$ MeV; T = 0.4, 0.6, 0.8, 1.0, and 1.4 radiation lengths; ○) individual calculated points for T = 0.4; □) the same for T = 0.8; b) $E_- = 70$ MeV; T = 0.4, 0.6, 0.8, 1.0, and 1.4 radiation lengths; ○) individual calculated points for T = 0.6; □) the same for T = 1.0.

Translated from Atomnaya Énergiya, Vol. 40, No. 1, pp. 70-72, January, 1976. Original article submitted May 4, 1975.

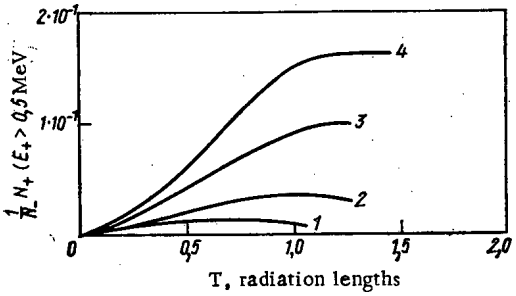

Fig. 3

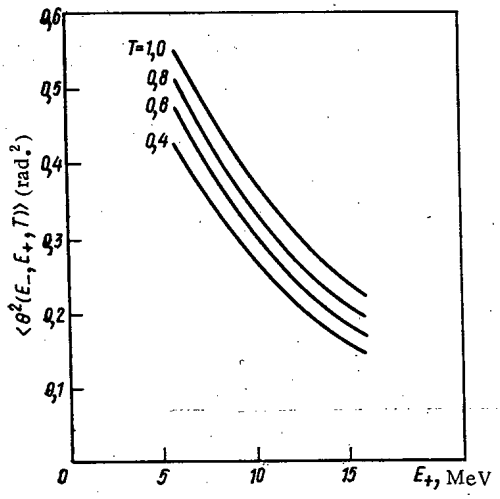

Fig. 4

Fig. 3. Total yield of positrons of all energies in the forward direction in the solid angle $\Omega = 2\pi$ as a function of target thickness T: 1) $E_- = 20$ MeV; 2) $E_- = 30$ MeV; 3) $E_- = 50$ MeV; 4) $E_- = 70$ MeV.

Fig. 4. Mean-square spatial angle of positrons emerging from a target as a function of E_+ for various values of T and $E_- = 20$-70 MeV.

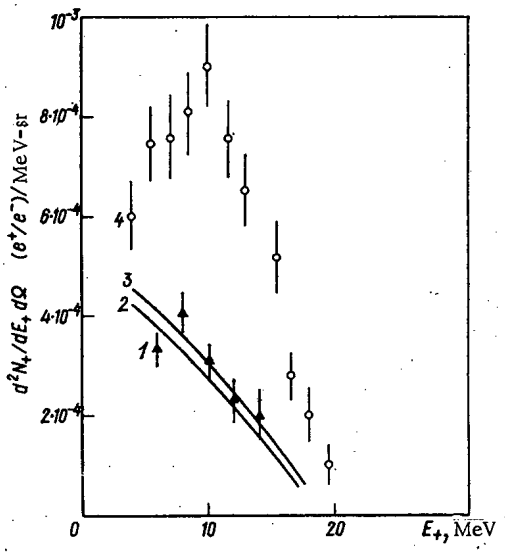

Fig. 5. Comparison of Monte Carlo calculations with experimental data and analytic calculations for $E_- = 25$ MeV and T = 0.2 radiation lengths: 1) present work (▲), tungsten; 2) experiment [1] (—), platinum; 3) analytic calculation [5] (—), tungsten; 4) experiment [3] (○), tungsten.

several tens of MeV but it is easier in practice to obtain higher electron currents. In order to calculate the positron current one can have in a storage ring as well as optimal conversion conditions, knowledge of the energy and angular positron spectra is needed. At these electron energies, spectral measurements of $d^2N_+/dE_+d\Omega$ at $\theta = 0°$ [1-4] are of a fragmentary nature and are not always in agreement. Analytic calculations [3, 5-7] were made under conditions which reduced their accuracy and area of application.

The present paper gives calculated results for the spectra $dN_+/dE_+(E_-, E_+, T)$ and for the mean values of the angular distributions $\langle\theta^2(E_-, E_+, T)\rangle$ of the positrons obtained by Monte Carlo simulation of the electron—photon cascade in matter. All the calculations were performed by means of a program [8] which is similar to other programs for the calculation of electron—photon cascades [10, 11]. The difference from [10-13] is that those programs investigated the integral characteristics of cascade electrons and positrons. The present calculations were performed for tungsten targets of thickness T = 0.2-1.4 radiation lengths and for initial energies $E_- = 20$, 30, 50, and 70 MeV. The trajectories of the initial electrons were assumed parallel in the calculations. Figures 1 and 2 show the spectra of positrons emerging in the forward direction from a converter target within the solid angle $\Omega = 2\pi$ for various initial energies and for targets of varying thickness. The curves were drawn within the limits of statistical error on the basis of histograms obtained from the Monte Carlo calculation. The errors were assumed to be $\pm\sqrt{N_+}$, where N_+ is the number of particles per histogram step ΔE_+; $\Delta E_+ = 1$ MeV for Figs. 1 and 2. The figures also show several computed points with their errors. Only cascade particles with energies greater than 5 MeV were considered in the calculations since the inclusion of lower energies leads to a marked increase in computing time, which is mainly determined by multiple scattering of low-energy electrons and positrons. Figure 3 shows the dependence of the total yield of positrons of all energies on converter thickness T for $E_- = 20$, 30, 50,

and 70 MeV. The curves were obtained by crude integration of the spectra in Figs. 1 and 2, which have a maximum in the neighborhood of $E_+ \approx 2$-3 MeV as indicated by measurements [1]. For the choice of optimal conversion conditions for any E_+, it makes sense to consider the thickness T up to the point of maximum total yield of positrons. The initial portions of the curves in Fig. 3 can be approximated within ~10% by a linear dependence on T:

$$N_+/N_- \approx 2.4 \cdot 10^{-4} \cdot E_-^{3/2}\,(\text{MeV}) \cdot T\ (\text{rad. length}) \qquad (1)$$

where $T \leqslant T_c$, $T_c \simeq 0.25 \cdot \ln E_-$ (MeV).

The relationship $N_+ \propto E_-^{3/2}$ can be explained by the fact that the energies considered belong to an intermediate range between low energies where $N_+ \propto E_-^2$ [3, 7] and high energies where $N_+ \propto E_-$ [9]. (Low energies are energies $E \leqslant E_S$, where E_S is the characteristic energy for Coulomb scattering, $E_S = 21$ MeV; high energies are energies $E \gg E_S$.) Figure 4 shows curves for $\langle \theta_+^2(E_-, E_+, T)\rangle$, the mean square spatial angle of positron emergence, as a function of E_+ and T. Within the limit of statistical error, $\langle \theta_+^2(E_-, E_+, T)\rangle$ can be considered independent of E_- and also Gaussian, as shown by analysis of the angular distributions. In order to judge the reliability of the results obtained, the Monte Carlo calculations were compared with experimental data [1-4]. Spectra for $d^2N_+/dE_+d\Omega$ from [1, 3, 5] are compared in Fig. 5 with the spectrum obtained for $E_- = 25$ MeV and $T = 0.2$ radiation lengths. The spectrum from [1] was increased by a factor 2.7 in accordance with the note at the end of that paper; points on the curve were obtained by interpolation of data for $T = 0.15$ and 0.3 radiation lengths. The spectra from [1] and [5] and the Monte Carlo calculation are in good agreement but are roughly a factor of two lower than the results of [3]. However, it was pointed out in [3] that the absolute scale of the experimental curves may contain a factor of the order of two. On the whole, the comparison of the Monte Carlo calculations with experimental data [1-4] showed that the agreement between them is good.

In conclusion, the author takes great pleasure in thanking B. V. Chirkov, B. I. Grishanov, R. A. Salimov, and A. D. Bukin for valuable discussions.

LITERATURE CITED

1. M. Bernardini et al., CEA Report N 2212 (1962).
2. C. Jupiter et al., Phys. Rev., 121, 866 (1961).
3. L. Katz and K. Lokan, Nucl. Instrum. and Methods, 7, 7 (1961).
4. T. Aggson and L. Burnod, ORSAY, Preprint LAL-27 (1962).
5. V. Jacobs et al., Nucl. Instrum. and Methods, 61, 166 (1968).
6. R. Sund and R. Walton, Nucl. Instrum. and Methods, 27, 109 (1964).
7. V. A. Tayurskii and B. V. Chirikov, Preprint 73-73, IYaF, SO Akad. Nauk SSSR (1973).
8. F. M. Izrailev et al., Preprint 63-73, IYaF, SO Akad. Nauk SSSR (1973).
9. S. Z. Belen'kii, Cascade Processes in Cosmic Rays [in Russian], Gostekhizdat, Moscow (1948).
10. W. Messel et al., Nucl. Physics, 39, 1 (1962).
11. H. Nagel, Zeits. für Physik, 186, 319 (1965).
12. M. Tamura, Prog. of Theor. Phys., 34, 912 (1965).
13. M. Ya. Borkovskii and S. P. Kruglov, Yad. Fiz., 16, 349 (1972).

DEPENDENCE OF ASYMMETRY IN THE PHOTOFISSION OF ^{233}U AND ^{239}Pu ON THE MAXIMUM BREMSSTRAHLUNG

M. Ya. Kondrat'ko, V. N. Korinets, and K. A. Petrzhak

UDC 539.173.3

The fission yields of certain products of the symmetric and near-symmetric fission of ^{233}U and ^{239}Pu by means of the bremsstrahlung from a betatron are determined over a range of energy maxima E_0 = 10-24 MeV. The procedure for similar experiments is described in [1-5]: irradiation of targets using special equipment, inserted in the accelerating chamber of the betatron; buildup of radioactive fission products in the form of nuclear recoil; radiochemical analysis, and measurements of β activity in proportional 4π counters. The fission products were identified by their half lives. Experimental decay-buildup curves were fitted by the method of least squares, utilizing tabular values for the half lives and branching ratios. The yields were determined with respect to the standard ^{140}Ba. Cumulative yields of identified isotopes were scaled to the values of the total yields of branches with a corresponding mass number. In addition, numerical estimates of individual yields of daughter isotopes and published data on the branching of decay with the formation of short-lived isomers were utilized.

The results are presented in Tables 1 and 2. The values of the relative yields, the error in which has not been noted, are determined with a relative error of 5-7%. The error in the maximum energy E_0 is due mainly to a drift in the standard values during irradiation and consisted of approximately ±150 keV. The yield ratios of ^{139}Ba and ^{140}Ba, equal to 1.11 ± 0.06 and 1.13 ± 0.05 when E_0 = 16-20 and 24 MeV, respectively, are also determined for the photofission of ^{239}Pu.

A comparison of the results shows that the ratios $Y^{115}Cd/Y^{140}Ba$ for ^{233}U and $Y^{117}Cd/Y^{140}Ba$ for ^{239}Pu, representing the case of the most symmetric fission, are similar in magnitude and energy dependence. A systematic reduction in the yields is observed for ^{239}Pu upon switching from near-symmetric (^{111}Ag) to most-symmetric (^{117}Cd) fission. However, in the photofission of ^{233}U, the relative yields of ^{113}Ag are less than with $^{115,117}Cd$. It is possible that this irregularity is connected with the manifestation of a central peak in the mass distribution of the symmetric fission. A similar phenomenon has been observed in the photofission of ^{235}U [5].

TABLE 1. Relative Yields of ^{233}U Photofission Products

E_0, MeV	Y_{113Ag}/Y_{140Ba}	Y_{115Cd}/Y_{140Ba}	Y_{117Cd}/Y_{140Ba}
10	0,0031±0,0008	0,0078±0,0010	0,005±0,001
12	0,022±0,005	0,034±0,002	0,032±0,002
14	0,037	0,060	0,060
16	0,053	0,068	0,061
20	0,068	0,095	0,086
24	0,100	0,126	0,128

TABLE 2. Relative Yields of ^{239}Pu Photofission Products

E_0, MeV	Y_{111Ag}/Y_{140Ba}	Y_{113Ag}/Y_{140Ba}	Y_{115Cd}/Y_{140Ba}	Y_{117Cd}/Y_{140Ba}
10	0,046±0,005	0,020±0,006	0,013±0,002	0,010±0,002
12	0,075±0,005	0,031±0,003	0,027±0,002	0,024±0,003
14	0,100	0,058	0,059	0,049
16	0,144	0,081	0,073	0,071
20	0,176	0,099	0,102	0,094
24	0,202	0,121	0,127	0,127

Translated from Atomnaya Énergiya, Vol. 40, No. 1, pp. 72-73, January, 1976. Original article submitted May 21, 1975.

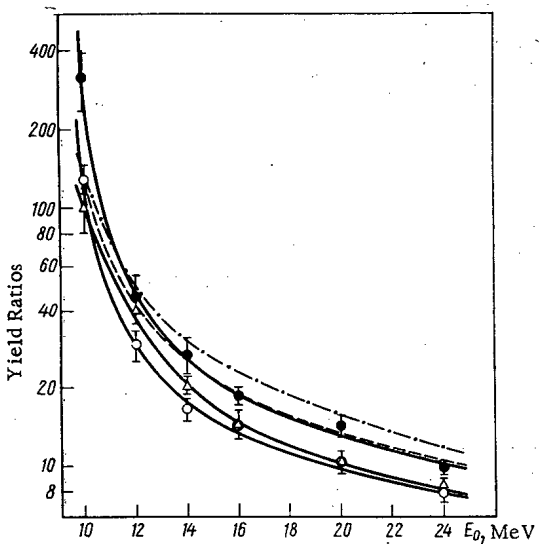

Fig. 1. Yield ratios "peak to trough" for photofission. Data of present paper for the reaction ^{233}U (γ, f): ○) $Y_{110}Ba/Y_{115}Cd$; ●) $Y_{140}Ba/Y_{113}Ag$; for the reaction ^{239}Pu (γ, f): △) $Y_{140}Ba/Y_{117}Cd$. Data in [1] for the reaction ^{235}U (γ, f): – – –) $Y_{140}Ba/Y_{115}Cd$; in [6] for the reaction ^{238}U (γ, f): —·— ·—·) $Y_{140}Ba/Y_{115}Cd$.

The energy dependences of the "peak to trough" ratios are given in Fig. 1. The $Y^{140}Ba/Y^{117}Cd$ ratios for the photofission of ^{235}U [1] and ^{238}U [6] are given there also. A reduction in the "peak to trough" ratio is observed in the series $^{233}U - ^{235}U - ^{238}U$, i.e., with a given nuclear charge Z, the probability of the most symmetric fission is lower, the greater the mass number A.

LITERATURE CITED

1. M. Ya. Kondrat'ko and K. A. Petrzhak, At. Énerg., 23, No. 6, 559 (1967).
2. M. Ya. Kondrat'ko, O. P. Nikotin, and K. A. Petrzhak, At. Énerg., 27, No. 6, 544 (1969).
3. M. Ya. Kondrat'ko, O. P. Nikotin, and K. A. Petrzhak, Pribory i Tekh. Éksperim., No. 3, 47 (1964).
4. M. Ya. Kondrat'ko, V. N. Korinets, and K. A. Petrzhak, At. Énerg., 34, 52 (1973).
5. M. Ya. Kondrat'ko, V. N. Korinets, and K. A. Petrzhak, At. Énerg., 35, No. 3, 214 (1973).
6. R. Duffield, R. Schmitt, and R. Sharp, in: Proceedings of the 2nd International Conference, Geneva, Vol. 15 (1958), p. 678.

SYNTHETIC PITCHBLENDE: COMPOSITION, STRUCTURE, AND CERTAIN PROPERTIES

V. A. Alekseev and R. P. Rafal'skii

UDC 542.65:549.514.8:549.12

Pitchblende with a highly defined collomorphic structure has been synthesized previously under hydrothermal conditions by the reduction of hexavalent uranium by elementary arsenic [1]. However, investigation of the products of the synthesis was not accompanied by systematic determinations of the O/U ratio and water content. Additional experiments were conducted in order to obtain this information.

A wafer of natural arsenic was placed in a quartz ampoule with a solution of UO_2SO_4, which was maintained at a fixed temperature after being evacuated and sealed. After rapid cooling, the ampoule was opened and we washed the wafer, coated with a thin layer of pitchblende, with water and alcohol and dried it in vacuum at room temperature. We carefully removed the thin layer; we used part of it for determining the content of tetravalent and ordinary uranium and water, as well as for x-ray analysis. A polished section was prepared from the remainder.

We calculated the O/U ratio from the data of chemical analysis performed by the ferrophosphatevanadate method [2]. The material subjected to analysis contained from 2.4-7.2 mass % of arsenic; however, it has been established that the presence of arsenic and its oxides do not have any effect on the accuracy of determining the uranium. We determined the water content by the Penfield method. During the heating of the sample, not only the water, but also arsenic trioxide, which together with the water was condensed in the form of a white deposit in an enlarged section of the tube, was driven off. During the drying of the latter in vacuum (110°C; 0.5-1 h), evaporation of As_2O_3 did not occur, a fact which was established by control weighing.

In order to prepare the polished sections of the thin layer, we introduced an epoxy resin, after the solidification of which we produced the thin section and the polishing. Investigation of the polished sections was followed by structural pickling in a 20% solution of iron chloride. We measured the reflecting

TABLE 1

Expt. No.	Exptl. conditions				Composition and properties of the synth. pitchblende			
	t, °C	heating time, h	initial concn. of uranium in sol., g/liter	volume of sol. at 25°C, ml	O/U	water content, %	reflecting power, %	abs. microhardness, kgf/mm²
1	150	10,5	2	5	2,38	9,62	Not determined	Not determined
2	150	17,5	3	5	2,36	5,88	»	»
3	150	16,5	2	12	2,28	4,67	»	»
4	150	33	2	5	2,32	6,90	10,1	160
5	150	32	4	100	2,26	3.35	9,5	310
6	150	9	21,8	10	2,35	Not determined	Not determined	Not determined
7	150	33	21,8	16	2,36	»	»	»
8	150	33	21,8	18	2,33	6,27	10,5	185
9	200	32,5	4,1	100	2,25	2,66	12,4	410
10	200	9	6	10	2,19	2,33	13,3	420
11	200	6	21,8	10	2,19	1,84	11,9	320
12	250	8,5	21,8	7	2,21	0,96	Not determined	Not determined
13	300	31,5	4,1	100	2,12	0,12	16,9	650
14	320	8,5	21,8	7	2,16	0,76	14,3	450
15	320	8,5	21,8	7	2,09	0,79	14,7	505

Translated from Atomnaya Énergiya, Vol. 40, No. 1, pp. 73-76, January, 1976. Original article submitted May 21, 1975.

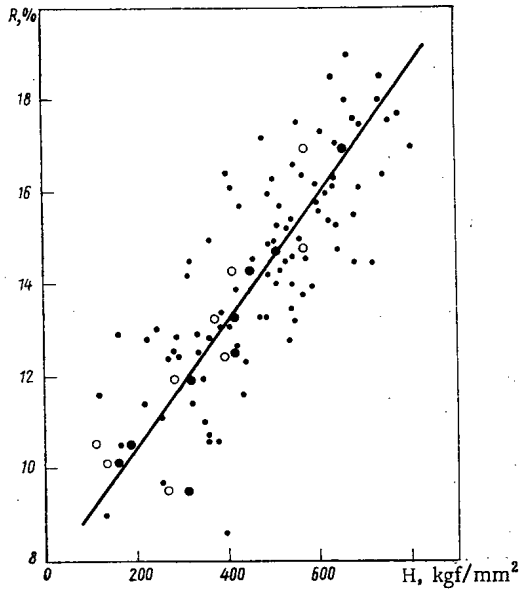

Fig. 1. Dependence between reflecting power and microhardness of uranium oxides: ○) Synthetic pitchblendes (microhardness is calculated from optimal load); ●) the same, microhardness is calculated for 14-μ diagonal of replica; ⊙) natural uraninites and pitchblendes.

power in a POOS device in air in the visible region of the spectrum (435-660 nm). The etalon was STF-2 silicon glass. The deviation in the arithmetical mean of the value of R for a single sample equaled 3.6% due to the inhomogeneity of the material. We utilized the value of R at λ = 580 nm for comparison with the microhardness.

We measured the microhardness in a PMT-3 device, calibrated to halite, at loads of 15-100 gf. The deviation in the arithmetical mean of the value of H with a single load comprised 16% due to the inhomogeneity of the material. For comparison with the reflecting power, the microhardness was determined by two methods: at optimal load for a given class [3] and for a constant length of a diagonal of the replica. In the latter case, we found the microhardness from the points of intersection of the straight line, obtained by utilizing the well-known formula $H = (1.8544P)/d^2$ (kgf/mm^2) and the corresponding diagonal length at 14 μ (the magnitude of which is limited by the size of the thin layers), with curves describing the H — P dependence for individual samples.

The conditions under which the experiments were conducted and the results of the study of the synthetic pitchblendes are given in Table 1. In spite of significant fluctuations in the O/U ratio in pitchblendes obtained at the same temperature, a distinct tendency of this ratio to fall with a rise in temperature is observed. Simultaneously with a decrease in the oxygen coefficient, the water content in the pitchblendes is reduced and their reflecting power and microhardness increases. The largest correlation coefficients are obtained between O/U and C_{H_2O} (0.93), as well as between R and H (0.89 and 0.93 when calculating the microhardness according to the optimal loads and for a constant diagonal length, respectively). Calculation of H by the second method should convert the systematic error due to the effect of the surface layer into a constant quantity which is smaller the greater the diagonal length. If one omits the anomalous point corresponding to the minimum reflecting power, the correlation coefficient in the last case increases to 0.98. At the same time, the dependence between the microhardness and the reflecting power (Fig. 1) is expressed by the following equation of a straight line, the coefficients of which are calculated by the method of least squares:

$$R = 0.0137H + 7.71$$

with the variances of the coefficients S_a = 0.0056 and S_b = 0.92.

The straight line corresponding to this equation agrees in direction and passes throug the center of the correlation ellipse of the values of R and H for natural pitchblendes and uraninites [4]. It is noteworthy that the reflecting power and microhardness of synthetic pitchblendes with the highest O/U ratio (2.33) are the same as for natural pitchblendes with a O/U ratio equal to ~2.70.

The dependence of the morphology of the separating out of the synthetic pitchblendes on the temperature presents considerable interest. Pitchblendes synthesized at 150°C and characterized by the highest O/U ratios form principally small oölites of concentrically zonal structure (Fig. 2a); a collomorphically banded microtexture is observed in particular cases. The latter moreover is most characteristic of pitchblendes obtained at 200°C (Fig. 2b). The pickling reveals a thin stratification (Fig. 2c); the individual layers are .1 μm thick and extend over the entire thin layer. Of the characteristics of the crystalline structure of pitchblendes synthesized at 150 and 200°C, it is not observed during microscopic study. However, thin layers of pitchblendes with the lowest O/U ratios, formed at 300 and 320°C, have a distinct crystalline structure. At the same time, they are combined with spheroidolites (Fig. 2d), sometimes changing into dendrites (Fig. 2e).

As is known, the rate of chemical reactions increases with an increase in temperature (2-4 times every 10°C on the average) and the concentrations of the original reagents. In this connection, one would expect that at higher temperatures and concentrations of uranium in the initial solution the dispersion of

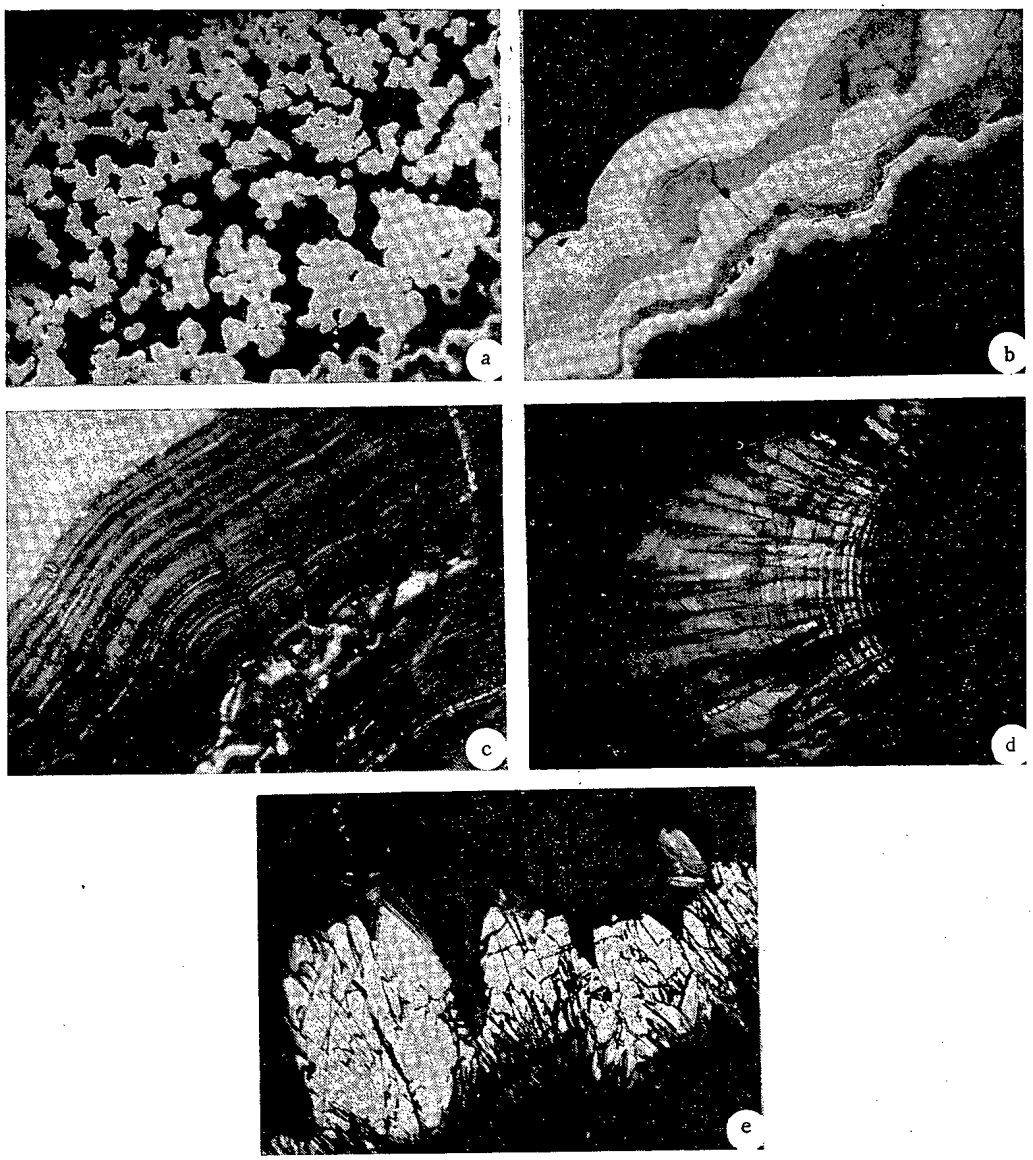

Fig. 2. Morphology of the separating out of synthetic pitchblende (the ordinal number of the experiment in Table 1 and the magnification are indicated): a) 5, 440; b) 9, 340; c) 11, 440, pickled; d) 13, 750, pickled; e) 13, 440, pickled (the filler is indistinct).

pitchblende deposits should increase due to the increase in the rate of reduction of hexavalent uranium and the formation of large quantities of the deposit per unit time. In fact, with an increase in temperature, the dispersion is reduced and the deposits have an increasingly distinct crystalline structure. The experimental results indicate the absence of an appreciable effect of the initial concentration on the size of the particles and the morphology of the separating out of the pitchblende, which agrees with the experimental data obtained in [1]. One can explain these discrepancies by the formation at different temperatures of pitchblendes with a distinct O/U, which is also the most important factor determining the structure and properties of the products of the synthesis. The higher this ratio, the higher the dispersion of the deposits and their water content and the lower the reflecting power and microhardness. This dependence is in good agreement with the results of the investigation of natural uraninites and pitchblendes. The effect of the O/U ratio is probably connected with the ordering of the crystalline structure UO_{2+x}, which occurs with the reduction of this ratio. Unfortunately, pitchblendes synthesized by the method described are distinguished by an increased crystal lattice parameter (up to 5.56 Å), which hinders the determination of the dependence of the parameter on the O/U ratio. It had been assumed previously [1] that the increase in the parameter is connected with the presence of water in the pitchblendes; however, it did not eliminate the possibility that the presence of As_2O_3 affects the parameter [5]. The available data does not permit one to solve this problem.

One can assume that the values of O/U given in Table 1 do not reflect stable phase ratios under experimental conditions and should decrease with an increase in time of the experiments. This question remains unclear: is the formation of pitchblendes with O/U > 2.38 possible at lower temperatures or for shorter experimental periods? This maximum O/U ratio, obtained in the experiments described, agrees with the limiting O/U ratio in the cubic phase UO_{2+x}, synthesized by a quite different method [6]. However, the possibility that this agreement is accidental is not excluded.

LITERATURE CITED

1. R. P. Rafal'skii, The Physicochemical Study of the Conditions of Formation of Uranium Ores [in Russian], Gosatomizdat, Moscow (1963).
2. V. K. Markov et al., Uranium, Methods of Its Determination [in Russian], Gosatomizdat, Moscow (1960).
3. S. I. Lebedeva, Trudy IMGRÉ, No. 6, 89 (1961).
4. M. V. Soboleva and I. A. Pudovkina, Uranium Minerals [in Russian], Gosgeoltekhizdat, Moscow (1957).
5. Yu. M. Dymkov, The Nature of Pitchblende [in Russian], Atomizdat, Moscow (1973).
6. R. P. Rafal'skii et al., Dokl. Akad. Nauk SSSR, 224, No. 5, 105 (1975).

MEASUREMENT OF THE ENERGY DEPENDENCE OF η^{233}U IN THE 0.02-1-eV REGION

V. A. Pshenichnyi, A. I. Blanovskii, N. L. Gnidak, and E. A. Pavlenko

UDC 539.125.5

Accurate data on the effective number of low-energy fission neutrons η^{233}U are important in the design of slow-neutron breeder reactors since the principal uncertainty in the breeding ratio for such reactors is introduced by the indeterminancy of η^{233}U. In view of this, the energy dependence of η^{233}U over the 0.02-1-eV range was determined in the VVR-M atomic reactor of the Institute of Nuclear Problems of the Academy of Sciences of the Ukrainian SSR with an accuracy of 1-2%. The measurements were conducted using the time-of-flight method with a resolution of ~12 μsec/m and normalized to the value when E = 0.0253 eV, assuming that η = 2.297 at this point. The neutron beam from the reactor was passed into a pulsating mechanical chopper with a rotor 300 mm in diameter and slots 2 mm wide. The sample and detectors were located 500 ± 5 cm from the chopper. The fission neutrons were recorded by a bank of 50 SNM-37 helium-filled counters with a moderator in the geometry near 2π. A cadmium shield was placed between the moderator and the counters in order to shorten the lifetime of the neutrons. The flux of incident neutrons was measured by the γ quanta from neutron captures by a sample of cadmium or indium. Such a (n, γ) detector consists of an NaI(Tl) crystal 70 × 70 mm in size and a PM-49. The transmission was measured by a SNM-5 boron-filled counter or by three SNM-37 helium-filled counters.

Theoretical corrections for the resolution, for the energy-dependence of the flux detector's sensitivity, and for multiple scattering of neutrons in the sample were introduced into the experimental results. The magnitude of the correction for multiple processes in the fissionable sample, calculated by a Monte Carlo method, was about 2.5% in the 0.025-eV energy region and increased to 3.5% in the vicinity of 1 eV. The correction for the resolution was about 2% in the 0.2-eV energy region relative to the value when E = 0.0253 eV. Inexact knowledge of this correction introduced a systematic error of the order of 0.5%, almost comparable with the statistical error in the measurements of ~0.7%.

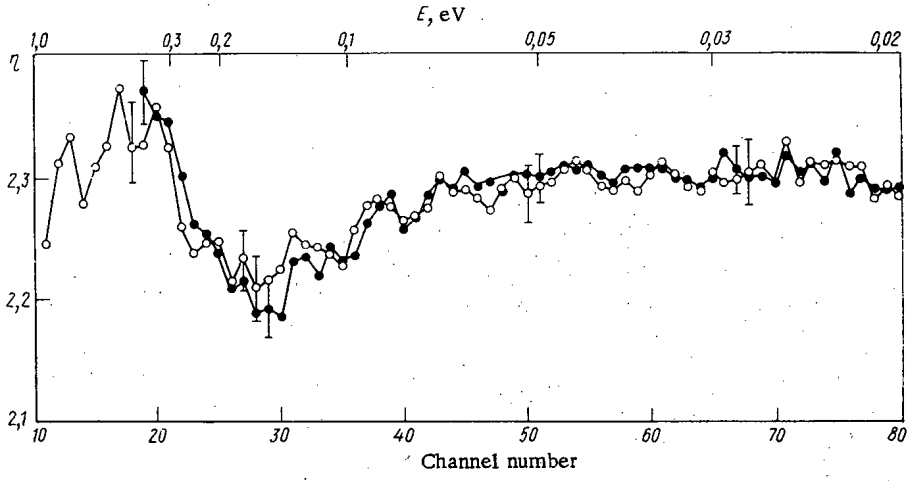

Fig. 1. Energy dependence of η^{233}U in the 0.02-1-eV region: ●) cadmium; ○) indium.

Translated from Atomnaya Énergiya, Vol. 40, No. 1, pp. 76-77, January, 1976. Original article submitted May 26, 1975.

The energy dependence of $\eta^{233}U$ (the flux was measured by an (n, γ) detector with samples of cadmium and indium) is shown in Fig. 1. Systematic discrepancies in the data obtained in the determination of the flux with indium and cadmium detectors are evidently connected with some indeterminancy in the flight distance in measurements with indium due to its greater thickness.

In the last five years, measurements of $\eta^{233}U$ were conducted in the 0.02-1-eV energy range [1, 2]. The results of these papers agree; the reduction in the value of η by 4.0-4.2% at 0.16 eV from the value at E = 0.0253 eV is emphasized. The energy dependence of η was determined by the simultaneous measurement of the fission and capture cross sections. In this paper, another technique is utilized: the energy dependence of the quantity $\bar{\nu}\sigma_f$ is measured indirectly. The results agree to within 1% with the data of the papers cited, although the reduction in the value of η at 0.16 eV, obtained in the measurement of the flux in cadmium, amounted to 5% of the value of η at E = 0.0253 eV. This agreement indicates that with the same precision the average number of fission neutrons remains constant in the thermal-energy region.

LITERATURE CITED

1. L. Weston et al., Nucl. Sci. Engng., 42, 143 (1970).
2. J. Smith and S. Reedez, in: 2nd Conference on Nuclear Cross Sections and Technology, Washington, 1968, Vol. 1, p. 591 (Proc. NBS Spec. Publication 299).

INFORMATION

NEXT PROBLEMS IN THE DEVELOPMENT OF OXIDE FUEL ELEMENTS FOR FAST POWER REACTORS

I. S. Golovnin

One of the chief features in the current development of nuclear power is the creation of nuclear power stations with fast reactors. Considerable advances have been made in a number of countries as to the technical design of such reactors. Experimental industrial stations with powers of the order of 300 million (electrical) kW each are already in the stage of adoption in the USSR, Britain, and France. Experience in the use of these installations and the more powerful versions now being built in the USSR and USA (BN-600 and FFTF) should over the next decade provide all the data required to create and introduce large electrical power stations of optimum parameters with fast sodium breeder reactors using mixed oxide fuel.

At the present time scientists are assiduously exchanging the results of research and technical experience. Several recent large international conferences have, in effect, summarized progress up to 1975 and pointed the way to future developments. This specially applies to the winter session of the American Nuclear Society (Washington, October 27-31, 1974),* the First European Nuclear Conference (Paris, April 21-25, 1975),† and the Congress of Specialists from the International Agency on Atomic Energy Regarding Possible Damage to Fast-Reactor Fuel (Seattle, USA, May 12-16, 1975). Earlier investigations were mainly aimed at demonstrating the potentialities of fast reactors and elucidating the basic problems, especially those concerning the fuel elements.

The limited amount of information available as to the influence of reactor conditions on the properties of materials prevents all the effects which began to appear on increasing the power, the neutron flux density, and the burn-up of the fuel in the experimental installations from being taken into account at the same time. One of the most important effects, which has not as yet been studied over a sufficiently wide range of irradiation (up to $4 \cdot 10^{23}$ neutrons/cm^2 at E > 0.1 MeV), is the softening of the construction materials, i.e., the fall in long-term strength and ductility, the acceleration of high-temperature embrittlement (austenitic stainless steels), and creep. Effects which have been discovered include the neutron-induced swelling of construction materials and the effect of the initial purity of the fuel and the accumulation of fission fragments on the compatibility of the fuel with the material of the fuel-element can. On the whole these effects lead to a certain (though not critical) reduction in the efficiency of fast reactors as compared with the original optimistic estimates, although the exact extent of the effect cannot yet be assessed.

Apart from design and technological developments, important features in the creation of efficient fuel elements include the study of materials and structures (both inside the reactor and after removal), analytical investigations into efficiency based on experimental data regarding the properties of materials, and an analysis of emergency situations from the point of view of their influence on the efficiency of the installation as a whole and its safety under service conditions. Experimental investigations based on both cooperative and independent programs are being carried out by scientists in the United States, Britain, France, West Germany, Japan, Italy, and the USSR. Many years' experience in the use of the first fast sodium reactors has shown that the number of fuel-element failures involving oxide and mixed oxide fuel is less than 1% for burn-ups of more than 10% of the heavy atoms. In individual cases fuel elements remain efficient up to a burn-up of 15-18% of the heavy atoms. Damage only appears visually in 0.1% of the total number of fuel elements studied.

*See At. Énerg., 38, No. 4, 268 (1975).
†See At. Énerg., 39, No. 3, 230 (1975).

Translated from Atomnaya Énergiya, Vol. 40, No. 1, pp. 78-80, January, 1976.

There are two main causes of damage: production defects and the exhaustion of efficiency. Experience in the manufacture of 25,000 fuel elements for the Phenix reactor (France) revealed that, subject to qualified technological monitoring, production defects could be completly eliminated. As yet it has not been found possible to predict the limit of efficiency exhaustion with a sufficient accuracy, since damage criteria have not been finally established, nor have the damage mechanisms been clearly formulated. Furthermore, experimental data regarding the influence of irradiation on the properties of materials are as yet insufficiently reliable. Hence the limiting degree of burn-up of the fuel in the fuel elements is to a large extent chosen on an approximate or empirical basis. For example, in the French Rhapsodie, Phenix, and Superphenix reactors the burn-up is specified as 8, 6.5, and 9% of the heavy atoms respectively. Criteria relating to can damage depend on the means of loading, and may be determined, firstly, by reference to the degree of nonuniformity of the plastic deformation of the material and the ductility limit, secondly from the deformation rate, thirdly from the steady creep velocity, and fourthly from the yield stress of the material.

Detailed study has been devoted to the interaction between the mixed oxide fuel cores and the austenitic stainless steel cans which arises at temperatures exceeding 500°C, mainly as a result of the action of volatile cesium, iodine, and tellurium fragments accumulating in the reaction zone at the high oxidizing potential of the medium. The rate of intercrystallite penetration is high until roughly 3% of the heavy atoms have been consumed, after which it rapidly diminishes. For almost stoichiometric fuel compositions the depth of intercrystallite penetration may amount to 70-120 μ for deep burnup, but it is much less for substoichiometric fuel. For superstoichiometric fuel, however, a uniform frontal oxidation of the inner surface of the can occurs to a depth of 10 μ, without intercrystallite rupture. A reduction in the density of the fuel, a rise in the linear power of the fuel element, and an increase in the gap between the can and the core, especially in the presence of eccentricity, intensify the interaction. West German research showed that the intercrystallite penetration depended on the composition of the steel. German types of steel may be placed in the following series of increasing interaction (the brackets indicate foreign analogs to the West German brands of steel): 1.4988 (AISI-318, FV-548); 1.4919 (AISI-319); 1.4981 (OKh16N15M3B); 1.4970 (12R72HV). The difference in the depth of intercrystallite penetration amounted to as much as 20% for different types of steel. The interaction due to the presence of fission fragments does not lead to any direct damage to the oxide-fuel fuel elements, but it weakens the can. A change to the use of carbide fuel fails to eliminate interaction: In this case carburization of the inner surface of the can may occur to a depth approaching 40 μ.

Visible damage to the fuel elements consists of longitudinal cracks in the upper and central parts of the cans arising as a result of the exhaustion of efficiency in the material. The central cracks correspond to the region of maximum diametral deformation of the fuel elements and are most probably associated with a gradual increase in the mechanical action of the swelling core and the gas pressure inside the fuel element. The cracks in the upper, hot part, in which the oxide fuel is almost completely softened, are associated with the transient operating conditions of the fuel element, involving a considerable loss of ductility by the can (thermal ratchet effect). These mechanisms go hand in hand, and it is as yet hard to say which is the most serious. For boosted irradiation conditions, cracks in the hot part of the fuel element predominate. Cracks in the middle are usually formed after diametral distortions of over 1%. The permissible deformation of the material in the upper part of the element can hardly be taken as greater than 0.1%. Under normal service conditions the initiation and development of damage in one fuel element does not have any major effect on the whole assembly. The time between the loss of hermetic properties and the opening of a crack may extend to several months. Investigations into the behavior of fuel elements with artificial defects have revealed a relationship between the development of damage and the formation of sodium uranoplutonate under the can. Only if the coolant flow is reduced or stops altogether, or if individual open cross sections of the assembly become clogged, is it possible for damage to propagate to the neighboring fuel elements; in the case of oxide fuel the emergency is localized within a single assembly.

The individual mechanisms leading to the exhaustion of the efficiency reserve of the fuel elements are quite closely associated, for example, with the redistribution of the fuel within the interior of the fuel element, the accumulation of fission fragments, gas evolution under the can, and so on. At the same time the influence of the neutron-induced swelling of the cans, which predominates over mechanical deformation at temperatures below 525°C, and also the role of radiation-induced creep, have not yet been studied anything like sufficiently. One has the impression that the main effort should be directed at creating very strong and ductile construction materials, although combating the swelling effect is still a matter of no

mean importance. It is quite possible that it will prove desirable in the future only to use low-swelling materials for the housings of the whole fuel-element assemblies.

Theoretical investigations play a major part in establishing the mechanisms of fuel-element damage. Mathematical models and computing programs developed by scientists in various countries have in general proved perfectly adequate. Differences between various theories have in the main been associated with the interpretation and assessment of individual properties, as well as the computing speed and accuracy. Some programs have been developed in great detail, and account for quite refined phenomena (the effect of changes in the isotopic composition of the fuel, the continuous change in contact thermal conductivity, radial nonuniformity of the neutron-induced swelling, etc.). These useful computing programs cannot yet be fully exploited in view of the absence of adequate experimental data relating to the properties of the materials. This factor also impedes the establishment of the limiting and statistically averaged values of the fuel-element efficiency criteria.

Special attention should be given to the behavior of fuel elements under transient conditions of operation. These include the rapid transient processes associated with the triggering of the emergency protection system, failure in the pumps of the first circuit, a surge in the power of the reactor, partial or complete blocking of the coolant flow through the fuel-element assembly, and finally repeated changes in power level. The aim of these investigations (the importance of which it is hard to overestimate) is to establish the limitations which will enable fuel-element efficiency to be maintained right up to the onset of an emergency situation. Such criteria include, for example, the limiting plastic deformation of the construction materials in various temperature ranges, for various loading rates, and for various doses of neutron irradiation and degrees of chemical interaction with the ambient; the permissible power surges; the permissible scales of fuel melting; the rupture of the can by gas pressure on overheating, and so on. The extension of steady-state and quasi-steady-state theoretical models to the case of rapidly changing parameters requires considerable development and careful comparison between the analytical results and experiment. It is important, for example, to allow for the transient nature of gas evolution, the redistribution of porosity in the fuel, mass transfer on melting, the transience of the mechanical interaction between the core and the can, the growth rate of the gas pressure (which may amount to hundreds of atmosphere), and so on.

A number of western countries and also Japan have undertaken combined and independent programs for studying the efficiency of fuel elements under transient conditions, including experiments inside the reactor involving power surges and coolant losses, and investigations aimed at establishing the influence of rapidly changing processes on the hydraulic and thermophysical characteristics of the fuel-element assemblies. It is also intended to carry out experiments on the heating of fuel elements irradiated to various burn-ups outside the reactor. The programs envisage the use of the TREAT pulse reactor (USA), which enables power surges to be introduced in a controlled way, with a visual assessment of the rupture process, and also loops of the experimental French thermal reactors, in which it is intended to carry out similar experiments with fuel elements previously irradiated in the fast Rhapsodie reactor. Individual experiments have already been carried out. The forming of the irradiated fuel on melting and the rupture of the can by gas pressure at points of overheating have been studied, and the rise in gas pressure in the fuel element following a power surge in the TREAT reactor has been estimated. Preliminary experiments have shown that the rupture of the fuel elements under transient conditions may be associated with the rapid evolution of gas from the molten fuel. Gas evolution from the solid fuel begins playing a major part in the transient process before the onset of melting, leading to additional mass transfer; the onset of can rupture depends on the original structure of the core. A brief power surge does not cause any serious damage to the fuel-element cans.

The effect of the efficiency of the fuel elements on the question of safety in the running of fast reactors is of importance in connection with the possible extension of any emergency situation (including that associated with anomalous working conditions) beyond the confines of the fuel-element assemblies, to embrace part or the whole of the active zone itself. Models are being developed to represent the mechanisms underlying the development of such hypothetical emergencies in order to establish the conditions under which the irregularity may be entirely contained within the fuel-element assemblies, so that a complete damaged assembly may be replaced without disturbing the running characteristics of the reactor as a whole. It is considered that when using oxide fuel it should be perfectly possible to make a reliable determination of the location and extent of the damage and to replace the fuel-element assembly quite safely, subject to the development of the necessary measuring devices recording the presence and type of activity of the fission fragments in the reactor.

THIRD CONFERENCE ON NEUTRON PHYSICS

A. I. Kal'chenko, D. A. Bazavov,
B. I. Gorbachev, A. L. Kirilyuk,
V. V. Kolotyi, V. A. Pshenichnyi,
A. F. Fedorova, and V. D. Chesnokova

The conference took place June 9-13, 1975 in Kiev. The participants were 300 Russian scientists from 42 institutes and science centers of the USSR and 50 foreign representatives from 16 countries. Ninety-two reports, including reviews and single communications, were presented. The conference took place in the form of 7 sections in which the most important modern problems of neutron physics were discussed.

Requirements in Regard to Nuclear Data and Their Evaluation. The Conference began with a presentation of the requirements in regard to nuclear data for reactor technology, thermonuclear reactors, astrophysics, and reactor physics. The reports put into evidence that to date the requirements in nuclear data and, even more, in neutron data by many fields of science and technology have now been formulated, have received the technological and economical foundation, and have been brought to the scientists. These requirements are heaviest in reactor technology and shielding from penetrating radiation.

L. N. Usachev (Physics and Power Institute, Obninsk) reported on mathematical studies of the Physics and Power Institute and on a set of programs of experimental investigations. He based his considerations on the conditions required for obtaining the desired accuracy of nuclear data with a minimum of expenses. N. M. Nikolaev (Physics and Power Institute, Obninsk) reported on the strategy of obtaining the required accuracy of neutron data; for this purpose, microscopical and integral experiments are combined in the best possible manner. Work was described which is done in the Soviet Union on experimental setups capable of satisfying a large number of the requirements of highest priority. G. E. Shatalov (I. V. Kurchatov Institute of Atomic Energy, Moscow) outlined problems related to the influence which nuclear constants have upon calculations of the blanket of a thermonuclear reactor in terms of neutron physics. The interest which scientists developing thermonuclear reactors have in neutron data increases from year to year. The expansion of the work on the evaluation of nuclear data caused great interest. Two complete files (data sets) on ^{235}U (Institute of Nuclear Physics of the Academy of Sciences of the Belorussian SSR, Minsk) and on iron (Physics and Power Institute, Obninsk) and some other papers dealing with the evaluation of the cross sections of nickel, chromium, gold, carbon, and other important construction materials and of stable nuclei (fission fragments) were presented.

Noteworthy was the contribution which the report of G. Salvi (France) made to the new information on the evaluation of nuclear data. The report dealt with a method of calculating the cross sections of capture, fission, and inelastic scattering in the case of heavy nuclei in the energy range 3 keV-1 MeV and calculating the cross sections of n, xn and n, xnf processes at energies of 2-20 MeV.

It follows from several reports that it is now possible to automatically obtain grouped constants from the files of microscopical data (mainly from the SOKRATOR system); methods have been developed for matching nuclear data obtained from integral experiments on the basis of the grouped constants.

A report by N. A. Vlasov (I. V. Kurchatov Institute of Atomic Energy, Moscow) on neutron reactions in stars was received with interest.* It was shown that it is possible to accurately determine the cross sections of radiative neutron capture at energies of 30-200 keV for solving the fundamental problem of the origin of elements.

*See also At. Énerg., 39, No. 2, 103 (1975).

Translated from Atomnaya Énergiya, Vol. 40, No. 1, pp. 80-82, January, 1976.

Fundamental Properties of Neutrons. This section assembled for the first time. The topics of this section put into evidence that it is justified to introduce this section into the program of the Conference, because, in addition to applied problems, problems involving important principles must be discussed. V. M. Lobashev (B. P. Konstantinov Leningrad Institute of Nuclear Physics) presented a review on the present state of research on the electric dipole moment of the neutron and the general knowledge of this matter. He reported on an experimental setup for measuring the dipole moment of the neutron with the aid of ultracold neutrons. This work, which involved experiments of very high accuracy, has proved that it is promising to use ultra-cold neutrons for further research work. V. I. Lushchikov (Joint Institute of Nuclear Research, Dubna) reported on the present state of work done with ultracold neutrons and reviewed several papers presented to the Conference on Ultracold Neutrons, particularly as far as the papers were related to the development of detectors, converters, neutron guiding means, and receptacles for retaining ultracold neutrons. This is a very promising direction of neutron physics and receives more and more attention.

B. G. Erozolimskii (I. V. Kurchatov Institute of Atomic Energy, Moscow) and Yu. A. Aleksandrov (Joint Institute of Nuclear Research, Dubna) spoke of new measurements of the angular spin-electron correlation in the decay of polarized neutrons, research of the n—e interaction, and the state of research done in our country and abroad on other fundamental properties of the neutron.

General Problems of the Interaction of Neutrons with Nuclei. Problems of the theory of nuclear structure and the mechanism of nuclear processes were discussed in review reports and communications which are traditional in nuclear physics work. We mention the model calculations of the density of nuclear states as a function of the excitation energy of the nucleus (V. G. Solov'ev and V. V. Voronov, Joint Institute of Nuclear Research, Dubna; and A. V. Ignatyuk, Physics and Power Institute, Obninsk), the various aspects of the optical model and its new versions, the fragmentation of separate single-particle states (V. G. Solov'ev, Joint Institute of Nuclear Research, Dubna), the structure of analog states (D. F. Zaritskii and M. G. Urin, I. V. Kurchatov Institute of Atomic Energy). A general rule can be recognized in the reports: Since the main institutes of the USSR are now equipped with modern computers, it is possible to treat and solve the problems within the existing concepts of nuclear structure, whereas it was earlier practically impossible to handle these problems. It is now possible to compare both theoretical and calculated results with experimental results in greater detail and on a larger scale so that our insight into the structure of the atomic nucleus has been improved. Characteristic in this respect is the work done by the group of theoreticians of the Joint Institute of Nuclear Research in which very laborious calculations of the density of nuclear states are made with the well-known phenomenological microscopical theory of the nucleus. The results are suitable for a direct comparison with the experimental data.

This section included a review report by G. Salvi (France) on the results of work done by four groups, who are concerned with the development of new versions of the optical model. Work on an optical model with a nonlocal real potential is of interest; this work requires considerable computer time. The report by G. Salvi dealt mainly with methodological aspects but papers presenting new results in terms of physics must be expected in the near future.

Experimental Investigation of the Interaction of Thermal Neutrons and Resonance Neutrons with Nuclei. Recently, research on the structure of resonances (compound states) has received increasing attention. Therefore, reports on the experiments which were done in the Joint Institute of Nuclear Research in investigations of (n, α)- and (n, $\gamma\alpha$)- reactions at resonances, in determinations of the magnetic moments of compound states, and in work on the details of capture-induced gamma radiation at resonances were accepted with great interest. Some general tendencies were recognized during the Conference and should be noted. First of all, we note an increased research activity with radioactive and transuranium nuclei, measurements of the energy dependencies of the neutron cross sections, and analyses of the parameters of neutron resonances (Institute of Nuclear Research of the Academy of Sciences of the Ukrainian SSR, Kiev; Institute of Theoretical and Experimental Physics, Moscow; NIIAR, Dimitrovgrad); besides that, machines working with polarized neutrons and nuclei have been put into operation and the first results have been obtained with them (V. P. Alfimenkov, Joint Institute of Nuclear Research, Dubna; K. Abrahams, The Netherlands).

Experimental Investigations of the Interaction of Fast Neutrons with Nuclei. Reports were discussed which were devoted to research on radiative capture and inelastic scattering of fast neutrons, neutron cross sections, the spectra of fast neutrons, and investigations of the structure of the atomic nucleus with the aid of fast neutrons (V. A. Tolstikov, Physics and Power Institute, Obninsk; M. B. Fedorov, Institute

of Nuclear Research of the Academy of Sciences of the Ukrainian SSR; O. A. Sal'nikov, Physics and Power Institute, Obninsk; and L. I. Govor, I. V. Kurchatov Institute of Atomic Energy). It was shown in the report by L. I. Govor that even in the future reactors will be successfully used as a source of both slow and fast neutrons for research in neutron physics. Z. Ziriax (Federal Republic of Germany) demonstrated again the experimental possibilities of the neutron spectrometer used on the base of the isochronous cyclotron in Karlsruhe. Therefore a time-of-flight neutron spectrometer of the nanosecond range should be put into operation as soon as possible for work with fast neutrons on the base of the U-240 Kiev cyclotron. The new possibilities which have been opened by spectrometers used on isochronous cyclotrons facilitate investigations in a wide energy range. The investigations can be made with an accuracy which the users of nuclear data for nuclear and thermonuclear reactors must have at the present time.

Cross Sections and Other Characteristics of the Fission of Heavy Nuclei by Neutrons. This problem was considered in a large number of papers (42 Soviet papers and 24 Western papers). The experimental facts were interpreted from the viewpoint of a double-hump fission barrier in theoretical work and in calculations. It was unanimously noted that, though there does not exist a straightforward experiment confirming the existence of a double-hump barrier, all the experimental evidence can presently be described only with the assumption of a barrier of this form.

The reports of the foreign participants (G. Specht and G. Pauli, Federal Republic of Germany; G. Blanc, France; Ch. Sykos, Hungary, and others) have shown that the concept of a double-hump barrier has been generally accepted and forms an important theoretical basis for new experiments and the development of new concepts.

It is very important to increase the accuracy of measurements of fission cross sections in a wide energy interval and to improve the absolute measurements of fission cross sections. As in the past, experiments with ^{252}Cf are of great interest both in regard to a deeper understanding of the fission process and to obtaining reliable constants for relative measurements using ^{252}Cf as a standard. The work encompasses detailed investigations of spectra of fission neutrons, emission times, and angular distributions. Attention was directed to the important role of the isotropic component of the spectrum of fission neutrons and to the need for further research on the problem.

The results of the latest measurements of fission cross sections of heavy isotopes of plutonium at energies of 1-7 MeV and precise values of the fission cross sections of ^{235}U, ^{238}U, ^{237}Np, and ^{239}Pu as obtained on the spectrum of the neutrons from ^{252}Cf fission were reported. For example, the fission cross section for ^{235}U was obtained with an error of 1.5% (1265 ± 19 mbar).

Results of excellent accuracy and resolution obtained in measurements made on ^{237}Np, ^{238}U, ^{243}Am and ^{239}Pu, ^{241}Am nuclei were described by D. Paye (France) and in the report by K. Attley (Great Britain) on measurements of the fission cross section of ^{239}Pu and the ratio of the fission cross sections of ^{238}U and ^{235}U.

Experimental Techniques of Neutron Physics. The problems related to obtaining and forming intense beams of cold polarized neutrons, the construction of pulsed sources of fast neutrons, and the automation of both collection and evaluation of data were considered. Some reports were devoted to neutron detection systems. The report "Neutron Sources and the Use of Laser Techniques" found great interest. It was shown in that report that it is possible to build pulsed sources with excellent parameters in regard to duration and intensity of the neutron pulse. The fact that it is possible to obtain cold polarized neutrons with high yield indicates that the reactor as a neutron source can be used on a broader scale in neutron physics research. Experimentalists and users of nuclear data are very interested, as in the past, in pulsed sources of resonance neutrons and fast neutrons. The participants of the Conference received with satisfaction the communication that the linear "FAKEL" accelerator has been put into operation (I. V. Kurchatov Institute of Atomic Energy, Moscow) and that the first stage of the GNEIS spectrometer has been built on the base of the phasotron of the Leningrad Institute of Nuclear Physics. The construction of a fast neutron spectrometer on the base of the isochronous U-240 cyclotron in the Institute of Nuclear Research of the Academy of Sciences of the Ukrainian SSR is expected in the near future.

Of the communications of foreign scientists, the report of M. Ashgar (France) on the construction of the LOHENGRIN spectrometer for undelayed fission products caused greatest interest. Since this device has been put into operation on the most powerful research reactor in Grenoble, detailed information on some characteristics of fission products has been obtained and the outlook on future work is very promising.

The Conferences on Neutron Physics, which have become a matter of tradition, are accepted with increasing interest. These conferences promote the exchange of opinions, ideas, and information and further fruitful discussions. All this stimulates further progress in this important field of nuclear physics.

The next conference on Neutron Physics will be held in 1977.

SCIENTIFIC SEMINAR ON THE COMPLEX OPTIMIZATION OF POWER INSTALLATIONS

Yu. I. Koryakin

The first session of the All-Union Scientific Seminar on complex methods of optimizing installations for the conversion of thermal and nuclear energy into electrical power was held on September 23-26, 1975, in the Siberian Power Institute, Siberian Branch, Academy of Sciences of the USSR, in the city of Irkutsk. The theme of this session was based on mathematical methods of simulating and optimizing the parameters of nuclear power stations, the form of the technological arrangements, and the profile of the equipment. Some 55 members of 21 organizations took part in the seminar; 27 contributions were presented and discussed. The President of the Seminar was Corresponding Member of the Academy of Sciences of the USSR L. S. Popyrin.

The papers may be roughly divided into the following groups: general questions regarding the mathematical simulation of nuclear power stations (nine papers); the mathematical simulation and optimization of nuclear reactors (six papers); the mathematical simulation of the heat-engineering parts of nuclear power stations (seven papers); mathematical models of nuclear/thermal power systems.

Practical experience of recent years has shown that many problems in nuclear power development, from the determination of the basic systems involved in its progress to the optimization of the parameters characterizing nuclear power stations (in part or whole) may and should be solved by using mathematical models (simulation). Mathematical simulation supplements design computations in relation to nuclear power stations; it facilitates the solution of problems associated with multivariant optimization procedures as applied to the technical and economic indices (chiefly in the initial design stages). Such problems arise in connection with multiparameter optimization, the indeterminacy and inaccuracy of the initial information, and the shortcomings of computing methods, and efficiency criteria, and also in connection with the continuous correction of technical solutions during the design process. Calculations based on the mathematical models of reactors and nuclear power stations may well reveal any promising tendencies as regards the combination of parameters, provide a great deal of information for engineering analysis, and point out the best directions for more detailed design and computing work.

One of the most important fields of application of mathematical models is the complex optimization of the objects of investigation, i.e., the deliberate selection of those values of the defining constructional and technical indices of the object (with due allowance for technical limitations) which will correspond to the optimum value of the chosen efficiency criterion (i.e., the target function, which is most frequently the calculated losses).

In order to provide a better understanding of the hierarchy of the mathematical models used in nuclear power, two papers regarding the mathematical simulation of a nuclear power system were presented to the Seminar. The results of model calculations indicate a strong link between the indices of nuclear power stations as objects of simulation and the indices of a real system of nuclear power stations; they also indicate the influence of methodological requirements and conditions on the approach to the method of attack, and the choice of limitations in the complex simulation of the nuclear power station itself.

Since the Seminar was essentially of a methodical nature and also the first of its kind, it was important to acquaint the participants as broadly as possible with the simulation procedures adopted by various organizations. It was also essential to assess the breadth and scale of contemporary research, the

Translated from Atomnaya Énergiya, Vol. 40, No. 1, pp. 82-84, January, 1976.

characteristics of various practical approaches, and other practical aspects of particular importance, to exchange opinions, and to make a concerted attempt at systematizing methods of mathematically simulating nuclear power stations already in use or in immediate prospect. It was therefore appropriate that the representatives of a fairly large number of organizations using mathematical methods of simulating nuclear power stations should be present, despite the fact that the main problems of these organizations in the field of nuclear power development varied quite widely and were concerned both with education and with the specific construction of various components and equipment for nuclear power stations. In other words, the main aim of the Seminar was to consider simulation questions broadly rather than deeply. It was considered that a deeper study of the mathematical simulation of nuclear power stations could be undertaken better at subsequent Seminars with a smaller number of participants. This should promote greater practical results in the complex mathematical simulation of nuclear power stations.

The methodical approaches discussed all tended to be similar, but there was a great variety of emphasis in the application of models to the objects under study. All the participants of the Seminar emphasized the importance of using methods of mathematical simulation for solving scientific-research and applied problems in nuclear power, in particular the importance and fruitfulness of mathematical simulation from the point of view of time economy and (largely) labor expense. A number of organizations have already developed models for the complex optimization of nuclear power stations and sections of these, and have put the models to practical use. In the majority of cases the use of the decomposition principle was indicated, i.e., the arbitrary division of the nuclear power station into two parts: the "expanded reactor" and the "expanded machine room." The first incorporates the reactor and the nuclear steam-generating equipment, the second incorporates the turbine system and heat-engineering apparatus. These two subsystems are first optimized in relation to their internal parameters and then matched with respect to the coupling parameters, which are either fixed or enter as external coupling factors in the subsystem being optimized. In order to describe the process in hand or the special characteristics of the objects, the algorithm of the model often employs approximating equations capable of being corrected as more accurate information becomes available. In order to establish the adequacy of the representation of the real nuclear power station by its mathematical model, the indices of the real object are usually compared with the indices calculated for the model, using the same initial data. This method has been used, for example, in the complex optimization of a nuclear power station with a water—graphite reactor, as described in the Seminar. Optimization was carried out by reference to the minimum calculated losses; it confirmed the adequacy of the model with respect to the real object. The majority of indices are determined by means of approximating equations with an absolute error of less than 10%.

Among other methods currently in use which were described at the Seminar, the "experiment-planning" method is one of particular importance. The essence of this method lies in the fact that the power installation (or part of the installation) is represented as a kind of "black box," i.e., the complex physico-technical relationships between its internal elements need not be kept continuously in view. Only the relationship between the input and output variables is essential. The first of these are the independent parameters of the power installation (or its elements), the second are the technicoeconomic characteristics, or "response functions," which are represented in the form of regression equations. The experiment lies in calculating the characteristics of the installation; it is carried out not with the real object but with its mathematical model. Optimization of the thermodynamic cycle of a nuclear power station using dissociating gas has been carried out by the experiment-planning method.

The Seminar also considered a method of separating essential and inessential factors for the object or process under consideration (so determining the optimum size of the model), and also the equivalence method, i.e., the conversion of one mathematical model into another, adequate (to a certain accuracy) with respect to the former, but simpler in format.

The broad introduction of methods of mathematical simulation into engineering practice reveals the weak link in this process — the great amount of labor required from highly qualified programmers in preparing the computing program. Furthermore, the program developed on a "manual" basis is not always the best possible, since its form and sequence are determined on the basis of the subjective considerations of the programmers. A paper by L. S. Popyrin described the Siberian Power Institute's improved automated method for constructing mathematical models of thermal power installations. This approach ensures both automation of the majority of the processes involved in setting up auxiliary procedures to describe individual technological processes and items of equipment, and also the automatic formation of a mathematical model of the installation in accordance with its technological scheme. This enables the extremely laborious work relating to the creation of mathematical models to be mechanized and the development time shortened by a factor of many tens. Many of the contributions laid main emphasis on the

mathematical simulation and optimization of the actual active zone of the power reactor. The rest of the reactor, with its complex combination of engineering devices, which ought also to be the subject of mathematical simulation for purposes of optimization, has not yet received sufficient attention.

An important question which arose during the work of the Seminar was that of optimization criteria. At the top level of the hierarchy of mathematic models in nuclear power engineering, i.e., that concerned with a whole system of nuclear power stations, it is inevitable that the optimization process should involve multiple criteria, owing to the wide variety of practical problems and development conditions of the nuclear power system; at the lower level, i.e., the simulation of individual nuclear power stations and their components, single-criterion optimization is better (the function being in the form of the calculated losses). However, in the course of discussion several participants of the Seminar remarked that this point of view was not the only one possible: Even in simulating a single nuclear power station (and its components), multiple-criterion optimization might become vital. Special attention was paid to the importance of using the criterion of minimum labor expenditure and labor resources. Thus the question as to the optimization criteria assumes independent significance, and as yet cannot be regarded as clear and agreed from a methodical point of view.

Another subject for discussion at the Seminar was the question of interaction between the human operator and the mathematical mode. On the whole this amounts to the fact that only strictly limited problems are susceptible to mathematical simulation, in the presence of duly considered technical decisions, whereas fundamentally new technical solutions may be created by heuristic methods, which the mathematical model is unable to realize. It was indicated in several papers that at the present time the role of mathematical simulation in the overall development and design of nuclear power stations is relatively slight. At the same time, mathematical models realized in electronic computers constitute a most effective tool for discovering optimum schemes and parameters in power-generating installations. The information employed in mathematical simulation is still incomplete. In this connection the importance of using optimization methods under conditions characterized by the indeterminacy, incompleteness, or low quality of the original data was emphasized, as well as the importance of creating an information system for mathematical simulation.

The discussions associated with each of the groups of papers indicated were extemely useful.

On the whole the Seminar laid the basis for the organized comprehension, generalization, and intensification of existing research into this undoubtedly promising new scientific direction, the complex optimization of nuclear power stations (and their components) by mathematical simulation.

The Seminar papers will shortly be published by the Siberian Power Institute.

SOVIET — AMERICAN SEMINAR ON FAST-BREEDER REACTORS

E. F. Arifmetchikov

In accordance with the collaboration program between the USSR and the USA in the field of fast-breeder reactors, a seminar on experience and problems in the design and utilization of fast breeders with sodium as the coolant was held in Obninsk in the summer of 1975. The American participants of the Seminar were representatives of the Energy Research and Development Administration (ERDA) and of companies working on the planning, the construction, and the utilization of installations having liquid-metal fast-breeder reactors (LMFBR); other US participants were from national laboratories working on LMFBR problems. Each side presented 11 reports.

The report of T. Nemseck et al. was concerned with the history of the development and the present state of the LMFBR program in the USA and the role of both the national laboratories and US industry in the development of the technological principles, the fuel, the materials, and the components for commercial LMFBR reactors. The other US reports dealt with the construction, the utilization, and experimental programs of the reactors EBR-II, Enrico Fermi, SEFOR, and FFTF and with the project of an atomic power station in Clinch River.

In 1974 the original plan of building three demonstrational atomic electric power plants with LMFBR reactors having a (electrical) power of 300-500 MW was replaced by the plan of building a 350-MW (elec.) reactor in Clinch River to concentrate the efforts on the completion of large-scale components and on a prototype of a commercial 1200-1500-MW (elec.) unit. The program envisages the full industrial implementation of LMFBR reactors by the 1990's. The Hanford Engineering Laboratory and the Design Center of Liquid Metals in Santa Susannah carry the bulk of the responsibility for the technological aspects of the LMFBR development work. They develop and test materials, components, and mechanical parts, as well as instruments for LMFBR reactors. The centers have: the FFTF reactor with a 400-MW thermal power for testing samples of both materials and fuel (the reactor is to be put into operation in 1978); a high-temperature sodium laboratory for testing huge reactor components in both air and sodium; a chemical engineering laboratory and a fuel-element laboratory (Hanford); stands for testing pumps operating with sodium, models of steam generators with a 35-MW thermal power, and models of steam generators with strong water discharge into sodium; and a stand for the purification of large equipment from sodium, etc. (Santa Susannah). It is planned to build a laboratory for testing large components of industrial 150-MW thermal-power LMFBR reactors (PCTF) in sodium, for destructive and nondestructive testing of irradiated fuel elements, and for the reprocessing of fuel elements.

As far as the aspects of physics are concerned, the program envisages further gathering of nuclear data of higher accuracy, the development of both a theory and methods of reactor calculations, and the execution of integral experiments. The latter make use of the zero-power reactors ZPP-6, ZPR-9, and ZPPR, of the reactors of the Argonne National Laboratory (AFSR, ATSR), and of the TSF unit. As to the safety aspects, theoretical and experimental investigations concern disturbances of the fuel-element cooling conditions (OPERA), an experimental investigation of the interaction of melted fuel with sodium when the coolant circulation is rapidly interrupted (TREAT; LOFT — Engineering Laboratory in Idaho Falls), and the possible clogging of the channel in the case of a sudden discharge of gaseous fission products from a fuel element (TFTF).

The US industry actively participates in the LMFBR work, works on experimental programs, and develops and produces fuel, materials of the core, and equipment. The Argonne National Laboratory and

Translated from Atomnaya Énergiya, Vol. 40, No. 1, pp. 84-85, January, 1976.

TABLE 1. Characteristics of the Cores of Some Reactors

	FFTF	Clinch River	Industrial reactor
Thermal power, MW	400	975	3800
Electrical power, MV	—	350	1500
Load factor	—	0,75	0,85
Temp. of coolant at entry to core, °C	422	388	380
Temp. of coolant at exit from core, °C	565	535	538
Fuel	Oxide	Oxide	Oxide
Shell	Steel 316	Steel 316	Steel 316 with low swelling
Ht. and diam. of core, m	0,914/1,24	0,914/1,89	1.24/3.11
Diam. of fuel rods, mm	5,8	5,8	6,9
Vol. fraction of fuel	0,329	0,325	0,342
Heat liberation (max./av.), kW/m	45,9/24,9	47,6/22,9	52,5/36,1
Max. burnup, MW·days/ton	80 000	150 000	150 000
Mult. factor	—	1,2	1,25
Doubling time, yrs.	—	23	12—15

the companies Babcock and Wilcox, General Atomics, General Electric, and others are producers of uranium — plutonium oxides. Carbides are produced by Atomics International, Westinghouse Electric, and the Los Alamos Laboratory; nitrides are produced by the Batelle Institute and the Oak Ridge National Laboratory. Various companies and laboratories participate in the development of instrumentation for the reactors, steam generators, mechanical pumps, etc.

The EBR-II reactor [62.5-MW thermal power, maximum neutron flux $3 \cdot 10^{15}$ neutrons/(cm^2·sec)] is presently the main station for the irradiation of materials in the USA. In this reactor the following burnup rates (% of the heavy atoms) and integral fluxes of fuel irradiation (10^{23} neutrons/cm^2) are reached: for carbide fuel — 12 and 1.2, respectively; for metal fuel — 15 and 1.2, respectively; and for oxide fuel — 17 and 1.5, respectively. During its ten years of operation, the reactor worked with an average load level of 42.6%. The low load figure is a consequence mainly of the experimental program and the large number of actuations of the control and safety rods due to spurious signals (280 since 1966).

The construction and operation of the Atomic Electric Power Plant "Enrico Fermi" (1963-1972) with a 200-MW thermal power have significantly contributed to the principal design schemes of an atomic electric power plant using an LMFBR reactor, to reactor technology, to the planning and the design of reactors, to the determination of nuclear characteristics, and to mechanical testing and utilization of large sodium-containing components of an LMFBR reactor. In 1966-1970, the atomic electric power plant was repaired because two fuel element assemblies had been partially melted and fission products had entered into the cooling system. At the end of 1972, the reactor operation was stopped owing to financial difficulties.

The experiments which were made in 1969-1972 on the SEFOR reactor (20-MW thermal power, UO_2 — PuO_2 fuel, sodium as the coolant) have convincingly proved stability and safety of operation of fast breeders having a composition, neutron spectrum, and temperature distribution typical for huge LMFBR reactors.

The next stage in the Anerican LMFBR program concerns the construction of a large experimental center for critical testing of fuel elements and materials in the FFTF reactor whose release is provided for 1978. The experimental conditions in the FFTF reactor allow a sodium-exit temperature of as high as 760°C and a maximum neutron flux of $1.3 \cdot 10^{16}$ neutrons/($cm^2 \cdot sec$). The construction of the FFTF reactor is completed to about 40%.

In 1973 work on the project of a demonstrational atomic electric power plant in Clinch River was initiated. The construction work is to begin in 1975 and the reactor is to become critical in 1982. The experience gathered with the LWR and FFTF reactors will be brought into account to the greatest possible extent in the projecting work and the construction of the Clinch River installation. Sufficient space for easy assembly of the huge components of the installation has been provided; models and prototypes have been used for the planning of the construction. Table 1 lists some project characteristics of the cores of the FFTF reactor, the Clinch River reactor, and an industrial reactor.

The Soviet reports were devoted to the experience gathered in the utilization of the fast breeder (BR-5, BOR-60, and BN-350) installations working in the USSR, to problems and engineering aspects of the projecting of fast breeders for industrial applications and, more specifically, to the selection and optimization of the characteristics, to the creation of cold traps for sodium impurities, to the purification of the protective gas from vapors and sodium aerosols, to the preparation of the coolant, etc. V. V. Orlov reported in his review on the basic stages of more than 25 years of USSR work on fast breeders. The experience, which has been accumulated, made it possible to start the construction of industrial pilot-types of fast breeders (BN-350 and BN-600) and to develop an industrial 1600 MW (elec.) reactor. However, the development of reliable steam generators, achieving high reproducibility, the solution of problems related to the chemical refining of the fuel, and obtaining competitive economic parameters relative to thermal reactors are preconditions for the industrial implementation of fast breeder reactors.

ALL-UNION CONFERENCE ON "DEVELOPMENT AND APPLICATION OF ELECTRON ACCELERATORS"

A. N. Didenko and V. K. Kononov

The traditional 9th Conference on Electron Accelerators took place from Sept. 3-5, 1975, in the Tomsk Polytechnical Institute. The first Conference on Electron Accelerators was held exactly 20 years ago. Since then these conferences were regularly convened in intervals of about 2 yr.

The present conference was an interesting example. About 400 scientists and engineers from 69 organizations of the Soviet Union participated. In addition to representatives of the well-known accelerator centers of the USSR, the co-workers of teachings organizations, scientific institutions, and industrial enterprises using accelerator devices in various fields of science and technology participated in the conference.

More than 300 reports were presented to the plenary session and the 11 sections. Besides that, there were sessions of the subsections "Superconducting Elements of Accelerators" and "Microtrons" of the Scientific Council of the Academy of Sciences of the USSR on problems related to the acceleration of charged particles. Review reports dealt with the state and the chances of investigations made with electron accelerators in nuclear physics and hypernuclear physics (G. A. Sokol, Moscow), with problems of the development of high-current electron accelerators and their utilization (A. N. Didenko, Tomsk), with the state and the future chances of the development of linear accelerators for low and medium energies (O. A. Val'dner, Moscow), of microtrons (V. N. Melekhin, Moscow), and of cyclic inductive accelerators with a constant guiding field (V. L. Chakhlov, Tomsk), and with the chances of using synchrotron radiation (A. A. Sokolov, Moscow). All reports presented to the sessions of the various sections can be subdivided into the following three subject groups: 1) development, construction, and improvement of classical electron accelerators (synchrotrons, betatrons, microtrons, and linear accelerators); 2) development and construction of straightforward high-current electron accelerators and the investigation of new acceleration methods with these accelerators; and 3) utilization of electron accelerators in various fields of the national economy.

The reports of the first group were discussed in four sections. The reports of the Scientific-Research Institute of Nuclear Physics of the Tomsk Polytechnical Institute on the modernization of the "Sirius" synchrotron (extraction of the electron beam, generation of a "plateau" on the pulse of the magnetic field, and generation of a beam of polarized electrons) were received with great interest. At the present time the electron beam is extracted with an efficiency of up to 60%; a "plateau" with a length of 22 msec and a stability of ±0.15% is created on the pulse of the magnetic field. The co-workers of the All-Union Scientific-Research Institute of Opticophysical Measurements reported on the construction of an ironless 50-MeV synchrotron as an intensity standard for the vacuum ultraviolet. Work done in the Institute of Nuclear Physics of the Siberian Division of the Academy of Sciences of the USSR on increasing the beam intensity of the B-4 synchrotron (injector and storage device VEPP-3) and in the Physics Institute of the Academy of Sciences on the slow extraction of electrons from the "Pakhra" synchrotron was reported and caused great interest.

The sessions of the section "Betatrons" in which 28 communications were reported dealt with the development of inductive accelerators. Certain progress, which was made in the development of new inductive accelerators and their utilization in industry and medicine, was noted. New small-size pulsed MIB-3 and MIB-6 betatrons were developed in the Tomsk Polytechnical Institute. The dose rate of these betatrons was increased more than 10 times. A compact high-power 25-MeV betatron with a weight two times

Translated from Atomnaya Énergiya, Vol. 40, No. 1, pp. 85-87, January, 1976.

smaller than that of previous models was also built in the Tomsk Polytechnical Institute. Multiorbit betatrons and betatron complexes (Tomsk Polytechnical Institute, Tomsk), inductive accelerators with constant controlling field (Physics Institute of the Academy of Sciences, Moscow; Scientific-Research Institute of Nuclear Physics, Tomsk), and ironless inductive accelerators (Leningrad State University, Leningrad) have been developed and built. New methods of generating controlling fields in betatrons have been designed.

Twenty two reports from 8 organizations were presented to the section "Microtrons and Linear Accelerators." A sector microtron for 25 MeV, which is to be used for the injection of electrons into the "Pakhra" synchrotron, is being built in the Physics Institute of the Academy of Sciences. The Saratov State University does extensive work on the construction of microtrons and on the improvement of their components. The great success attained by the Scientific-Research Institute EFA (Leningrad) and by the Moscow Engineering Physics Institute in the building of serial linear accelerators and their utilization in medicine and the national economy was outlined.

The results of work on the development of superconducting accelerator elements were discussed for the first time in a conference. The Scientific-Research Institute of Nuclear Physics (Tomsk), the Scientific-Research Institute (EFA, the Physicotechnical Institute of the Academy of Sciences of the Ukrainian SSR (Khar'kov), and the Radiotechnical Institute of the Academy of Sciences of the USSR (Moscow) have been most successful in this field. Results of investigations on superconducting resonators and on methods of treating and protecting their surfaces were reported by the co-workers of the Scientific-Research Institute of Nuclear Physics (Tomsk). Methods of nuclear physics were used for the first time in this work to analyze the state of the surface of a superconducting material. The co-workers of the Scientific Research Institute EFA told of an investigation of the parameters of a superconducting resonator of the 10-cm band made of niobium. The resonator was designated for an experimental superconducting 5-MeV electron accelerator.

A communication by representatives of the All-Union Scientific-Research Institute of Electrothermal Tooling (Moscow) on the development of an electrical superhigh vacuum furnace for the annealing of superconducting resonators was accepted with great attention. The basic design parameters of the unit are: temperature of operation 2200°C, pressure at the temperature of operation 10^{-8} mm Hg, and diameter and height of the articles to be annealed 250 and 500 mm, respectively. This furnace, which was built by order of the Radiotechnical Institute, has been brought to the Scientific-Research Institute of Nuclear Physics in Tomsk and assembled in it. The subsection "Superconducting Accelerator Elements" recommended that the work of all organizations capable of performing investigations with the aid of the furnace should be coordinated.

Reports of the second group caused very great interest. The reports were discussed in three sections. Twenty seven reports from 11 organizations were presented to the section "Straightforward Accelerators." Most of the reports dealt with the results of development work on straightforward high-current accelerators with energies of up to 2 MeV and currents of several ten thousand amperes in nanosecond or microsecond pulses. Several organizations reported on the development of new accelerators of this type. The large number of reports indicates that extensive work is being done in the USSR on the development of these accelerators and that these accelerators are increasingly used in modern science and technology. Particular interest in accelerators generating microsecond beams with a power in excess of 1 GW was noted in the reports. The participants of the conference were informed of the new Tonus-II accelerator of the Scientific-Research Institute of Nuclear Physics (Tomsk), which makes it possible to obtain 1.5-MeV electron beams with a current of 20 kA and a pulse duration of up to 7 μsec.

The reports were also concerned with physics research which is done with the aid of high-current electron accelerators. As far as the subject matter is concerned, these reports can be divided into four groups. The first group works on the theory and on experiments of self-acceleration and was represented by the Physicotechnical Institute of the Academy of Sciences of the Ukrainian SSR and the Khar'kov State University, the Scientific-Research Institute of Nuclear Physics (Tomsk), and the Physics Institute of the Academy of Sciences and the Moscow Engineering Physics Institute (Moscow). The main efforts are now directed to removing the low-energy component of electron beams. The second group of reports, which were presented by the Institute of Theoretical and Experimental Physics (Moscow), the Joint Institute of Nuclear Research (Dubna), and the Scientific-Research Institute of Nuclear Physics (Tomsk) is concerned with the development of electron rings. The Conference approved work done in this field and recommended to the scientists working in this field that they improve the coordination in the development of both the

mathematics and the automation of experiments on collective acceleration techniques. The third group considered the acceleration of ions in straight beams; the fourth group discussed the generation and transfer of powerful electron beams and their interaction with various media.

The utilization of electron accelerators in various fields of the national economy was considered in 116 reports from 52 organizations. The reports concerned the state and the chances of utilizing electron accelerators for nondestructive testing methods, for radiation chemistry, for radioactivation analysis, and for nuclear physics and medicine. The utilization of synchrotron radiation in physics experiments was discussed in a special section.

The resolution of the conference reflected the proposals and recommendations of the sections in regard to extending the work on electron accelerators. The conference was useful and up to date.

7TH INTERNATIONAL CONFERENCE ON CYCLOTRONS AND THEIR APPLICATIONS

N. I. Venikov

The above conference took place in Zurich (Switzerland) between Aug. 19-22, 1975. About 250 specialists from 22 countries participated in the conference; 55 reports were read and 70 reports were presented for information of the participants. Summarizing the main topics of the conference, it is noted that the technology of cyclotrons has branched out in the last few years: the number of operating cyclotrons increases rapidly, meson factories using isochronous cyclotrons and synthrocyclotrons have been put into operation, superconductivity was introduced into the technology of cyclotrons, new areas have been developed, and the old areas of cyclotron applications have been expanded.

Meson Factories. Two meson factories making use of huge isochronous cyclotrons (the SIN in Switzerland and the "Triumph" in Canada) have been put into operation; two other meson factories making use of synchrocyclotrons (CERN and Columbia University, USA) are working now. An external 590-MeV proton beam of about 30 μA, up to 95% of which are transmitted through a ring cyclotron, were obtained in the SIN accelerator; polarized protons have been accelerated and beams for physics experiments and practical applications have been introduced on a large scale. Owing to the beam losses (~30%) during the acceleration process, the external beam, with an energy of about 500 MeV, of the "Triumph" cyclotron reaches at most 0.3 μA, though 48 μA are reached in pulses. At the beginning of 1976 the average current was raised to 10 μA; the average current is to be increased to 100 μA in 1977. In the external beam of the CERN synchrocyclotron, several microamperes have been reached and the efficiency of the extraction system is as high as 70%. The internal beam of the Columbia University synchrocyclotron reaches several microamperes and work on beam extraction is in progress.

The participants were impressed by the project of the Laboratory of Nuclear Problems of the Joint Institute of Nuclear Research to develop a "supermeson factory" based on an isochronous cyclotron with an external beam intensity of several hundred milliamperes and a 800-MeV energy. This is possible in an external beam, provided that the extraction efficiency is 100%. This efficiency figure can be reached when one uses a new method of extracting the beam from an isochronous cyclotron. The method was proposed and developed by the co-workers of the Joint Institute of Nuclear Research and termed "method of expanding closed orbits in periodic magnetic fields."

Acceleration of Heavy Ions. As in the past, the interest in accelerating heavy ions has increased. Both operating cyclotrons and cyclotrons to be put into operation have been adapted to accelerate heavy ions; projects of new cyclotrons and setups with cyclotrons have been worked out. Work on the improvement of existing sources of multiply charged ions and the development of new sources of such ions are in progress. All proposals on the development of superconducting cyclotrons are directed to the acceleration of heavy ions (Michigan University, Chalk River, Oak Ridge, Berkeley). The reports of the conference dealt with both cyclotrons accelerating heavy ions (the most important of these cyclotrons are in Dubna, Berkeley, and Oak Ridge) and with existing proposals and projects. At the present time heavy ions are accelerated in at least 17 cyclotrons all over the world; records in regard to the selection of ions and the ion intensity have been set by the Laboratory of Nuclear Reactions of the Joint Institute of Nuclear Research, by Berkeley, and by Oak Ridge. Though new sources of multiply charged ions (laser sources, electron beam sources) have been developed and studied in many laboratories, the dominating opinion is that Penning sources of multiply charged ions will be most efficient for cyclotrons for a long time to come. The source having a heated cathode and used in the cyclotrons of the Laboratory of Nuclear Reactions of the Joint Institute of Nuclear Research is the best form of the Penning source.

Translated from Atomnaya Énergiya, Vol. 40, No. 1, pp. 87-88, January, 1976.

One must consider separately the acceleration of "semiheavy" ions, lithium and beryllium ions, which are of great interest for nuclear physics research. Lithium and beryllium ions were accelerated for the first time in the entire world in the cyclotron of the I. V. Kurchatov Institute of Atomic Energy and, as far as the intensity of the source is concerned, the source of the Institute of Atomic Energy has not been surpassed. The same ions are now obtained with similar intensity in the Berkeley cyclotron, but the ions issue from a completely different source. Triple-charged lithium ions were also accelerated in the Karlsruhe cyclotron (with an intensity of 0.005 μA, which is by two orders of magnitude lower than the intensity of the triple-charged lithium ions in the external beam of the Institute of Atomic Energy). There exist plans to generate these ions in the 0.1 μA internal beam of the recently finished cyclotron of Indiana (USA).

Several proposals concerning the acceleration of heavy ions in cyclotrons and synchrocyclotrons which are in operation, being built, or in the project stage were presented to the Conference. In 1976 the heavy-ion complex of the WIKSI (=Wissenschaftliches Institut für Kernforschung + SI) in West Berlin is to be put into operation. This complex comprises the existing electrostatic 6-MeV accelerator-injector and a 4-sector ring cyclotron. The complex can be used to accelerate ions up to argon ions with an energy of up to 200 MeV. It seems that in the same year heavy ions will be obtained in the external beam of the Indiana (USA) cyclotron complex. This complex comprises an electrostatic 600-kV accelerator and two ring cyclotrons. It was planned to put this complex into operation in 1972, but the operation was delayed for several reasons. One of the Oak Ridge projects is in the final stage: according to a contact with ORNL, the National Electrostatic Corporation builds an electrostatic charge-reversing vertical Π-shaped accelerator with a conductor potential of up to 25 MV. The total cost of this accelerator is 8.1 million dollars. A beam will be obtained for the first time in 1979. After a charge-reversing injection of a heavy ion beam into the existing ORIC cyclotron and the acceleration of the ions in the cyclotron, ions with an energy exceeding the Coulomb barrier energy of uranium will be available for experiments with ions having a mass of up to 160. It was suggested to replace the ORIC cyclotron by four separate magnets with BR = 25 KG $\cdot$ m, which would make it possible to generate uranium ions with an energy of up to 10 MeV/nucleon and carbon ions with an energy of up to 75 MeV/nucleon. This project can become operative in 1981.

Extensive work is done on the French GANIL project whose completion is planned for 1980. This project comprises a small cyclotron injector and two large ring cyclotrons with separate magnets and charge-reversing injection. The plan is to accelerate ions up to uranium ions with an energy of 8 MeV/nucleon. It has been proposed to accelerate heavy ions in the CERN synchrocyclotrons (ions up to neon with an energy of 70 MeV/nucleon) and in Uppsala (Sweden).

Utilization of Superconductivity in Cyclotrons. First suggestions with a solid foundation have been made in 1973 in regard to building a cyclotron with a superconducting base coil; these suggestions were made almost simultaneously in three laboratories, viz., in Chalk River, Berkeley, and Michigan University. All these proposals make use of the rich world-wide experience in the construction of large superconducting bubble chambers: the proposals comprise a fully stabilized niobium — titanium superconductor in a copper matrix, the cryostat and the refrigerators resembling in their design the components of bubble chambers, etc. The most important aspect of these projects is that the high-frequency system and the correction coils of the steel sectors are used at normal temperature. The azimuthal variation of the magnetic field is produced by saturated steel sectors rather than by superconducting coils. Michigan University has received an allocation for the building of a superconducting magnet with a cryogenic system for a cyclotron having three-sector structure with BR = 46 kG $\cdot$ m and an ejection radius of 0.65 m (K = 440). The ejection problem was solved mainly by creating a magnetic field which breaks off sharply at increasing radii and by using a pair of electrostatic deflectors with a high gradient; the ejection problem was, first of all, solved by a magnetic shield in the form of a superconducting tube made from a 50-μ Nb_3Sn superconductor. This tube was already prepared in Stanford and its inspection has been initiated. The magnet costs 0.7 million dollars.

The project of a superconducting cyclotron for the Chalk-River Laboratory is estimated at 2.2 million dollars; the cyclotron is to become operative in 1980. The average magnetic field is 50 kG and the exit radius is also 0.65 m. The injection into the cyclotron is effected from an existing electrostatic charge-reversing 13-MV accelerator. The ejection problems have not yet been fully resolved. It was proposed to generate uranium ions with an energy of up to 10 MeV/nucleon and carbon ions with an energy of up to 50 MeV/nucleon. The proposal of the Berkeley Laboratory considers two forms of superconducting cyclotrons which differ only by their geometrical dimensions (K = 400 and K = 800). One of the two forms

will be selected as a post-accelerator for the existing SUPERHIGHLAC or the 88-inch cyclotron. This will make it possible to reach the range of very heavy ions with an energy of several dozen MeV per nucleon. The basic difference to the above projects is that the required radial profile of the magnetic field is developed with the aid of the main superconducting coil which is divided in vertical direction into sections (the sections are separately supplied). The cost of the superconducting cyclotrons is 4.9 million dollars for K = 400 and 7.8 million dollars for K = 800. If these cyclotrons were not made superconducting, the costs would increase to 10.3 and 18 million dollars, respectively, i.e., by more than a factor of two.

Greatest attention should be paid to the proposal made by the Oak Ridge Laboratory that the coil of the ORIC cyclotron should be replaced by a superconducting coil while simultaneously the steel yoke should be reinforced (an additional steel mass of 1500 t should be added). This allows to increase four times the ampere-windings of the coil and to raise almost two times the average magnetic field strength (from 18.6 to 33.9 kG), i.e., it should be possible to increase K from 90 to 300.

The utilization of cyclotrons in other fields, particularly in medicine, increases at a higher rate than in nuclear physics. Compact isochronous cyclotrons have been installed in many hospitals. Widely discussed were proposals for a cyclotron which is optimal from the viewpoint of medicine and which allows cancer therapy with protons (proton energy 150-200 MeV) and the preparation of large quantities of radio isotopes required for disease diagnostics. Other applications of cyclotrons are expanded, e.g., the simulation of radiation defects of reactor materials and the radio activation analysis of superpure materials, mainly semiconductor materials and materials for reactors. New applications have come up: the cyclotron in Winnipeg (Canada) is extensively used to determine the amounts of protein in various cereals, whereas the cyclotrons in Melbourne (Australia) and Davis (USA) are used to analyze environmental contamination.

Some cyclotrons in the Federal Republic of Germany and in Great Britain are used to determine the wear of parts of machines (wheels of box cars, pinions, ball bearings, etc.) and the corrosion of constructions; in this case surface activation with a beam of accelerated particles is employed.

The conference also dealt with problems related to the automated control and the computer control of cyclotrons, with high-quality systems, magnetic systems, beam dynamics, beam injection, beam ejection, and beam transfer.

The next conference on cyclotrons and their application will be held in Aug.-Sept. 1978 in the USA.

CONFERENCE ON LASER ENGINEERING AND APPLICATIONS

V. Yu. Baranov and N. G. Koval'skii

This conference took place in the summer of 1975 in Washington. Similar conferences are organized by the Optical Society of America and the Committee on Quantum Electronics every other year and are a broad forum at which the latest accomplishments in various fields of laser applications are reported and the most interesting technical problems associated with lasers and the optical elements used in laser systems are discussed. Approximately 1400 people took part in the 1975 conference. The majority of the participants were representatives of U.S. research laboratories and industrial firms. The number of foreign experts (USSR, England, Canada, France, West Germany, Japan) did not exceed 150. About 200 talks were given which were divided into 19 sections according to themes. Each day three sections ran simultaneously in morning and evening sessions.

The conference covered a wide range of questions. Judging from the talks, there is great interest at present in a number of countries in the problem of laser isotope separation. However, no practical results were reported at the conference. As a rule, only individual physical experiments and theoretical considerations were presented. At the Lawrence Livermore Laboratory, Solarz has conducted experiments on the photoionization cross sections and lifetimes of excited states in uranium vapors at 2000°K. Here a commercial N_2 laser was used to pump a dye laser. At Los Alamos Scientific Laboratory the copper isotopes ^{63}Cu and ^{65}Cu were obtained by irradiating copper and iodine vapors with an argon ion laser. As always, there was great interest in the talks presented by the staff of the Institute of Spectroscopy of the Academy of Sciences of the USSR. R. V. Ambartsumyan, N. V. Chekalin, Yu. A. Gorokhov, V. S. Letokhov, G. P. Makarov, and E. A. Ryabov have for the first time obtained macroscopic isotope separation with a CO_2 laser using isotopically selective dissociation of complex molecules in the high radiation field. Experiments were done on the separation of the isotopes ^{10}B and ^{11}B by dissociation of BCl_3 and an enrichment coefficient of about 2800 was obtained for the sulfur isotope ^{34}S by dissociation of SF_6 molecules. The talk by V. N. Bagratashvili and others (also of the Institute of Spectroscopy) described the basic characteristics of a high pressure CO_2 laser with smoothly tunable frequency over a wide band. At a pressure of 5 atm the tuning range was 50 cm^{-1}. With this laser infrared luminescence resonances of ethylene in the visible range have been observed. The study of these resonances is important for understanding the mechanism of isotopically selective molecular dissociation.

The papers on the laser fusion program were presented mainly by physicists from Los Alamos and Livermore and can be divided into the following groups.

1. Theoretical and experimental studies of effects accompanying the propagation of subnanosecond light pulses through the amplifier cascades of powerful neodymium glass lasers; analysis and use of soft diaphragms and spatial filters for prevention of self-focussing of laser beams; choice of materials for optical elements; and perfection of disc amplifiers to avoid parasitic oscillations.

2. Discussion of the design of the large neodymium glass and CO_2 laser systems with energies of about 10 kJ in a short pulse which are under construction at this time in US laboratories.

3. Reports on the results of the latest experiments on demonstration of the compression of spherical glass targets, filled with a deuterium—tritium mixture, by laser pulses with energies of several tens of Joules. To achieve spherical symmetry in energy deposition on the compressible target when working with one or two laser beams, the surface of the glass sphere is coated with a layer of low Z material (ablator).

Translated from Atomnaya Énergiya, Vol. 40, No. 1, pp. 89-90, January, 1976.

4. The search for new gaseous media for powerful pulsed lasers in the range of 0.3-0.6 μ. American scientists believe that such lasers might be used in future thermonuclear power stations.

The talk by E. Teller before the start of the session on the use of lasers in thermonuclear research attracted great interest. In his opinion, thanks to work done at the KMS Company and at Los Alamos and Livermore, the possibility of laser initiated controlled thermonuclear fusion, first mentioned in 1972, has now become real. Apparently, in the next three or four years thermonuclear reactions will be demonstrated in compressed and heated deuterium — tritium targets. The basis for this conclusion is the rather good agreement between experimental and theoretical results. Construction of commercial laser-driven thermonuclear reactors is complicated by so much technical difficulty that energy will be obtained from such systems only in the 21st century. However, it may be hoped that in the next few decades high-power lasers will be widely used for isotope separation to great economic effect. Teller noted that the Russians do not lag behind the US in the application of lasers.

A large research program was described by the Livermore staff. In that laboratory a two-beam laser, "Janus" (20 J in each beam with pulse duration 100 psec), and a single beam laser, "Cyclops" (270 J in a 200-psec pulse), have been built and are working. Both machines are neodymium glass laser systems with disk amplifiers 35, 85, and 200 mm in diameter in the final stages. The goal of the Janus experiments is to demonstrate the compression effect in a spherical target. Along with the standard methods of determining the plasma temperature from soft x-rays using filters, x-ray pinhole cameras, and spectroscopic analysis of radiation scattered by the plasma, an x-ray image converter is being built directly on the test chamber to make streak photographs with a time resolution of 10 nsec. An x-ray microscope has been developed and is being used successfully. Of undoubted interest are the measurements of the energy spectra of the alpha particles produced in the D-T fusion reaction. At the relatively low (about 10^6) neutron yields in present laser target experiments it is extremely difficult to analyze the energy spectrum of the neutrons. Thus, this method is very useful and, apparently, makes it possible to judge whether the neutrons are of thermonuclear or nonthermonuclear origin.

On the Cyclops machine work is being done to perfect optical elements for laser systems, and to test soft diaphrams, spatial filters, and Faraday rotators. Various ways of battling parasitic oscillations in disc amplifiers are being studied. In fact, the Cyclops laser is a module for later multibeam systems. At Livermore work has begun on construction of the Argus system which will consist of two Cyclops lasers operating in parallel.

Work is proceeding at a fairly fast rate on construction of the 20-beam "Shiva" system, which will have an energy of 10 kJ in a short pulse. According to the plans, the experiments are to begin in the end of 1977. With this machine, American scientists hope to obtain significant thermonuclear energy yields (10-20% of the laser energy delivered to the target) in 1977-1979, and in the next year or two it may be possible to proceed to experiments in which the energy release is on the order of the laser pulse energy. The possibility is foreseen of operating at the second and fourth harmonics of the neodymium laser light.

The Livermore staff members also presented a talk on a pulsed CO_2 laser (project "Valkyrie") with an energy of 50 J in a 1-nsec pulse. The amplifier stages have been built by the Maxwell company. When it acts on a 5-μ-thick CH_2 foil, about 6% of the CO_2 laser light at a power density of 10^{14} W/cm^2 is backscattered into a solid angle of 0.1 sr. Work on pulsed CO_2 lasers for thermonuclear studies is being actively done at Los Alamos. The master oscillator and the preamplifier chain form a 1-nsec pulse, which is divided into two parts, expanded, and sent into the two chambers of the final amplifier, which are located on both sides of a cathode from which electron beams excite the working gas mixture in both chambers at once. After amplification, the energy in each of the two beams, at a diameter of 35 cm, is 1.25 kJ. The machine is one of four modules of a projected 10-kJ laser system.

Interesting results have been obtained by McCall's group at Los Alamos in a study of the processes responsible for the anomalously low thermal conductivity of the plasma formed when spherical and plane solid targets are irradiated at supercritical densities. Experiments have been conducted on two machines. One of these is a two-beam neodymium laser with an energy of 30 J in each beam and a pulse length of 150 nsec, and the other is a single-beam CO_2 laser with a 150-J, 1.5-nsec pulse.

Also attracting interest is the work of Sheppert (Los Alamos) in which a number of subtle effects have been studied which have an important effect on the operation of CO_2 lasers. Simultaneous lasing on several lines has been achieved by placing cells with different gases (Élegaz, butane, etc.) in the cavity. When amplifying short pulses, the dispersion effects may differ for different rotational — vibrational

transitions so the total pulse after amplification may be longer. The time variation in the rotational temperature was analyzed, the maximum efficiency of a CO_2 laser was estimated theoretically, and a method was proposed and the technology explored for measuring the size of the focal spot and energy density (using a diffraction grating).

German scientists (G. Brederlau et al. at Garching) presented a design for an iodine laser, "Asterix III," with an energy of 1 kJ in a nanosecond pulse at a wavelength of 1.315 μ. Its use in thermonuclear research was proposed.

It should be noted that a large-scale effort is under way in the US to study new active gaseous laser media. In particular, much attention is devoted to the development of chemical lasers, metal vapor lasers, and lasers using mixtures of noble gases and oxygen.

SOVIET—AMERICAN WORKING MEETING ON OPEN TRAPS

D. A. Panov

A Soviet—American working meeting on the problems of plasma containment and stability in open traps was held from Sept. 15-21, 1975 in Novosibirsk at Akademgorodok. The meeting was organized within the framework of the agreement on scientific and technical cooperation between the USSR and the USA.

The center of attention was a discussion of the results of studies of collisional plasmas in minimum B traps: PR-6, PR-7 (I. V. Kurchatov Institute of Atomic Energy, Moscow), 2X2, and 2X2B (Lawrence Livermore Laboratory, California). A plasma of density up to $3 \cdot 10^{12}$ cm^{-3} with an ion temperature of about 0.5 keV is investigated in the PR-6 and PR-7 machines. Observations of the decay of the plasma have shown that after some period of stability, oscillations develop in the plasma which are produced by anomalously rapid particle losses through the magnetic mirrors. A number of previous experiments show that the delay in the development of the instability is connected with the stabilizing effect of the cold plasma which lies outside the region of containment of the hot plasma. To investigate this effect an additional pulsed winding was installed in the PR-6 to develop a flux of lines of force between the plasma injector and mirror regions. It is shown that this flux discontinuity, in breaking contact between the cold and hot plasma, is in fact, accompanied by the onset of an instability.

Along with studies of plasma confinement physics, the "X" series machines at Livermore are also intended to gradually achieve thermonuclear reactor parameters. A significant step in this direction has been made on the 2X2B machine, on which experiments were begun in the summer of 1975, shortly before the beginning of this meeting. A beam of fast atoms with energies of 10-20 keV and intensities of up to 370 equivalent amperes was injected into a plasma target (produced as in the 2X2, by injection of a plasma and then compressing it adiabatically). A plasma with very high parameters has been obtained in the experiments, which because of insufficient time cannot be regarded as complete: density $4 \cdot 10^{13}$ cm^{-3}, ion temperature 13 keV, containment time 5 msec or more, and ratio of the kinetic to the magnetic pressure $\beta = 0.4$. An unchanging condition for creating a plasma with these parameters is stabilization of the instability of the cold plasma which is being injected into the target throughout the buildup along the magnetic field lines. Injection of fast atoms with the flux of cold plasma turned off was accompanied by the development of powerful oscillations at a frequency close to the ion cyclotron frequency and by plasma decay with a time constant of about 100 μsec. Thus, the experiments at the Institute of Atomic Energy and at Livermore have shown that if special measures are not taken in minimum B traps, an instability develops and is accompanied by anomalous plasma losses. At the same time, the instability can be stabilized by a cold plasma flux. The results of experiments on the Ogra-3 machine (Kurchatov Institute) in which a feedback system was used to suppress the flute instability of a simple mirror plasma at densities of 50 times the threshold for appearance of the instability, were discussed with interest.

A number of experiments at US laboratories involve development of target plasmas. In the LITE experiment vaporization and ionization of grains of LiH by a laser beam is used to produce a plasma whose decay constant in the density range 10^{14}-10^{12} cm^{-3} is about 0.5 msec, which renders it suitable for planned experiments on injection of a beam of several hundred equivalent amperes into a minimum B trap. A special system for injecting ammonia droplets with a complex device for aiming the droplets at a given point in space has been developed for the Baseball-2 magnetic trap. The ammonia droplet will be evaporated and ionized by a laser beam as it passes through the machine.

Translated from Atomnaya Énergiya, Vol. 40, No. 1, pp. 90-91, January, 1976.

In connection with the negative ion injectors being developed at the Kurchatov Institute, the requirements imposed on the material of which the charge exchange gas target is made (which must be sodium as shown by analysis) were discussed. On the presently existing negative ion sources, the ones with the best parameters are the surface ionization sources developed at the Institute of Nuclear Physics of the Siberian Branch of the Academy of Sciences of the USSR. A report of this was received with great interest. The authors of the 2X2B experiment presented for discussion an injector system for the device with design parameters of 600 equivalent amperes at a particle energy of 20 keV. A modernization of the sources which would allow an increase in the energy of the atoms to 40 keV was reported.

The study of various kinds of open traps for building a thermonuclear reactor in our time, when the problem of controlled fusion has not yet been finally solved, is very important. A system for containing a dense plasma in a chain of simple mirror traps, developed at the Institute of Nuclear Physics of the Siberian Branch of the Academy of Sciences of the USSR, was discussed with great interest. The kinetic pressure of the plasma in this system is balanced by the chamber walls while the role of the magnetic field amounts to reducing the thermal conductivity of the plasma. Arranging the field in the form of a chain of traps must impede escape of the plasma along the field lines. This has been confirmed experimentally in experiments with an alkali plasma. It has been shown that a plasma can be produced and confined in experiments with a simple mirror trap and a system of annular high-voltage electrodes in the magnetic plugs. From a theoretical analysis of the stability of the plasma in such a trap, it is clear that by producing certain profiles of the radial electric field it is possible to satisfy the conditions for hydrodynamic stability.

As before, confinement systems with cusped magnetic field, which ensure complete hydrodynamic stability of the plasma, attracted great attention. At the Kharkov Physicotechnical Institute the possibility is being studied of reducing plasma losses from such traps through the annular magnetic gaps by means of an electrostatic barrier. In the Jupiter machines developed there, a plasma has been obtained with a density 10^{12} cm^{-3}, an ion temperature of about 1 keV, and a lifetime of up to 5 msec. No signs of instability were observed. At the University of California the escape of a low-pressure plasma through a magnetic wall with opposing currents was measured and it was shown that the outflow is proportional to the geometric mean of the ion and electron Larmor radii. A power reactor with cusped magnetic fields computed on the basis of these losses is within the realm of contemporary technical possibility.

It was not a special goal of this meeting to discuss the present state of the theory of plasmas in open systems. On the whole it was noted that the majority of the theoretically predicted instabilities have been observed experimentally. The results of the initial stages of an analysis of the nonlinear limitations on the level of instability oscillations have been definitely confirmed experimentally. The linear theoretical analysis of the conditions for stabilization of the flute instability agrees numerically with experiment. Factors are theoretically observed which increase the range of parameters over which plasma stability is ensured with respect to drift cone oscillations.

In a discussion of the prospects for open traps as reactors the substantial progress in obtaining high plasma parameters was noted. The possibility of stabilizing the drift cone instability with the cold plasma was demonstrated. Up to the present time no signs of the RF cone instability have been observed. At the same time the existing data do not yet permit a reliable analysis of the energy balance of reactor systems in which the energy losses associated with the leakage of cold plasma needed for stabilization are taken into account. It was emphasized that the weak point of open traps from the standpoint of future systems is their small margin of energy efficiency, even if the plasma should be completely stable. It is necessary to devote much attention to the analysis of methods for increasing the plasma lifetime in traps.

SEVENTH ALL-UNION CONFERENCE ON SCINTILLATION TECHNOLOGY

O. P. Sobornov

A conference on the synthesis, production, and use of scintillators took place in Khar'kov on September 23-25, 1975. Papers on work executed since 1971 were read, and consideration was given to the prospects of technological development and the production of scintillators and scintillation materials in the Tenth Five-Year Plan. Participants included leading scientists working on the creation and study of scintillation materials, detectors, photomultipliers, and scintillation units, as well as representatives of various industrial and scientific-research organizations using nuclear-radiation detectors based on NaI(Tl), CsI(Tl), CsI(Na) plastic and other scintillators. The conference proceedings indicated that Soviet industry had made notable advances in the production of detectors and in the improvement of their properties. Production of large NaI(Tl) spectrometric detectors (200 × 200 mm in diameter) has become a routine matter.

Of great practical interest are the industrially adopted CsI(Tl) detectors, which have a greater efficiency than NaI(Tl), as well as a greater mechanical strength, and are capable of operating subject to sharp changes of temperature. For counters recording tritium radiation and the extremely weak luminescence of living tissues, phc tomultipliers with the first dynode made of gallium phosphide have been developed; by virtue of the amplification of the dynode the signal/noise ratio has been increased by a factor of more than 20 times. Many research workers have studied the counting, spectrometric, and background (noise) characteristics of detectors and scintillation devices intended for recording β , γ and x radiations. A number of papers considered problems of improving the technology of making scintillators and detectors based on the latter.

On the whole the conference demonstrated considerable progress in scintillation technology, which has greatly extended its useful range over the past few years. The proceedings of the conference will shortly be published.

Translated from Atomnaya Énergiya, Vol. 40, No. 1, p. 92, January, 1976.

INTERNATIONAL CONGRESS ON ENGINEERING CHEMISTRY, CHEMICAL ENGINEERING, AND AUTOMATION

V. N. Koshkin

An International Congress on Engineering Chemistry, one of the series organized by the Czechoslovakian Academy of Sciences once every three years, was held in Prague on Aug. 25-29, 1975. The scientific schools of a variety of countries concerned with the development and study of fundamental problems in engineering chemistry were widely represented at the Congress.

The section devoted to mixing processes considered theoretical and applied problems involved in the design of systems with various types of mixers for homogenization, the mixing of suspensions and viscous liquids, dispersion, and the mixing of gases. K. Molen of Holland described a determination of the intensity of turbulence in various zones of a reactor based on Doppler measurements of velocities with lasers. Soviet scientists presented an interesting communication in which they discussed the construction and modeling of devices for the production of wet-process phosphoric acid at a rate of 280-300 thousand tons of P_2O_5 per year.

A considerable number of the papers on the mixing of solids were devoted to the further development of mixing theory.

The fluidization Section considered theoretical problems of agglomeration and heat and mass-transfer processes in fluidized beds, gas–solid systems, and liquid–solid systems (ion exchange).

In the field of liquid extraction and the structure of flows in chemical apparatus, all the research workers concentrated their attention on three types of extracts: rotor-disk columns (East Germany, Austria, Switzerland, West Germany), pulsation columns (USSR, Bulgaria, East Germany), and vibrational columns (Czechoslovakian SSR, USSR, Yugoslavia). A combined paper by Bulgarian and French scientists compared various types of extracts in the acetone–benzoic acid system. It was shown that the best technological and economic indices were those of rotor-disk and pulsation columns. A series of contributions presented by the USSR included one on a study of the vibrational extractor and five on hydromechanics and mass transfer in pulsation columns with a diameter of 200-3400 mm.

Translated from Atomnaya Énergiya, Vol. 40, No. 1, p. 92, January, 1976.

V. I. Sidorov, N. I. Loginov, and F. A. Kozlov FUNDAMENTALS OF HEAT PHYSICS IN ATOMIC POWER INSTALLATIONS*

Reviewed by M. Kh. Ibragimov

A large number of scientific-research and experimental-design investigations are now being carried out with a view to establishing a sound basis for the design of nuclear power installations. Most of these investigations are concerned with heat physics. The execution of research and the servicing of nuclear power installations demand the attention of a large number of specialists, including the workers and operators of nuclear power stations. The education of such personnel is impeded by the lack of heat-physics reference books duly reflecting the present level of nuclear science and technology.

The book under consideration satisfies this need; it systematizes information relating to hydrodynamics and heat transfer, coolant technology, and temperature and flow measurements in the active zones of nuclear reactors.

The first chapter considers the basic problems of liquid and gas mechanics: the laws of hydrostatics and hydrodynamics, and the operating principles of instruments for measuring pressure and rate of flow; the characteristics of liquid motion (laminar and turbulent) are explained, relationships are given for calculating the pressure drop and velocity distribution in channels containing moving liquids. The second chapter sets out the fundaments of heat transfer and considers the laws of conduction, convection, and radiation in relation to the transmission of heat, as well as heat transfer in boiling and condensation, and methods of calculating the performance of heat exchangers. A special section is devoted to the characteristics of heat transfer during the flow of coolant in the channels of nuclear power stations. The third and fourth chapters provide a detailed description of instruments and sensors for measuring coolant temperature, flow rate, and velocity. Special attention is given to a description of small coolant temperature and flow sensors for making precision measurements. The physical bases of the electromagnetic method of measuring coolant flows are set out. The fifth chapter gives information regarding various coolants used in nuclear technology and makes recommendations as to their use in nuclear power equipment. The sixth and seventh chapters are devoted to problems involved in the use of liquid sodium as coolant for nuclear reactors. Questions as to the monitoring of impurity content (oxygen, hydrogen, carbon, and nitrogen) are considered, as well as ways and means of decontaminating the sodium.

Taken as a whole, the book contains all the information necessary for educating and instructing the middle technical personnal of nuclear power stations and improving their qualifications. Unfortunately, owing to its small size, the book is unable to reflect or to rigorously expound such questions as safety technology when operating with liquid-metal test-beds and reactors, emergency situations, and so on. The small number (1610) printed is surprising as the book is rapidly selling out.

*Atomizdat, Moscow (1975).

Translated from Atomnaya Énergiya, Vol. 40, No. 1, p. 94, January, 1976.

L. S. Sterman, L. T. Sharkov, and S. A. Tevlin

THERMAL AND NUCLEAR POWER STATIONS*

Reviewed by Yu. I. Klimov

This book is intended as a reference book for students of the higher educational establishments studying courses in "Water and fuel technology in thermal power stations" and "Automation of thermal power processes"; it is based on a course of lectures read by the authors in the Moscow and Ivanovsk Power Institutes. The authors consider identical components and services in thermal and nuclear power stations in relation to their functional purposes, with a parallel exposition and description of their special characteristics.

A considerable space is given to general problems of the power industry and its economic aspects. The authors briefly set out the principles and special characteristics of gas-turbine and gas-steam power stations and those containing MHD generators, which cannot as yet be regarded as widely employed in power production.

The book gives the impression of a very fundamental treatise; it contains 26 chapters embracing practically every aspect of the construction, operation, and special characteristics of thermal and nuclear power stations (except for heat-generating systems such as the steam boiler in thermal and the nuclear reactor in nuclear power stations, which as the authors indicate are treated in special courses).

The authors give considerable attention to the description of technological solutions employed in specific operating power stations. This emphasizes the practical nature of the book. Of course, as regards nuclear power stations, which are experiencing a period of rapid technical progress and intensive technical and economic evolution, it is as yet impossible to assert that any particular description of their characteristics has become generally accepted and canonical. This applies to general problems of nuclear power (the choice of sites for nuclear power stations, the types of stations to be built, and their functions in the nuclear-power system), which constitute the subject of serious and often mutually competitive discussions and considerations. Naturally the book is not intended to reflect every view as to the future of power (especially nuclear-power) production. The authors have nevertheless succeeded in distinguishing and expounding some reasonably general problems and tendencies. In this sense the book is a great aid to the development of competent specialists for such a vast and vitally important branch of the popular economy as power production.

*Atomizdat, Moscow (1975).

Translated from Atomnaya Énergiya, Vol. 40, No. 1, p. 94, January, 1976.

breaking the language barrier

WITH COVER-TO-COVER ENGLISH TRANSLATIONS OF SOVIET JOURNALS

The Soviet Journal of Bioorganic Chemistry

Bioorganicheskaya Khimiya

Editor: **Yu. A. Ovchinnikov**
Academy of Sciences of the USSR, Moscow

Devoted to all aspects of this rapidly-developing science, this important new journal includes articles on the isolation and purification of naturally-occurring, biologically-active compounds; the establishment of their structure; the mechanisms of bioorganic reactions; methods of synthesis and biosynthesis; and the determination of the relation between structure and biological function.

Volume 1, 1975 (12 issues) $225.00

The Soviet Journal of Coordination Chemistry

Koordinatsionnaya Khimiya

Editor: **Yu. A. Ovchinnikov**
Academy of Sciences of the USSR, Moscow

The synthesis, structure and properties of new coordination compounds; reactions involving intraspheral substitution and transformation of ligands, homogeneous catalysis; complexes with polyfunctional and macromolecular ligands; complexing in solutions; and the kinetics and mechanisms of reactions involving the participation of coordination compounds are among the topics this monthly examines.

Volume 1, 1975 (12 issues) $235.00

The Soviet Journal of Glass Physics and Chemistry

Fizika i Khimiya Stekla

Editor: **M. M. Shul'ts**
Academy of Sciences of the USSR, Leningrad

This new bimonthly publication presents in-depth articles on the most important trends in glass technology. Both theoretical and applied research are reported.

Volume 1, 1975 (6 issues) $95.00

Soviet Microelectronics

Mikroélektronika

Editor: **A. V. Rzhanov**
Academy of Sciences of the USSR, Moscow

Offering invaluable reports on the latest advances in fundamental problems of microelectronics, this new bimonthly covers • theory and design of integrated circuits • new production and testing methods for microelectronic devices • new terminology • new principles of component and functional integration.

Volume 4, 1975 (6 issues) $135.00

Lithuanian Mathematical Journal

Lietuvos Matematikos Rinkinys

Editor: **P. Katilyus**

A publication of the Academy of Sciences of the Lithuanian SSR, the Mathematical Society of the Lithuanian SSR, and the higher educational institutions of the Lithuanian SSR.

In joining the ranks of other outstanding mathematical journals translated by Plenum, *Lithuanian Mathematical Transactions* brings important original papers and notes in all branches of pure and applied mathematics. Topics covered in recent issues include complex variables, probability theory, functional analysis, geometry and topology, and computer mathematics and programming. Translation began with the 1973 issues.

Volume 16, 1976 (4 issues) $150.00

Programming and Computer Software

Programmirovanie

Editor: **N. P. Buslenko**
Academy of Sciences of the USSR, Moscow

This important new bimonthly is a forum for original research in computer programming theory, programming methods, and computer software and systems programming.

Volume 1, 1975 (6 issues) $95.00

send for your free examination copies!

PLENUM PUBLISHING CORPORATION, 227 West 17th Street, New York, N.Y. 10011

Prices slightly higher outside the US. Prices subject to change without notice.